Dissertation zur Erlangung des Doktorgrades
der Fakultät für Chemie und Pharmazie
der Ludwig-Maximilians-Universität München

Aggregation of polyQ-expanded huntingtin interferes with cytosolic protein quality control by sequestering critical chaperone factors

Yury Kukushkin

aus

Moskau, Russland

2015

Erklärung

Diese Dissertation wurde im Sinne von § 7 der Promotionsordnung vom 28.
November 2011 von Herrn Prof. Dr. F. Ulrich Hartl betreut

Eidesstattliche Versicherung

Diese Dissertation wurde eigenständig und ohne unerlaubte Hilfe erarbeitet.

München, am 08.06.2015

....
Yury Kukushkin

Dissertation eingereicht am

1. Gutachter: Professor Dr. F. Ulrich Hartl

2. Gutachter: Professor Dr. Roland Beckmann

Mündliche Prüfung am 05.08.2015

Acknowledgments

Contents

1   Summary

Neurodegenerative diseases like Huntington's, Alzheimer's and Parkinson's diseases are incurable conditions associated with protein misfolding and aggregation. In this work, we used a yeast model of Huntington's disease to study how polyglutamine (polyQ) aggregates interfere with protein quality control in the cell. We used a set of misfolded proteins located in different compartments as reporters for polyQ interference. These proteins normally undergo rapid degradation via the ubiquitin proteasome system. By employing a combination of yeast genetics, biochemistry and proteomics, we found that the polyQ-expanded protein, 96QmCh, stabilized misfolded model proteins in the cytosol (CG*; misfolded cytosolic carboxypeptidase Y* fused to GFP), nucleus (NLS-CG*), ER lumen (CPY*; misfolded secretory carboxypeptidase Y*) and ER membrane (CTG*; CPY* fused to a transmembrane domain and cytosolic GFP) by interfering with their proteasomal degradation. This effect was neither due to a direct inhibition of the proteasome by the polyQ-expanded protein, nor to lack of ubiquitination, as CG* was properly ubiquitinated despite the presence of polyQ protein.

In the second part of the study, we showed that neither 96QmCh alone nor a combination of 96QmCh and CG* induced a strong stress response. Moreover, we have found that misfolded proteins strongly affect the ability of the cell to upregulate the heat shock response, and this effect helps to explain why protein aggregates exert toxicity.

To investigate how the aggregation of polyQ-expanded protein interfered with the degradation of misfolded cytosolic proteins, we used quantitative proteomnics and analyzed the polyQ protein interactome in the yeast system. We identified about 100 different 96QmCh interactors. Among them the essential Hsp40 Sis1 was highly associated and its functional depletion by 96QmCh caused the stabilization of CG*. Overexpression of Sis1 rescued CG* and NLS-CG* degradation in the presence of 96QmCh, while CPY* and CTG* remained unaffected. We could show further that Sis1 shuttles between the cytosol and nucleus and is required for effective CG* degradation by proteasome complexes in the nucleus. Upon depletion of Sis1 by 96QmCh, CG* formed cytoplasmic inclusions. Interestingly, the observed stabilization of CG* by expression of 96QmCh was dependent on the status of the yeast prion [PIN+]. In [pin-] cells,96QmCh

did not form detergent insoluble aggregates and the sequestration of Sis1 and other chaperones was reduced.

In summary, these results show that the aggregation of polyQ-expanded protein interferes with cytosolic protein quality control by sequestering critical chaperone factors. Moreover, we discovered that the Hsp40 Sis1 has an essential role in transporting misfolded proteins from the cytosol into the nucleus for degradation.

2 Introduction

2.1 Protein folding

Proteins perform the majority of biological functions in the cell, including metabolism, movement and transport, inter- and intracellular communication as well as the replication of the genetic material. They form the cytoskeleton that maintains cell shape and the extracellular matrix of tissues and organs.

Proteins are polymers made of the 21 different amino acids. In order to acquire biological activity, for most proteins the linear chain of amino acids must adopt a well defined three-dimensional conformation. This process is known as a protein folding.

There are four levels to describe protein structure: primary, secondary, tertiary and quaternary structures. Primary structure describes the amino acid sequence in a linear polypeptide chain as it is encoded by the corresponding mRNA. Secondary structure describes relatively short regions of the polypeptide chain where the amino acids are arranged in defined backbone conformations, most prominently α-helices and β-strands, the latter forming β-sheets (Pauling and Corey, 1951; Pauling et al., 1951). Secondary structure is supported by hydrogen bonds between peptide backbone amino- and carboxyl groups. The amino acids exhibit different ability to form various secondary structure elements. For example, glycine and proline can disrupt the regularity of the α-helical backbone conformation. Both amino acids have unusual conformational abilities and are commonly found in turns. There is a group of amino acids that prefer to adopt helical conformations in proteins: methionine, alanine, leucine, glutamate and lysine. Another group of amino acids tends to adopt β-strand conformations – among them we find amino acids with large aromatic residues, tryptophan, tyrosine and phenylalanine, and amino acids with branched side chains, isoleucine and valine.

Tertiary structure concerns the whole polypeptide sequence and contains information about the arrangement of α-helixes and β-sheets and their interactions in space. At this level we can describe a protein as globular (if it is relatively compact and has a spherical shape) or as fibrillar (if one axis of the folded polypeptide is significantly longer compared to another). Quaternary structure refers to the assembly of two or more folded protein molecules to oligomeric complexes. The correct three-dimensional structure is generally

essential for function. This operative and functional conformation of the polypeptide is called native state. Protein folding is driven by the reduction in free-energy arising from polypeptide compaction and the burial of hydrophobic amino acid side chains (Dobson, 2004; Jahn and Radford, 2008).

Initially it was believed that protein folding is generally a spontaneous process, based on the demonstration by Anfinsen that bovine pancreatic ribonuclease (a small globular protein with molecular weight ~14kDa) could reach its folded conformation from the denatured state without additional factors (Anfinsen, 1973). However, larger proteins and proteins with complex fold topologies often do not refold spontaneously and rather tend to undergo aggregation, mediated by the exposure of hydrophobic amino acids during the initial stages of the folding process (Eichner and Radford, 2011; Chiti and Dobson, 2006). The rate of aggregation increases in the crowded cellular environment, where the protein concentration reaches 300 g/L and more (Zimmerman and Trach, 1991). Under these conditions the rate constants of many reactions increase, particularly association reactions such as aggregation (Minton, 2000; Zimmerman and Minton, 1993). To suppress these aggregation reactions, cells have evolved a specialized machinery of so-called molecular chaperones, which assist in the folding of newly-synthesized polypeptides and stabilize preexistent proteins against aggregation during cell stress (Hartl, 1996;Bukau and Horwich, 1998; Frydman, 2001; Hartl and Hayer-Hartl, 2002). Chaperones recognize the hydrophobic amino acid residues that are exposed by non-native polypeptides and transiently shield those hydrophobic surfaces, thereby preventing aggregation. Folding is mediated by cycles of binding and release, often regulated by an inbuilt ATPae activity and by further cofactors. There are several classes of sequence related molecular chaperones. Many of them are referred to as stress or heat shock proteins (Hsp's) as their expression is induced under stress conditions such as heat stress. Chaperones are not only involved in folding and assembly but in a wider range of process in which protein conformation is modulated, including the transport of proteins across membranes and protein degradation. Multiple chaperone factors and other components cooperate in a large functional network to ensure protein homeostasis (or proteostasis). The different chaperone classes are typically defined by their molecular weight. In the following sections we will describe the most important chaperone families and their role in the cell.

2.2   Hsp70 system

Hsp70s are a family of conserved 70kDa proteins with essential functions in protein folding, protein transport and in the protection of the cells from stress. They form a central part of the proteostasis network. This family of proteins is expressed ubiquitously in almost all prokaryotes and eukaryotes (Folgueira et al., 2008).

All Hsp70s consist of an N-terminal ATP binding domain and a C-terminal domain that binds to the substrate, also known as substrate binding domain (SBD)(Flaherty et al., 1990; Zhu et al., 1996). The N-terminal domain consists of two parts, each containing two subdomains. The subdomains encompass a nucleotide-binding cleft (Bukau and Horwich, 1998; Zuiderweg et al., 2013). The C-terminal domain consists of a β-sandwich subdomain and anα-helical lid. The substrate-binding site is located in the β-sandwich subdomain (Bukau and Horwich, 1998). The substrate binding domain binds to a peptide stretch. This peptide stretch contains hydrophobic amino acids and is surrounded by positively charged amino acid residues. The peptide and SBD interaction is mediated by hydrogen bonds and hydrophobic contacts (Mayer, 2010). Substrate binding and release by the C-terminal domain of Hsp70 is regulated by ATP binding and hydrolysis in the N-terminal domain. In order to recognize unfolded polypeptides Hsp70 uses a cleft in its peptide-binding site that promotes binding with the peptide in an extended conformation (Zhu et al., 1996). If ATP is bound, the SBD is in an open conformation and binds or releases substrate rapidly. If ADP is bound, then the lid of the SBD is closed and bound peptide is held tightly (Hartl, 1996). Interconversion between ATP and ADP states is critical for substrate cycling and folding. This process is regulated by so-called co-chaperones, as has been best described for the bacterial system.

Analysis of the substrate specificity of Hsp70 has demonstrated that this chaperone recognizes linear polypeptide sequences enriched in hydrophobic amino acids (Rüdiger et al., 1997; Blond-Elguindi et al., 1993; Flynn et al., 1991). These motifs are only exposed in the non-native state but are buried in the folded structure. Most polypeptide sequences have such hydrophobic regions approximately every 40 residues (Rüdiger et al., 1997).

In *E. coli* the main Hsp70 homolog is called DnaK. There are two other cochaperones important for Hsp70 function - DNAJ and GrpE proteins (Szabo et al., 1994). DNAJ belongs to the family of Hsp40 proteins. These proteins contain special J-domain that interacts with Hsp70. Hsp40s also bind to unfolded proteins independently of Hsp70 and can recruit Hsp70 to non-native substrates (Langer et al., 1992). DnaJ binds to DnaK and

stimulates its ATP hydrolysis, thereby allowing DnaK to bind an unfolded polypeptide stably.

GrpE is a dimeric cochaperone for DnaK, which functions as a nucleotide exchange factor. GrpE is required for ADP release from the N-terminal domain of Hsp70 (Harrison et al., 1997). Rebinding of ATP results in the dissociation of DnaK-substrate complex and leads to the release of peptide. The cycle is shown in Figure 1. This process of binding and releasing was shown to be sufficient to fold a model substrate: firefly luciferase (Szabo et al., 1994). However if the substrate protein remains unfolded during cycling, then the Hsp70 system can transfer the substrate to another type of chaperone for folding (Langer et al., 1992). For example, many proteins are transferred to a so-called chaperonin for final folding. The chaperonins are large cylindrical complexes of ~800 kDa which provide a compartment for single protein molecules to fold in isolation, unimpaired by aggregation (Hartl and Hayer-Hartl, 2002).
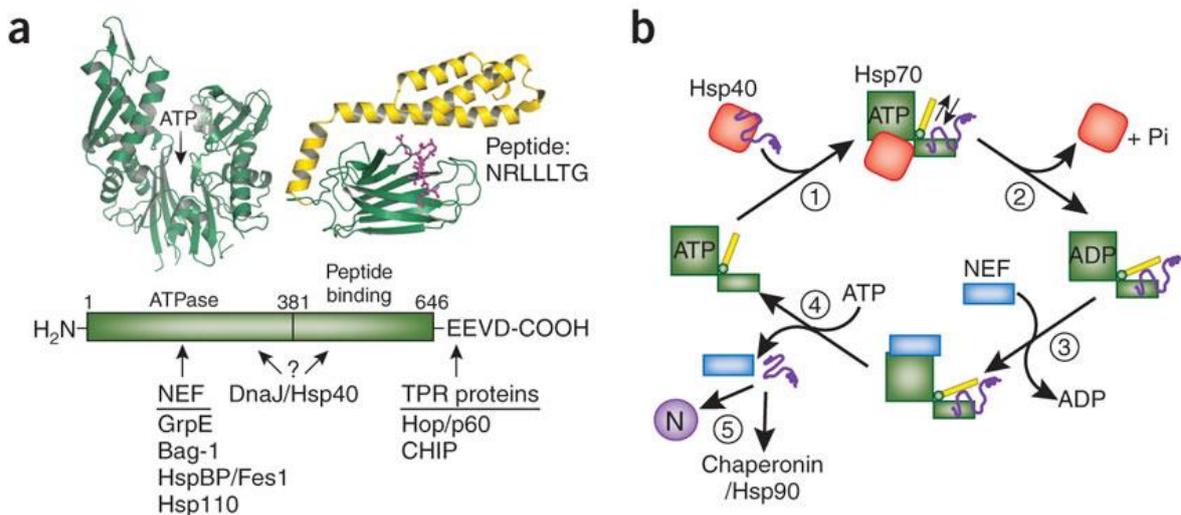
Figure 1. Hsp70 system

Hsp70 system. (A) Structures of the N-terminal ATP binding domain and the C-terminal peptide-binding domain of Hsp70 shown for *E. coli* DnaK (Zhu et al., 1996). The α-helical lid of the PBD is yellow and the peptide substrate is pink. ATP points at the ATP binding site position in the Hsp70 structure. Hsp70 interaction with cofactors is shown schematically. COOH-terminal sequence EEVD present only in eukaryotic Hsp70s (Scheufler et al., 2000). (B) Hsp70 chaperone cycle. (1)Polypeptide substrate delivered to ATP-bound Hsp70 with Hsp40 assistance. (2) Hsp40 binding accelerated ATP to ADP hydrolysis. As a result Hsp70 a-helical lid is closed and substrate was tightly bound by Hsp70. After the hydrolysis, Hsp40 dissociates from Hsp70 complex.(3) NEF triggers the dissociation of ADP. (4) ATP binding result in opening of the a-helical lid and

subsequent substrate release. (5) Substrate could either fold to native state (N), rebind to Hsp70 or transferred to chaperonin/Hsp90 chaperones. Nucleotide-exchange factor (NEF) is blue. NEF represented by GrpE for *E. coli* DnaK and by HspBP1, Bag, Hsp110 for eukaryotic cytosolic Hsp70 (from Hartl and Hayer-Hartl, 2009).

Eukaryotic cells contain Hsp70 members in various compartments, including cytosol, mitochondria, chloroplasts and endoplasmic reticulum (ER). Some of these proteins are constitutively expressed, referred to as Hsc70, or stress inducible, referred to as Hsp70 proper. The class of Hsp70 chaperones has been expanded in fungi. In the yeast *Saccharomyces cerevisiae* Hsp70 homologues are represented by the Ssa subfamily of proteins: Ssa1, Ssa2, Ssa3, Ssa4 and also by Ssb (Ssb1, Ssb2), Sse (Sse1, Sse2) and Ssz families (Willmund et al., 2013; Mukai et al., 1993; Werner-Washburne et al., 1987). They have roles in folding, disassembling aggregates of misfolded proteins and in misfolded protein degradation (Deshaies et al., 1988; Glover and Lindquist, 1998; Hartl, 1996). Ssa family proteins have a 84-99% homology within the group (Boorstein et al., 1994). Strains with mutations in SSA3 and SSA4 genes are indistinguishable from the wild-type. Ssa3 and Ssa4 are not expressed during vegetative growth and are stress inducible (Werner-Washburne et al., 1987;Young and Craig, 1993).

Ssa1 is constitutively expressed in the cytosol under normal conditions. Heat shock and some other forms of stress enhance its expression (Werner-Washburne et al., 1989). Transcriptional activator Hsf1 mediates the upregulation. It can bind to the regions called HSE (heat shock elements) in SSA1 gene promoter and enhance Ssa1 mRNA synthesis. Ssa1 function is important for yeast to survive under heat shock conditions as well as in conditions characterized by an increased level of misfolded proteins.

2.3   Hsp40/DnaJ system

The Hsp40s are a family of evolutionarily preserved chaperones and regulators of Hsp70 proteins (Walsh et al., 2004). The Hsp40s have been highly conserved from bacteria to eukaryotes and are characterized by the so-called J-domain, a small helical domain of ~70 amino acids, which mediates interaction with Hsp70 (Pellecchia et al., 1996; Hartl et al., 2011).

The J-domain contains a highly conserved loop with histidine, proline and aspartic acid residues. This so-called called HPD motive connects the second and third helices (Qian et al., 1996). Mutation of any of these residues results in the loss of the respective Hsp40 to stimulate the ATPase activity of its Hsp70 partner (Cheetham and Caplan, 1998; Greene et al., 1998).

According to their domain structure Hsp40 could be categorized in 3 different types (Cheetham and Caplan, 1998). These types of Hsp40 members are depicted in the Figure 2.
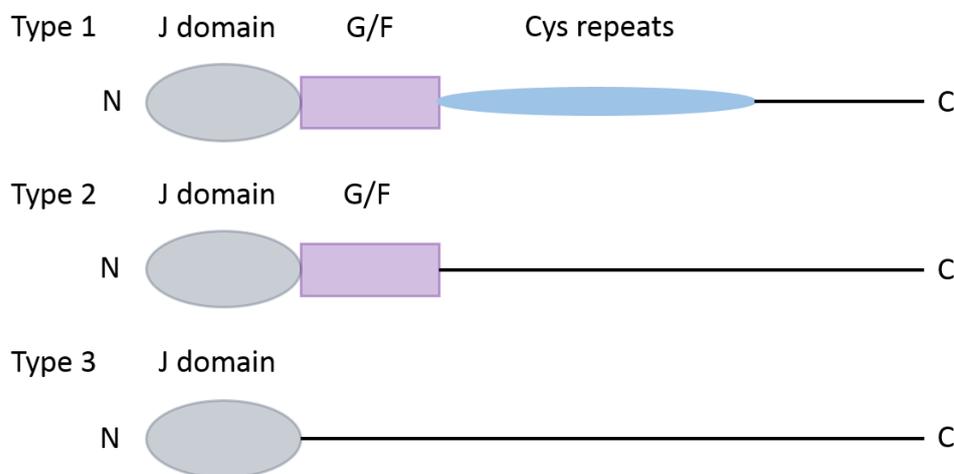
Figure 2. Classification of Hsp40 family proteins.

J-proteins are classified into 3 types: type 1, type 2 and type 3. Schematic representation of each class depicted in the figure. Type 1 possess J domain, G/Fregion and cys repeats. Type 2 has J domain and G/F repeats. Type 3 has only J domain.

Type 1 Hsp40 proteins contain a J domain, a glycine/phenylalanine (G/F)-rich region and a cysteine repeat region which is also known as zinc-finger domain. The G/F region is required for stability and precise positioning of the J-domain when Hsp40 interacts with Hsp70 (Rajan and D'Silva, 2009). The zinc-finger domain (cys repeats) consists of two clusters with two amino acid sequences CXXCXGXG, where X is any amino acid. Two clusters coordinate two zinc ions (Martinez-Yamout et al., 2000). This domain is implicated in substrate binding and assists in interaction with Hsp70. Proteins from this group have similar structure to the classical *E.coli* DnaJ. Type 2 proteins have a J-domain and G/F--rich region but do not have a zinc-finger domain. Proteins from the type 3 group have a J-domain located anywhere in the protein (Cheetham and Caplan, 1998). Type 1 and 2 can bind to non-native substrates and are considered to have quite similar

functions and activity, while type 3 members are not binding to non-native proteins and therefore cannot function as chaperones on their own (Kelley, 1998). There is also evidence that the zinc finger domain can interact with non-native substrates. In addition to the described regions, Hsp40 can have additional domains, which may determine functional diversity of DnaJ group of proteins. For example, the C-terminal region of DnaJ is essential for dimerization and chaperone activity (Shi et al., 2005).

Like their Hsp70 partners, Hsp40 family members are also found in different compartments. There are 6 Hsp40 members in *Escherichia coli*, 22 in *S. cerevisiae* and about 41 in humans (Qiu et al., 2006). Moreover, according to the Human Genome Resource 140 genes are annotated in humans as DnaJ-related. DnaJ-related proteins could have structures similar to normal members of this family but lack the HPD motif. Therefore, they probably interact with Hsp70 but do not stimulate its ATP hydrolysis. The number of Hsp40 family members is growing with increasing complexity of the organism. Higher eukaryotes have more Hsp40 because it is believed that they could provide broad substrate specificity for the conserved Hsp70 family members (Cheetham and Caplan, 1998). Hsp40s bind to different substrates according to their specificity and deliver them to Hsp70 or they target Hsp70 to various locations in the cell (Kampinga and Craig, 2010). For example human has only 11 Hsp70s and 13 NEFs but 41 Hsp40 proteins.

Yeast have 22 Hsp40 family members located in different compartments. The classification of yeast Hsp40 members with localization of these proteins is described in Table 1:

Table 1. Hsp40 members in yeast *Saccharomyces cerevisiae* (Gong et al., 2009**;** SGD, *http://www.yeastgenome.org).*

	Class	Localization	Function
Ydj1	Type 1	Cytosol	Protein folding, regulation of Hsp90 and Hsp70 functions, involved in protein translocation across membranes
Xdj1	Type 1	Mitochondria	Mitochondrial analog of Ydj1p
Apj1	Type 1	Mitochondria, cytosol?	Overexpression interferes with propagation of [PSI+] prion
Mdj1	Type 1	Mitochondria	Cochaperone, stimulating ATPase activity of Ssc1p (mitochondrial Hsp70), folding and refolding of mitochondrial matrix
Scj1	Type 1	ER lumen	With Hsp70 Kar2 mediating maturation of proteins

		Cytosol,	Cochaperone for cytosolic Hsp70, increased in response to
Sis1	Type 2	Nucleus	DNA replication stress
Djp1	Type 2	Cytosol	Peroxisomal protein import and assembly
Caj1	Type 2	Nucleus	Binds to non-native substrates for presentation to Ssa3, has a function for protein translocation, assembly and disassembly
Hlj1	Type 2	Anchored to ER membrane	Cooperates with Ydj1 and promotes ER-associated protein degradation of integral membrane substrates
Zuo1	Type 3	Cytosol	Ribosome associated chaperone, functions in ribosome biogenesis together with Ssz1 and Ssb1/2
Swa2	Type 3	Cytosol	Auxillin-like protein involved in vesicular transport, clathrin - binding protein required for uncoating of clathrin-coated vesicles
Jjj1-3	Type 3	Cytosol	Cochaperone that stimulates ATPase activity of Ssa1p in a late step of ribosome biogenesis
Cwc23	Type 3	Cytosol?	Component of complex Cef1p, involved in pre-mRNA splicing
Mdj2	Type 3	Associated with mitochondria	Constituent of mitochondrial import motor associated with presequence translocase, stimulates ATPase activity of Ssc1p to drive mitochondrial import
Pam18	Type 3	Associated with mitochondria	Constituent of mitochondrial import motor (PAM complex), stimulate ATP activity of Ssc1p to drive mitochondrial import
Jac1	Type 3	Mitochondria	Specialized J-protein that functions with Hsp70 in Fe-S cluster biogenesis in mitochondria, involved in iron metabolism
Jid1	Type 3	ER membrane?	Probable Hsp40 cochaperone, involved in ER degradation of misfolded proteins
Jem1	Type 3	ER membrane	Nuclear membrane fusion during mating, has genetic interactions with Kar2
Sec63	Type 3	ER membrane	Essential subunit of Sec63 complex, with other components forms a channel competent for signal recognition particle(SRP) dependent and SRP independent protein targeting and import in the ER
Erj5	Type 3	ER lumen	Important for folding capacity preservation in the ER

2.4   The Hsp40 Sis1

Sis1 is a type 2 Hsp70 cochaperone. This protein is essential and it plays an important role in protein aggregation prevention and proteasomal degradation of misfolded proteins. Sis1 is delivering misfolded proteins to Hsp70 (Lee et al., 2002). Sis1 is also essential for initiation of translation (Zhong and Arndt, 1993). It interacts with Ssa1 and Ssa2 proteins on translating ribosomes (Horton et al., 2001). At a non-permissive temperature, a strain with *sis1*ts mutation rapidly accumulates 80S ribosomes and has a decreased amount of polysomes. Sis1 was also shown to associate with 40S ribosomes and probably mediates the dissociation of 80S ribosomes (Zhong and Arndt, 1993). Sis1 is widely distributed in the cell and could be found both in cytosol and nucleus. However, it is ~3-fold more concentrated in the nucleus. Sis1 could interact with Ssa1 in yeast instead of Ydj1, however overexpression of Ydj1 cannot substitute for Sis1 deletion (Luke et al., 1991).

Sis1 consists of J-, G- and C-terminal domains, the latter mediating substrate binding (Fan et al., 2004). The experiments of crystallization of C-terminal domain of Sis1 have demonstrated that several patches of hydrophobic side chains are required for substrate binding (Sha et al., 2000). The conserved J-domain contains the HPD loop and mediates interaction with Hsp70. The G-domain is an extended glycine-rich region of 104 residues, composed of a region rich in phenylalanine residues (G/F) followed by region rich in methionine residues (G/M). This domain plays an important role in yeast prion maintenance of [RNQ+]. Single alterations in amino acid sequence in this region result in loss of prion maintenance (Lopez et al., 2003). Moreover, the G-domain mediates substrate selectivity. A fusion construct of the J-domain of Ydj1 with the G-domain of Sis1 can replace Sis1 for growth but a chimera containing the J-domain of Sis1 and the G-region of Ydj1 could not rescue the Δ*sis1* lethality (Yan and Craig, 1999). Substrate binding is mediated by hydrophobic residues in the C-terminal domain (Stirling et al., 2003).

Although Sis1 and Ydj1 are structurally similar, they have different functions. Ydj1 is a type 1 Hsp40 while Sis1 belongs to type 2. Both proteins form homodimers via a C-terminal dimerization domain (Figure 3). Interestingly, the structural difference between the proteins relates to only one region. Ydj1 has zinc fingers following G/F domain, while Sis1 has glycine/methionine-rich region (Fan et al., 2004; Kampinga and Craig, 2010). As an example, Sis1 promotes elongation of yeast prion and supports maintenance of

[RNQ+] status of the cell while Ydj1 antagonizes the maintenance of this prion. It was shown that these specificities were determined by the G/F domain of Sis1 (Yan and Craig, 1999; Lopez et al., 2003).
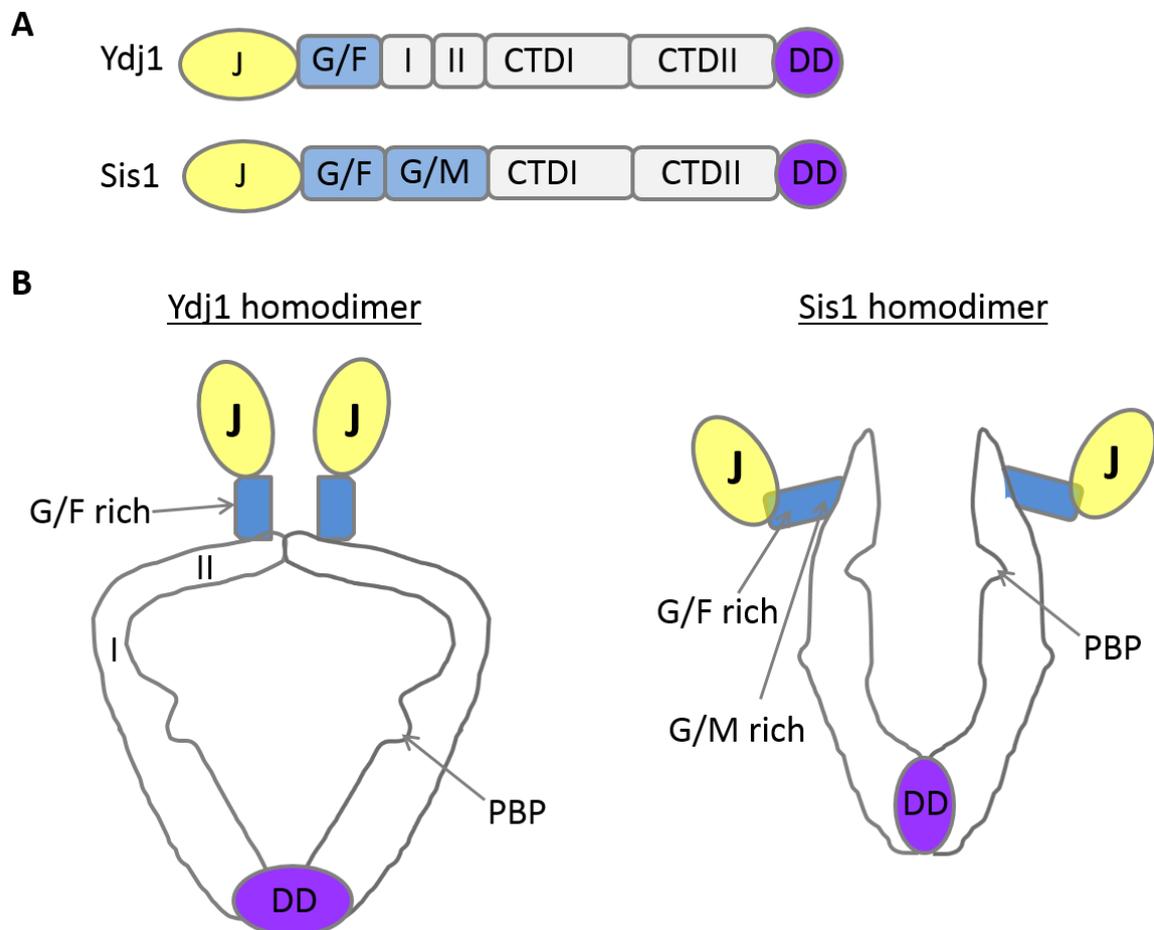
Figure 3. Ydj1 and Sis1 structure compared (adopted with modifications from Summers et al., 2009).

Ydj1 consists of Zinc fingers (denoted as I and II), Glycine/Phenylalanine rich region (G/F), C-terminal domain (CTD) and DD (dimerization domain). Sis1 contains glycine/methionine G/M domain which has essential functions (Luke et al., 1991). Both proteins have polypeptide binding pockets (PBP) for association with unfolded polypeptides. Adapted with modifications from Summers et al., 2009.

The closest Sis1 homologue in human is Dnajb1. The main function of this protein is interaction with Hsp70 and stimulation of ATPase activity of this protein and it could stimulate association between Hsc70 and Hip (Ohtsuka, 1993). Dnajb1 is a stress-inducible protein. Under normal conditions, it is expressed at low levels and diffusely distributed in the cell. If cells are stressed with heat shock it translocates rapidly from the cytoplasm to the nucleus (Hattori et al., 1992).

In the mammalians, Hsp70-Hsp40 chaperone cycle is more complex and has some unique features. Hsp70 reaction cycle is regulated by J-domain proteins and nucleotide exchange factors (NEFs). Different combination of J-domain proteins with NEFs could adapt cycling rates to various substrates. Hip attenuates Hsp70 cycle by stabilizing Hsp70-ADP-substrate state, therefore increasing the substrate "holdase" activity of Hsp70 (Höhfeld et al., 1995). Hip attenuates cycle by binding to the Hsp70 site which is mutually exclusive with NEFs binding site. Extended residence of the substrate on Hsp70 may prevent aggregation or promote transfer to degradation machinery or to Hsp90(Li et al., 2013).

2.5   Yeast prions

Prions are infections misfolded proteins which are capable of self-replicating. They cause neurodegenerative diseases in mammals (for example Creutzfeldt - Jakob disease), while in *S. cerevisiae* prions are epigenetic elements. Prions are transmitted via non-Mendelian protein only interaction (Wickner, 1994). There are at least seven confirmed prion proteins in *S. cerevisiae:* Sup35, Rnq1, Ure2, Swi1, Mot3, Cyc8 and Mod5. Importantly, most of the yeast prions are based on glutamine or asparagine-rich sequences (except HET-s and Mod5). Therefore, the data observed for the yeast prions could be partially applied to huntingtin polyQ model in yeast.

The Sup35 protein of *S. cerevisiae* yeast is a homologue of the polypeptide chain release factor 3 (eRF3) of higher eukaryotes (Paushkin et al., 1996). Sup35 has glutamine and asparagine rich N-terminal region that causes its aggregation. It could form a [PSI+] prion phenotype in yeast *S. cerevisiae.* [PSI+] strain is auxotrophic for adenine due to a nonsense mutation (Patino et al., 1996). In fact, [PSI+] phenotype is the result of self-propagation of misfolded form of Sup35 protein. In the yeast cell with [PSI+] phenotype, misfolded Sup35 protein forms amyloid-like aggregates (Tuite et al., 2008).

Interestingly, Ssa1 plays a role in prion propagation in yeast. Ssa1 overexpression could cure [PSI+] and [URE3] prion phenotype (Schwimmer and Masison, 2002; Mathur et al., 2009). Some prion types could be cured not only by Ssa but even by Ssb overexpression (Kushnirov et al., 2000). Conversely, Ssa family members overexpression promotes prion formation and suppresses the ability of Hsp104 to cure the prion phenotype, suggesting a

complex interplay between chaperones (Allen et al., 2005). Influence of different chaperones on [PSI+] propagation were reviewed by Sweeny and Shorter, 2008.

De novo formation of the yeast [PSI+] requires the presence of another yeast prion, [PIN+]. Prions in [PIN+] strain might act as "seeds" for the polymerization of [PSI+] and other prions (Sharma and Liebman, 2013). [PIN+] formed by abnormal version Rnq1 protein, which is forming amyloid arranged in the parallel beta sheets structures (Wickner et al., 2008). [PIN+] phenotype is not required for [PSI+] maintenance (Sondheimer and Lindquist, 2000).

2.6   Huntington's disease and polyglutamine aggregation

In 1872, George Huntington published a paper in the *Medical and Surgical Reporter of Philadelphia*. This paper described a hereditary disease that results in chorea, henceforth referred to as Huntington's disease (HD). HD has autosomal dominant inheritance (Walker, 2007).This disorder usually has an onset in the late 30s-40s of the affected individual. Huntington's disease is characterized by progressive neuronal dysfunction and neuronal loss and it leads to death 10-20 years after onset (Hardy and Orr, 2006).HD is associated with neuronal cell death occurring in a selective way mostly in the cortex and striatum (Vonsattel et al., 1985).

HD is caused by a protein called huntingtin, which contains a polymorphic polyglutamine (polyQ) tract. Heritable expansion of this polyQ tract is causally linked with the disease. The expression of normal and mutant forms of huntingtin was observed in the central nervous system at similar levels and also in peripheral tissues (Trottier et al., 1995). In the brain, huntingtin is expressed mostly in the cell bodies, dendrites, and nerve terminals of neurons. Huntingtin was described using immunohistochemical and electron microscopy method as a cytosolic protein. Moreover, it was shown that it is associated with vesicles and/or microtubules and therefore may play a part in cytoskeletal fixing or vesicular transport (DiFiglia et al., 1995;Gutekunst et al., 1995;Sharp et al., 1995). Huntingtin was also found in the nucleus (Hoogeveen et al., 1993;De Rooij et al., 1996), but its functions in the nucleus remain unknown.

HD is caused by expansion of the polyQ tract in huntingtin. Glutamine is encoded by CAG repeats in the respective gene and there is a number of diseases that are caused by a CAG expansion in the genome occurring during replication. All these diseases cause

progressive neuronal degeneration and include: dentatorubral pallidoluysian atrophy (DRPLA), spinobulbar muscular atrophy (SBMA, or Kennedy's disease), spinocerebellar ataxias (SCA1, SCA2, SCA3/MJD, SCA6, SCA7 and SCA17) and HD (Kanazawa, 1999; Kennedy et al., 1968; Mutsuddi and Rebay, 2005; Lebre and Brice, 2003). For all of these diseases certain threshold length of the polyQ stretch must be reached for disease manifestation. Moreover, the longer the polyQ-expanded tract, the earlier the age of onset (Duyao et al., 1993).

HD is the most common among all the polyQ expansion diseases. The CAG repeat expansion results in an increased number of glutamines in the N-terminal part of the protein. If polyQ stretch is shorter than 35 glutamines, it does not cause the disease. However if the number of the repeats is greater than 36 glutamines, HD manifestation will occur. The polyQ expansion strongly increases the propensity of the protein to form cytotoxic aggregates. There have been cases reported of HD patients with 240 glutamines, however normally such long polyQ tracts cause death during embryonic development (Nance et al., 1999). The CAG expansion mechanism appears to be unique to the human genome. PolyQ tracts are often not conserved in other mammals and appear not to have a necessary function (Hardy and Orr, 2006).

It is practically very hard to overexpress whole huntingtin in yeast, because the full protein has 3144 amino acids, is encoded in over 67 exons and the predicted mass of the protein is around 350 kDa. It was shown, that expression of exon 1 huntingtin (67 amino acids long plus variable length for polyQ tract) is sufficient to cause HD pathology(Singer et al., 2010).

Interestingly, there is substantial variability in age of onset and lifespan for individuals with the same length of polyQ repeat. The exact reasons for these differences are not known, but it is conceivable that protein quality control plays a role. In any case, the late age of onset of the disease suggests that cellular control systems can cope with the expanded polyQ protein for decades, until eventually the resistance mechanism become insufficient, presumably as a result of aging.

The toxicity of the expanded polyQ tract is attributed to a gain of function that correlates with the ability of the protein to form fibrillar, amyloid-like aggregates. Poly-L-glutamine forms sheets of β-strands through hydrogen bonds between their main chain and side chain amides, so-called polar zippers (Perutz et al., 1994).

According to a widely held view, polyQ toxicity is caused by aberrant interactions of the mutant protein with key cellular factors, resulting in transcriptional dysregulation and interference with the function of the ubiquitin-proteasome system (UPS)(Gerber et al., 1994; Bence et al., 2001; Faux et al., 2005; Bennett et al., 2005).

The latter effect may be attributed to the sequestration by the polyQ aggregates of molecular chaperones or factors of the ubiquitin-proteasome system (Ciechanover and Brundin, 2003; Sakahira et al., 2002). The polyQ aggregate inclusions were demonstrated to be ubiquitin-positive. They may engage proteasomes but resist degradation, leading to proteasome inhibition (Bennett et al., 2007; Pandey et al., 2007). It was also shown that polyglutamine proteins can alter nuclear and cytoplasmic proteins (Harjes and Wanker, 2003; Li and Li, 2004).

Another possible mechanism of toxicity is damage to membrane structures through formation of ion-permeable pores (Hirakura et al., 2000; Monoi et al., 2000; Trushina and McMurray, 2007). These mechanisms can also cause mitochondrial damage that may provoke ATP deficits, Ca2+ release, depletion of antioxidants and overproduction of reactive forms of oxygen (reviewed in Trushina and McMurray, 2007). One more mechanism that appears to explain polyQ toxic effect is the physical block of axonal and dendritic transport that can affect the soma structure and, in turn, result in cell death (Piccioni et al., 2002). Observing these mechanisms, we can conclude that all of them may contribute to neuronal dysfunction in neurodegenerative diseases.

Brains of the people affected by HD have small neuronal inclusions. These inclusions contain huntingtin as well as chaperones, parts of proteasome machinery and other factors. These inclusions are amyloid-like and mainly consist of huntingtin protein (Figure 4). Remarkably, aggregates of huntingtin are very stable and cannot be dissolved in SDS. In general, "amyloid fibrils" *in vitro* are termed "intracellular inclusions" *in vivo* and can be detected with the Congo red dye (Westermark et al., 2005;Sipe and Cohen, 2000). Strikingly, the precursor proteins differ substantially in structure, but the associated fibrils originated from these proteins have very similar properties and appearance (Sunde and Blake, 1997;Tycko, 2004). Within the cell, the inclusions are usually found in neuronal

nuclei and in the peri-nuclear space. The regions harboring these inclusions belong to the mid-frontal gyrus, mid-temporal gyrus, caudate nucleus, amygdaloid nucleus and globus pallidus (McGowan et al., 2000).

While the inclusions were initially considered harmful, more recent studies suggest that soluble precursors of the inclusions (oligomers) may be the major toxic species(Arrasate et al., 2004;Behrends et al., 2006) (Figure 4). The sequestration of soluble oligomers into insoluble inclusions may even be protective by reducing the exposed surface available for aberrant interactions (Leitman et al., 2013). Moreover, chaperones seems to play an important role is shifting toxic soluble oligomers to fibrillar aggregates (Hipp et al., 2014).
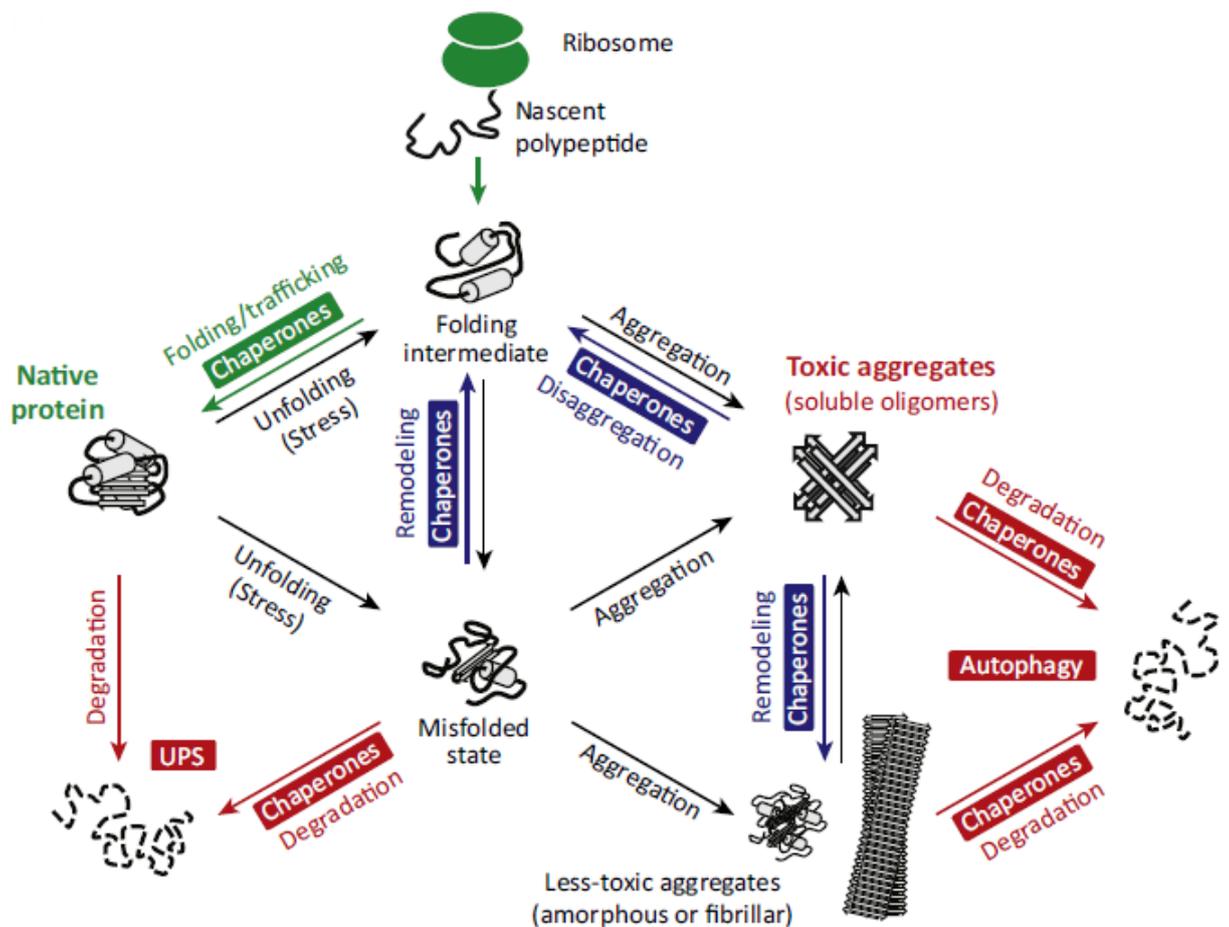
Figure 4. Protein misfolding, degradation and homeostasis(Hipp et al., 2014).

Protein homeostasis is achieved by controlling the levels of functional proteins and preventing the formation of toxic aggregates. Proteins involved in protein biogenesis labelled green, in conformational maintenance - blue, in degradation by UPS or autophagy – red. Toxic aggregates (mainly diffusible, oligomeric states) may be converted to less toxic, insoluble inclusions of amorphous or fibrillar (amyloid-like) structure.

It is very important to understand the cause of toxicity for Huntington's and other neurodegenerative diseases because this will allow the development of effective therapeutic strategies.

2.7   Ubiquitin proteasome system in protein quality control.

The accumulation of misfolded proteins is a significant threat to cellular health. Cells rely on molecular chaperones to hold (in order to prevent aggregation) and to refold misfolded proteins (Hartl and Hayer-Hartl, 2002). If a protein cannot be refolded, it is targeted for degradation via the UPS. Generally, the ability of a cell to refold or to destroy misfolded proteins is known as quality control.

The UPS is the most important pathway to degrade misfolded and incorrectly assembled proteins. Proteins that are degraded via the proteasome are generally labelled by covalent attachment of polyubiquitin (poly-Ub) chains to the lysine of target protein. The poly-Ub chain is recognized by the 26S proteasome (Wolf and Hilt, 2004; Hershko and Ciechanover, 1998). Canonical signal for protein degradation is poly-Ub chain linked at the 48th lysine residue (Komander and Rape, 2012). If this chain connected via lysine 63, it has different functions. In this case it regulates different processes in the cell: inflammation, endocytic trafficking, translation and DNA repair (Miranda and Sorkin, 2007). Poly-Ub could be formed via other lysine residues (Lys6, lys11, Lys27, Lys29, or Lys33) of ubiquitin; however, their role is poorly understood.

Ubiquitin is a regulatory protein with molecular weight 8.5 kDa which is found in all eukaryotic organisms (Goldstein et al., 1975). This protein is highly conserved and almost invariant in yeast and humans (96% sequence identity). Ubiquitin is a highly stable protein with a compact β-fold structure and a flexible C-terminal tail (Vijay-Kumar et al., 1987). Most of its core residues are not flexible; however, β1/β2 loop with Leu8 is flexible. This flexibility is important for recognition of ubiquitin-binding proteins, since binding to them leads to conformational change (Lange et al., 2008). All lysine residues, which are used for chain assembly are exposed at the surface of the ubiquitin molecule. Lys6 and Lys11 are located in the flexible region of the protein, which is binding to ubiquitin-

binding domains of different proteins. Lys27 is located inside the molecule. Poly-Ub association with it leads to the structural changes in the protein structure. Lys48 and Lys63 association does not lead to significant changes in the ubiquitin structure (Komander and Rape, 2012).

A cascade of enzymes carries out the process of attachment of ubiquitin to the proteasome. Enzymes activate free ubiquitin and label the target protein with it (Figure 5). These enzymes are E1, E2 and E3. E1 is an ubiquitin activating enzyme, which activates and transfers ubiquitin to the carrier protein E2. E2 is an ubiquitin-conjugating enzyme, which needs another interacting partner in order to label the protein. E3 is an ubiquitin ligase and it is a partner of E2. E3 recognizes a protein that needs to be degraded and labels it with ubiquitin. Ubiquitination is repeated several times, which creates a poly-Ub chain that targets proteins for degradation or plays a part in many other processes in the cell (Wilkinson, 1999;Pickart, 2001). There is only one E1 protein, however there are approximately 20 E2 and hundreds of E3 ligases (Pickart, 2001). This ratio allows control of degradation and other processes where ubiquitin is involved very precisely.
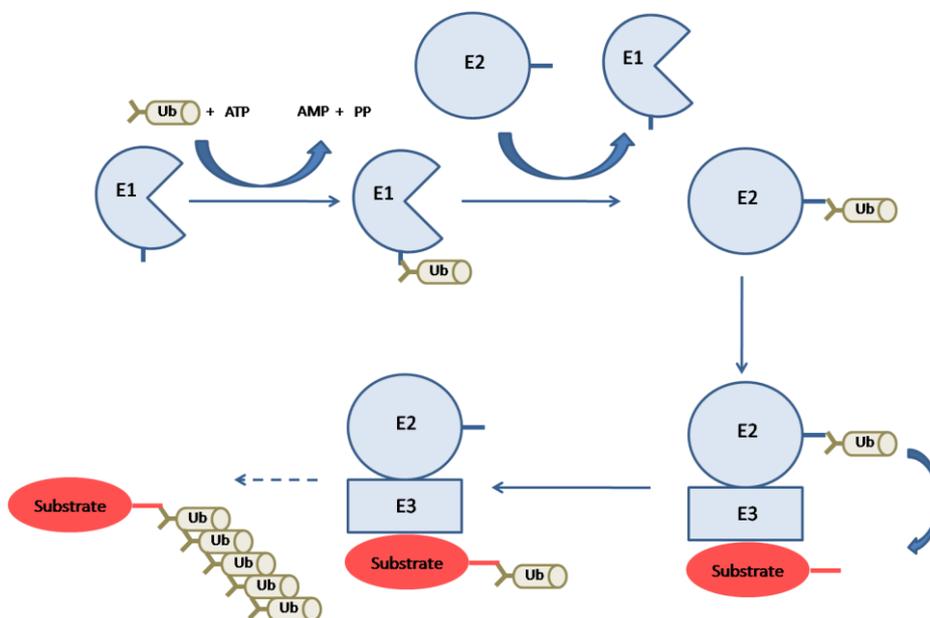
Figure 5. Ubiquitination of substrate protein.
The main steps of protein ubiquitination are described:
1. Ubiquitin activating enzyme (E1) adenylates an ubiquitin molecule and transfers it to the active site with cystein residue. One ATP is hydrolyzed.
2. Adenylated ubiquitin transferred to ubiquitin conjugated enzyme (E2).
3. Ubiquitin ligase (E3) recognizes the target protein and ubiquintinates it with assistance of E2 protein. It transfers poly-Ub chain from ubiquitin to the conjugated enzyme. Target protein should have a chain of at least four ubiquitins to be recognized by proteasome(Thrower et al., 2000). However for some proteins monoubiquitination is enough to be degraded (Sun et al., 2011).

After the protein has been labeled by poly-Ub chains with Lys48 connections it is recognized by the 26S proteasome. This structure is found in the nucleus and in the cytosol in eukaryotes and archaea and it is responsible for degradation of most proteins (Peters et al., 1994). It is a very abundant and complex structure, constituting approximately 1-2% of total cell mass (Voges et al., 1999). In the proteasome, proteins are linearized and poly-Ub chain is removed. The linearized protein is injected into the central core of the proteasome where it is digested to short peptides of about seven to eight amino acids length. Peptides are degraded to amino acids by peptidases.

26S proteasome is a very large protein with molecular weight of 2000kDa, which consists of a 20S core particle and two regulatory 19S particles on both ends of the core structure. 20S core particle have three different proteolytic activities and degradation occurs in an ATP-dependent manner (Kisselev et al., 2002). The core particle is responsible for degradation of the target protein. 19S particles recognize ubiquitinated proteins via ubiquitin binding sites, de-ubiquitinate them and deliver them into catalytic core.

Degradation of misfolded proteins happens in different compartments in the cell. The ER has its own protein quality control system. Misfolded proteins in the ER are degraded via ER-associated protein degradation (ERAD) (Lippincott-Schwartz et al., 1988). Misfolded proteins are recognized, translocated back to the cytosol, ubiquitinated and subsequently degraded via the proteasome. In addition, some folded and active proteins are also degraded via ERAD. For example, 3-hydroxy-3-methylglutary1-acetylcoenzyme-A reductase (HMGR) a pivotal enzyme in sterol synthesis is degraded as ERAD substrate (Gil et al., 1985;Varga et al., 2004;Song et al., 2005).

Newly-synthesized proteins enter the ER in an unfolded state via a narrow Sec61 translocon channel (Rapoport, 2007). Polypeptide chain emerges into the ER and immediately starts to fold. Some of these proteins might be modified by glycosylation and disulfide bond formation. (Braakman and Hebert, 2013). Some proteins fold spontaneously and do not require special factors for this process. Other proteins need special assistance in this process. There are many factors enhancing folding in the ER lumen, for example Hsp70 and Hsp90 chaperones. Another important enzyme is protein disulfide isomerase (PDI), which oxidizes pairs of cysteine and creates chemical bonds

between them. PDI usually oxidizes and reduce cysteine bonds in few cycles, which allows a protein to attain the native conformation. Secretory proteins in the ER also get modifications by oligosaccharides. There are few enzymes involved in this process like calnexin, calreticulin and lectins. Protein modification by sugars makes them more hydrophilic (Aebi et al., 2010).

Despite the presence of chaperones, a fraction of proteins fail to acquire native conformation (Hartl and Hayer-Hartl, 2009). ERAD has multiple branches with different specificity for different topology of misfolded proteins (Taxis et al., 2003; Bernasconi et al., 2010; Christianson et al., 2012). Despite this diversity, ERAD substrates undergo similar steps on their way to the degradation in the proteasome (Figure 6). These steps include recognition of substrate in the ER, retrotranslocation of the substrate back to the cytosol, ubiquitination, extraction from the membrane in ATP-dependent manner and degradation by the proteasome. These steps are regulated by E3 ligases. Activity of these proteins specified by RING domain, which mediates the interaction with E2 protein. E3 facilitates the direct transfer of ubiquitin from E2 to lysine residue of the substrate. There are two main ERAD E3 ligase complexes in yeast – Hrd1 and Doa10 (Bays et al., 2001; Swanson et al., 2001).
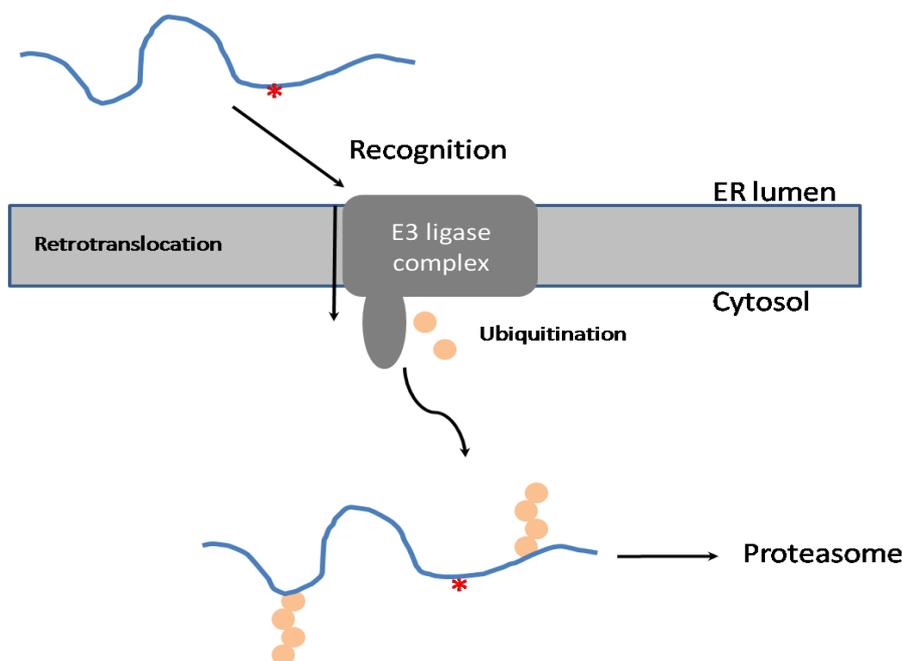
Figure 6. Steps required for degradation of all types of ERAD substrates.

A generic misfolded (red star) ER lumenal substrate is a subject for ERAD. E3 ligase complex coordinate substrate recognition, retrotranslocation and ubiquitination. Ubiquitin is illustrated as a small brown circles. With modifications from Ruggiano et al., 2014.

Recognition of the misfolded proteins in the ER is tightly regulated, because ineffective detection results in their accumulation and affects the cell (Jonikas et al., 2009). Misfolded or wrongly assembled proteins expose hydrophobic regions, may have unpaired cysteine residues and possibly could have abnormal sugar modifications. These abnormalities are recognized by different enzymes, such as lumenal Hsp70 and Hsp40 members, calnexin, and calreticulin and protein disulphide isomerases. These proteins cooperate with E3 ligase complexes, which have a major role in mediating ERAD substrate specificity. Recognition of lumenal substrates requires Hrd3, Kar2 and for glycosylated proteins – Yos9 lectin (Plemper et al., 1997; Szathmary et al., 2005; Carvalho et al., 2006). Der1 membrane protein might be also involved in substrate recognition (Stanley et al., 2011). Some ERAD substrates with membrane domain could be directly recognized by E3 ligase Hrd1 (Sato et al., 2009).

Incorrectly folded glycoproteins are recognized and degraded by ERAD. Typically, newly synthesized proteins enter the ER lumen and are modified at asparagine residues with glycan moieties. This moiety is a well-defined structure that consists of 3 glucoses, 9 mannoses and 2 N-acetylglucosamine residues and is referred to as Glc3-Man9-GlcNAc2 (Braakman and Hebert, 2013). Glc3-Man9-GlcNAc2 is N-linked to asparagine residues and can be modified by several enzymes. Glycosidases and other early processing enzymes modify the glycan moiety and increase the binding affinity of glycoproteins towards lectins, which assist in the folding of glycoproteins. Late processing enzymes, such as Htm1 mannosidase, trigger the binding of different types of lectins that guide proteins to ERAD (Quan et al., 2008;Clerc et al., 2009). Through this process, newly synthetized proteins have time to acquire their native conformation and traffic away from the ER. Conversely, glycoproteins that remain in the ER for a long period of time likely encounter folding problems. These incorrectly folded proteins are labeled by Htm1 with α 1,6-linked mannose, which is recognized by Yos9, a lectin that is involved in ERAD recognition (Quan et al., 2008; Clerc et al., 2009). Interestingly, the simultaneous recognition of specific N-linked glycans by Yos9 and an unstructured polypeptide motif by HRD3 is required for ERAD-mediated degradation of these incorrectly folded substrates (Denic et al., 2006;Xie et al., 2009).

Proteins containing lumenal, cytoplasmic and membrane-spanning domains are degraded via ERAD-L, ERAD-C and ERAD-M, respectively (Denic et al., 2006;Vashist and Ng, 2004; Huyer et al., 2004). However, these pathways have not been clearly identified in

mammals (Ballar et al., 2011). For substrates that reside in the ER membrane, ubiquitination occurs prior to or simultaneously with translocation. ERAD-C substrates are regulated by the Doa10 E3 ligase protein complex, while ERAD-L and ERAD-M substrates are regulated by the Hrd1 E3 ligase protein complex. The composition of these complexes is depicted in Figure 7.

The Hrd1 complex is responsible for the degradation of lumenal misfolded proteins (ERAD-L). These substrates are ubiquitinated in cooperation with the E2 ubiquitin-conjugating enzymes Ubc1 and Ubc1-Cue1. E3 ligases accept an ubiquitin (Ub) molecule from their cognate E2 ligase and transfer the ubiquitin molecule to the substrate thereby promoting substrate degradation. ERAD-M substrates are also processed by the Hrd1 E3 ligase complex; however, fewer components are required to mediate ERAD-M substrate degradation through this mechanism (Bordallo et al., 1998; Gardner et al., 2000; Gauss et al., 2006). The Doa10 complex mediates the degradation of substrates containing misfolded cytosolic domains. ERAD-C substrates are ubiquitinated by the Doa10 ubiquitin ligase in cooperation with the E2 Ub-ligases Ubc6 and Ubc7-Cue1 (Ravid et al., 2006; Carvalho et al., 2006). Interestingly, despite differences in their recognition and in the complexes required for ubiquitination, ubiquitinated substrates in the late stages of ERAD-mediated degradation are extracted by the same Ufd-Npl4-CDC48/p97 AAA+ ATPase complex resulting in their delivery to the proteasome (Bays et al., 2001b; Rabinovich et al., 2002).

In mammalian cells, many E3 ligases exist, such as Trc8, Rfp2, Rnf170 and Rma1/Rnf5, but most mammalian E3 ligases are poorly characterized. The best-studied E3 ligases are Hrd1 and Gp78. Hrd1 and Gp78 are homologs of yeast Hrd1 but can target different types of substrates for degradation (Schulze et al., 2005;Christianson et al., 2012;Burr et al., 2013).
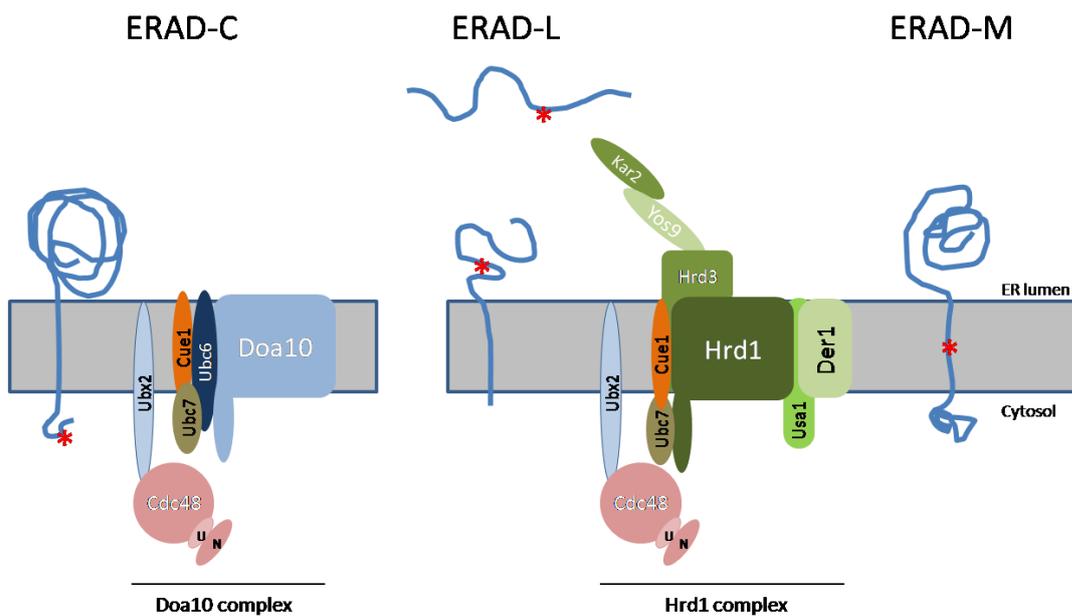
Figure 7. ERAD-C, ERAD-L and ERAD-M pathways for the degradation of misfolded proteins.

The Doa10 and Hrd1 complexes involved in ERAD-mediated protein degradation in *S. cerevisiae* and their substrate specificities. ERAD-C substrates, which contain a misfolded domain in the cytoplasm, are degraded with the assistance of the Doa10 complex. ERAD-L substrates, which consist of proteins containing a lumenal misfolded domain, are degraded via the Hrd1 complex. ERAD-M substrates, which contain other misfolded domains, are also degraded via the Hrd1 complex. U and N denote the Cdc48 cofactors Ufd1 and Npl4. Misfolded domains within proteins are marked by a red star. Reproduced with modifications from Ruggiano et al., 2014.

After a misfolded protein is recognized by ERAD, the protein is retrotranslocated to the cytoplasm. For lumenal proteins, the entire polypeptide is transported across the ER membrane. Membrane proteins are partially retrotranslocated and subsequently extracted from the ER membrane. Retrotranslocation occurs via Sec61 or possibly via a different protein. Many studies have shown that Sec61 plays a part not only in translocation but also in retrotranslocation; however, this observation has yet to be confirmed with additional studies (Wiertz et al., 1996; Schmitz et al., 2000; Pilon et al., 1997). Moreover, some of the proteins that aberrantly engage Sec61 on their way to the ER can become substrates of the Hrd1 ligase, which could explain the interactions reportedly observed between ERAD and Sec61 (Rubenstein et al., 2012). Therefore, Sec61 interaction with proteins undergoing retrotranslocation could represent an artifact of the ER protein translocation system. However, even if Sec61 is involved in retrotranslocation, whether two distinct families of proteins function as translocons and retrotranslocons remains unclear. Alternatively, Sec61has different functions depending on the protein with which it interacts.

E3 ligase complexes contain many multispanning membrane proteins and thus represent good candidates for retrotranslocons. E3 ligases themselves could conduct retrotranslocation (Ye et al., 2001;Horn et al., 2009;Mehnert et al., 2014). For example, overexpression of the E3 ligase Hrd1 results in the degradation of lumenal ER substrates in the absence of Der1, Usa1 and Hrd3 (Carvalho et al., 2010). Other proteins, such as Der1, are crucial for the degradation of many lumenal ERAD substrates (Carvalho et al., 2006; Wahlman et al., 2007).

Target proteins are usually ubiquitinated during retrotranslocation on the cytoplasmic side of the ER. Moreover, ubiquitination may assist in protein retrotranslocation (Nakatsukasa et al., 2008;Richly et al., 2005). Ubiquitination allows proteins to be recognized by the Cdc48/p97 ATPase complex. Cdc48 plays a role in the retrotranslocation of target proteins. Cdc48 is an AAA+ ATPase that acts to extract proteins in an ATP-dependent manner. Moreover, Cdc48 can distinguish between polyubiquitinated and non-polyubiquitinated proteins and can assist with the delivery of proteins to the 19S regulatory subunit of the proteasome (Jentsch and Rumpf, 2007). Cdc48/p97 is also associated with de-ubiquitinating enzymes (DUBs), which remove ubiquitin chains prior to proteolysis by the proteasome (Rumpf and Jentsch, 2006;Jentsch and Rumpf, 2007).

After the proteins are retrotranslocated and extracted from the membrane (if necessary), they are maintained in a soluble form and are transferred to the proteasome by chaperones such as the BAG6 complex (Claessen and Ploegh, 2011;Wang et al., 2011). In addition, Dsk2 and Rad23, both of which are shuttle factors, can bind ubiquitinated proteins and deliver them to the proteasome and can also deliver ERAD substrates to the proteolytic core (Medicherla et al., 2004).

3 Materials and Methods

3.1 Materials

3.1.1 Instruments

Amersham Pharmacia Biotech: electrophoresis power supply EPS;

Beckman Coulter: Avanti 30 Centrifuge;

Beckman Coulter: Avanti J-25I ultracentrifuge;

Beckman Coulter: GS GR Centrifuge;

Beckman: DU 640 UV/VIS spectrophotometer;

Biometra: T3 PCR- Thermocycler

Bio-Rad: electrophoresis chambers MiniProtean 2 and 3;

Bio-Rad: Mini Trans-Blot cell (liquid blotting);

Eppendorf: Centrifuge 5424 and 5415R;

Eppendorf: Pipets (2, 10, 20, 100, 200, 1000 µl);

Eppendorf: Thermomixer Comfort;

Fisher Scientific: pH meter Accumet Basic;

Fujifilm: Image Reader LAS 3000;

Hoefer Scientific Instruments (San Francisco, USA): SemiPhore blotting transfer unit;

Mettler Toledo: balances AG285, PB602;

Millipore: deionization system MilliQ plus PF;

NanoDrop Technologies Inc.: NanoDrop-1000 Spectrophotometer;

New Brunswick Scientific: orbital shaker and incubator Innova 4430;

Zeiss: Microscope Axiovert 200M;

3.1.2 Chemicals

Quality of chemicals was Pro Analysi (p.a.) and mostly reagents were supplied by Sigma-Aldrich.

Amersham Pharmacia Biotech: ECL+ Detection Kit;

BD Bioscience: Doxycycline;

BioRad: Protein Assay Kit;

Calbiochem: TWEEN-20;

DIFCO: Bacto agar, Bacto peptone, Bacto tryptone, Bacto yeast extract, Yeast nitrogen base w/o amino acids;

Fermentas: PageRuler Prestained Protein Ladder Plus, GeneRuler 1 kb and 100bp DNA Ladder;

Fluka: DMSO;

Life Technologies: SYBR Safe - DNA Gel Stain;

Merck: Benzonase, EDTA, 2-Mercaptoethanol;

Molecular Probes: DAPI;

New England Biolabs: restriction endonucleases, prestained protein marker broad range, T4 DNA Ligase, CIP;

Pierce: Coomassie protein assay reagent;

Promega: Wizard Plus SV Minipreps, PureYield Plasmid Midiprep system, Wizard SV gel and PCR clean-up system salt;

Qiagen: QIAquick PCR purification and gel extraction kits;

Roche: Complete Protease inhibitor, DTT, ampicillin;

Schleicher & Schuell: Protran (nitrocellulose transfer membrane), nitrocellulose acetate membrane filter;

Seikagaku: Zymolyase-20T;

Serva: Acrylamide-Bis solution 30% (37:5:1), Coomassie, Serva BlueR, PEG-4000, PMSF, Citifluor;

Stratagene: PfuTurbo DNA Polymerase II, Yeast Carrier DNA;

3.1.3 Buffers

10X TBS

For 1L	For 10L	Final concentration
87.66 NaCl	876.6g NaCl	150 mM NaCl
12.11g Tris	121.1g Tris	20 mM Tris
~4ml HCl	~40ml HCl	
adjust pH to 8.0	adjust pH to 8.0	

1X TBS

100 ml of 10X TBS and 900ml of ddH$_2$O

1X TBST

For 1L
100ml 10X TBS
0.5ml 100% Tween (final 0.05% v/v)
899.5ml ddH$_2$O

Blocking buffer

5% skim milk in TBST

Antibody buffer

0.5% skim milk in TBST

TAE

For 1L 50X solution	Final concentration

242g Tris Base	40mM Tris Base
57.1 ml of Glacial Acetic Acid	20mM Acetate Acid
100ml 0.5M EDTA	1mM EDTA
Fill H$_2$0 up to 1l	

1.5M Tris HCl, pH = 8.8

For 1L	Final concentration
181.65g Tris base	1.5M Tris HCl
800 ddH20	
Adjust pH with 37%HCl	
Fill H$_2$0 up to 1l	

1.0M Tris HCl, pH = 6.8

For 0.5L	Final concentration
78.8 g of Tris-HCl	1.0M Tris HCl
400 ddH20	
Adjust pH with 37%HCl to 6.8	
Fill H$_2$0 up to 0.5l	

4X SDS-PAGE sample loading buffer

For 7.5 ml	4X	Final concentration 1X
1.5 mL of 1 M Tris-HCl pH 6.8	200 mM Tris-HCl pH 6.8	50 mM Tris-HCl pH 6.8
3 mL of 1 M DTT	0.4M DTT	0.1M DTT
0.6 g of SDS	8% SDS	2% SDS
0.05 g of bromphenol blue	0.08 % bromphenol blue	0.02 % bromphenol blue
2.4 mL of glycerol	32% glycerol	8% glycerol
Fill H$_2$0 up to 7.5ml		

4M and 8M UREA sample buffer

For 40ml 4M UREA	For 40ml 8M UREA	Final concentration
8ml 1M Tris/HCl pH=6.8	8ml 1M Tris/HCl pH=6.8	200mM
9.6g UREA	19.2g	4M or 8M

2g SDS	2g SDS	5% SDS
8µ 0.5 EDTA	8µ 0.5 EDTA	0.1mm EDTA
0.05g	0.05g	0.075mM Bromphenol blue
0.6 DTT	0.6 DTT	1.5% DTT

4M and 8M Urea sample buffers were aliquoted in 1.5ml eppendorf tubes and stored in -20°C.

WB stripping buffer

For 40ml	Final concentration
8ml 10% SDS	2% SDS
5ml 1M pH6.8 Tris-HCl	0.125M pH6.8 Tris-HCl
+243µl β-me	6mM β-me
26.7 ddH$_2$O	

SDS running buffer

For 10l of 10X SDS-PAGE Running Buffer	For 1l of 10X SDS-PAGE Running Buffer	Final concentration 1X
303 g Trisbase	30.3 g Trisbase	25 mM Tris
1440 g glycine	144.0 g glycine	192 mM glycine
100 g SDS	10.0 g SDS	0.1% SDS
Fill H$_2$O to 10l	Fill H$_2$O to 1l	

Transfer buffer

For 10l of 1X Transfer Buffer	Final concentration 1X
29g Glycine	0.0387M
58g Tris	0.0479M
3.7g SDS	0.00128M
2l MetOH	4.95mol/L
Fill H$_2$O to 10l	

Cycloheximide solution

Cycloheximide solution was used in concentration 10mg per 1 ml of H$_2$O. This solution was always prepared freshly.

Glass beads lysis buffer

Final concentration 1X
25 mM Tris/HCl pH7.5
50 mM KCl
5% Glycerol
10 mM MgCl$_2$
1 mM EDTA
1 mM PMSF
1X protease inhibitor cocktail (Roche)

Stocks in -20°C

DTT (1 M)

5 g of DTT (FW 154.25) were resolved in 32.5ml of 10 mM NaAc with pH = 5.2. Solution was filtered with 0.22 µm filter (Millipore). Aliquots of 0.5ml were made and stored in -20°C freezer.

PMSF (100 mM)

3.48g of PMSF (FW 174) was dissolved in 200ml of isopropanol and was stored in -20°C freezer.

1000X Ampicillin

5g of ampicillin was dissolved in 50ml of ddH20 and was filtered through 0.22 µm filter (Millipore). Sterile solution was aliquoted in 1.5 ml eppendorf tubes and was stored in -20°C freezer.

1000X Kanamycin

1.25g of Kanamycin was dissolved in 50ml of ddH20 and was filtered through 0.22 µm filter (Millipore). Sterile solution was aliquoted in 1.5 ml eppendorf tubes and was stored in -20°C freezer.

3.1.4 Cultivation media

YPD

2% peptone (Difco)
1% yeast extract (Difco)
2% glucose
(+ 2-3% agar for solid medium)

2X CM

For preparing 3.1 l of synthetic media:

12.4 g drop out mix without amino acids

41.5g nitrogen base

pH should be adjusted to 5.6

Final CM - is diluted 2XCM with 2% glucose or 2% Galactose/Raffinose

Drop out mix

L-alanine, l-arginine, l-asparagine, l-aspartic acid, l-cystein, l-glutamine, l-glutamic acid, l-glycine, l-methionine, l-isoleucine, l-phenylalanine, l-proline, l-serine, l-threonine, l-tyrosine, l-valine, myo-Inositol – 2g.

PABA (4-Aminobenzoic acid) 0.2 g

LB

For 1l
Bacto-tryptone 10g
Bacto-yeast extract 5g
10g NaCl
Adjust PH to 7.0

Resulting mixture was sterilized by autoclave. For solid LB, 2% of agar was added.

SOB

For 1l
Bacto-tryptone 20g
Bacto-yeast extract 5g
NaCl 0.5g
10ml of 250mM KCl
Adjust PH to 7.0

Resulting mixture was sterilized by autoclave.

3.1.5 Yeast and *E. coli* strains used in this work

Escherichia coli strains:

Strain	Genotype	Reference
DH5αF′	*F'/endA1 hsdR17(rK-mK+) supE44 thi-1 recA1 gyrA (Na1r) relA1 D(lacZYA-argF)$_{U169}$(m80lacZDM15)*	Novagene
SURE	*e14- (McrA-) D(mcrCB-hsdSMR-mrr)171 endA1 supE44 thi-1 gyrA96 relA1 lac recB*	Novagene

S. cerevisiae strains

YPH499	*MATa ura3-52 lys2-801 ade2-101 trp1Δ63 his3Δ200 leu2Δ1*	Sikorski and Hieter, 1989
YPH499	*MATa ura3-52 lys2-801 ade2-101 trp1Δ63 his3Δ200 leu2Δ1*[pin-]	This study

		Park et al., 2013
YPK010	*MATa ura3-52 lys2-801 ade2-101 trp1-Δ63 his3-Δ200 Leu2::His6-Ub*	
R1158	*MATa his3-1 leu2-0 met15-0l URA::CMV-tTA*	Open Biosystem
Tet-Off SIS1	*MATa his3-1 leu2-0 met15-0l URA::CMV-tTA pSIS1::KanR-TetO7-TATA*	Open Biosystem
BY4741	*MATa his3Δ1 leu2Δ0 met15Δ0 ura3Δ0*	EUROSCARF
Δpdr5	*BY4741 Δpdr5::Kan-R*	EUROSCARF
crm^{1-1ts}	*BY4741 MATa his3Δ1 leu2Δ0 met15Δ0 ura3Δ0 crm1-1ts*	EUROSCARF

3.1.6 Plasmids

Plasmid	Description	Reference
CG* (p413GAL-ΔssCPY*-GFP)	CPY*-GFP without signal sequence under *GAL1* promoter (*CEN6, HIS3*)	Park et al., 2013
NLS-CG* (p413GAL-NLS-ΔssCPY*-GFP)	CPY*-GFP without signal sequence but with N-terminus nuclear localization sequence under *GAL1* promoter (*CEN6, HIS3*)	This study
NES-CG* (p413GAL-NES-ΔssCPY*-GFP)	CPY*-GFP without signal sequence but with nuclear export sequence under *GAL1* promoter (*CEN6, HIS3*)	This study
p16 (pRS413ADH-ΔssCPY*-GFP)	CPY*-GFP without signal sequence under *ADH1* promoter expressed on a centromere plasmid (*CEN6, HIS3*)	Park et al., 2007
p17 (pRS423ADH-ΔssCPY*-GFP)	CPY*-GFP without signal sequence under *ADH1* promoter expressed on a multicopy plasmid (2μ, *HIS3*)	Park et al., 2007
CTG* (pRS413-CPY*-TM-GFP)	CPY*-TM-GFP under *GPD* promoter expressed on a centromere plasmid (*CEN6, HIS3*)	This study
CPY*-HA (pRS413-CPY*-HA)	CPY* under *GPD* promoter expressed on a centromere plasmid (*CEN6, HIS3*)	This study
Ub-GFP (p415GAL-Ub^{G76V}-GFP)	Ubiquitin conjugated with GFP under *GAL1* promoter, centromere plasmid (*CEN6, LEU2*)	Park et al., 2013
His$_6$-Ub (YIplac128ADH-His$_6$-Ub)	His6 tagged Ub expressed under *ADH1* promoter	Kalocsay et al., 2009
20Q (pYES2-myc-20Q)	Yeast plasmid expressing fragment of first exon of huntingtin with 20Q tract (2μ, *URA3*)	Park et al., 2013
96Q (pYES2-myc-96Q)	Yeast plasmid expressing fragment of first exon of huntingtin with 96Q tract (2μ, *URA3*)	Park et al., 2013

20QmCh (pYES2-myc-20QmCh)	Yeast plasmid expressing fragment of first exon of huntingtin with 20Q tract with C-terminus mcherry fluorescent protein (2µ, *URA3*)	Park et al., 2013
96QmCh (pYES2-myc-96QmCh)	Yeast plasmid expressing fragment of first exon of huntingtin with 96Q tract with C-terminus mcherry fluorescent protein (2µ, *URA3*)	Park et al., 2013
20QcODC (pYES2-myc-20QcODC)	Yeast plasmid expressing fragment of first exon of huntingtin with 20Q tract with C-terminus cODC degron (2µ, *URA3*)	Park et al., 2013
96QcODC (pYES2-myc-96QcODC)	Yeast plasmid expressing fragment of first exon of huntingtin with96Q tract with C-terminus cODC degron (2µ, *URA3*)	Park et al., 2013
20QcODC* (pYES2-myc-20QcODC_C441A)	Yeast plasmid expressing fragment of first exon of huntingtin with 20Q tract with C-terminus cODC degron mutation (2µ, *URA3*)	Park et al., 2013
96QcODC* (pYES2-myc-96QcODC_C441A)	Yeast plasmid expressing fragment of first exon of huntingtin with 96Q tract with C-terminus cODC degron mutation (2µ, *URA3*)	Park et al., 2013
pUBR1 (pRS425ADH-Flag-UBR1)	Yeast plasmid expressing Ubr1 (2µ, *LEU2*)	Du et al., 2002
pSSA1 (pESC-LEU-SSA1)	Yeast plasmid expressing Ssa1 under *GAL1* promoter (2µ, *LEU2*)	Park et al., 2013
pYDJ1 (pESC-LEU-YDJ1)	Yeast plasmid expressing Ydj1 under *GAL1* promoter (2µ, *LEU2*)	Park et al., 2013
pSIS1 (pRS414GPD-SIS1)	Yeast plasmid expressing Sis1 under *GPD* promoter (CEN6, *TRP1*)	Addgene#18687
pHA-SIS1 (p415GAL-HA-SIS1)	Yeast plasmid expressing Sis1 under *GAL1* promoter (*CEN6, LEU2*)	Park et al., 2013
pSIS1_AAA (p415GAL-HA-SIS1_AAA)	Yeast plasmid expressing Sis1 carrying mutations in HPD loop under *GAL1* promoter (*CEN6, LEU2*)	Park et al., 2013
pSIS1_ΔJ (p415GAL-HA-SIS1_ΔJ)	Yeast plasmid expressing Sis1 carrying J domain deletion under *GAL1* promoter (*CEN6, LEU2*)	Park et al., 2013
pNLS-SIS1 (p415GAL-HA-NLS-SIS1)	Yeast plasmid expressing Sis1 with N-terminus nuclear localization sequence under *GAL1* promoter (*CEN6, LEU2*)	Park et al., 2013
pNES-SIS1 (p415GAL-HA-NES-SIS1)	Yeast plasmid expressing Sis1 with N-terminus nuclear export sequence under *GAL1* promoter (*CEN6, LEU2*)	Park et al., 2013
Ssa3-LacZ-Leu	Yeast cytosolic stress reporter plasmid (2µ, *LEU2*) with β-Galactosidase linked to SSA3 promoter	Polier et al., 2008
Ssa3-LacZ-Ura	Yeast cytosolic stress reporter plasmid (2µ, *URA3*) with β-Galactosidase linked to SSA3 promoter	This study, market swap

p415Gal	Yeast expression vector (*CEN6, LEU2*), *GAL1* promoter	Mumberg et al., 2004
p425Gal	Yeast expression vector (2µ, *LEU2*), *GAL1* promoter	Mumberg et al., 2004
p423Gal	Yeast expression vector (2µ, *HIS3*), *GAL1* promoter	Mumberg et al., 2004

3.1.7 Clonning strategy

NLS-CG* (p413GAL-NLS-ΔssCPY*-GFP). The N-terminal tandem SV40 NLS sequence (DPKKKRKVDPKKKRKV) was attached to ΔssCPY*-GFP protein (Fischer-Fantuzzi and Vesco, 1988). P413Gal plasmid was cut with spe1 and hpa1 restriction endonucleases (NEB). P413Gal-ΔssCPY*-GFP plasmid was used as a template for PCR for amplification of ΔssCPY*-GFP. Forward primer for this reaction had sequence AAGTCCACTAGTATGGCTTCTCCTAAGAAGAA ACGTAAAGTTATCTCATTGCAAAGACCGTTGGGT. Reverse primer had sequence CATCACCTTCACCCTCTCCACTGAC. PCR product was cut with spe1 and hpa1. PCR product was separated in 1% agarose gel and isolated from the gel with Wizard® SV Gel and PCR Clean-Up System. Insert and vector were mixed in 2:1 ratio and ligated by T4 ligase overnight at 16°C.

NES-CG* (p413GAL-NES-ΔssCPY*-GFP). Engineered NES sequence (NINELALKFAGLDL) sequence was attached to ΔssCPY*-GFP protein (Guttler et al., 2010). P413Gal plasmid was cut with spe1 and hpa1 restriction endonucleases (NEB). P413Gal-ΔssCPY*-GFP plasmid was used as a template for PCR for amplification of ΔssCPY*-GFP. Forward primer for this reaction had sequence AAGTCCACTAGTATGGCTTCTAACATTAATGAGCTCGCACTTAAGTTCGCCGGTTT AGACCTGATCTCATTGCAAAGACCGTTGGGT. Reverse primer had sequence CATCACCTTCACCCTCTCCACTGAC. PCR product was cut with spe1 and hpa1. PCR product was separated in 1% agarose gel and isolated from the gel with Wizard® SV Gel and PCR Clean-Up System. Insert and vector were mixed in 2:1 ratio and ligated by T4 ligase overnight at 16°C.

CTG* (pRS413-CPY*-TM-GFP). pMA plasmid was cut with Sma1 restriction endonuclease in Tango Y (Fermentas, now Thermo Scientific) and with Swa1 in double tango buffer consequently (Taxis et al., 2003). Vector was cut from the agarose gel and purified from gel (Wizard® SV Gel and PCR Clean-Up System) and ligated with T4 ligase (Neb) overnight at 16°C.

CPY*-HA (pRS413-CPY*-HA). pRS413-CPY*-TM plasmid was cut HindIII and BstE2 and vector was isolated from the agarose gel. pCT42 plasmid was cut with HindIII and BstE2 and insert was isolated from the agarose gel(Taxis et al., 2003). Vector was cut from the agarose gel, purified from gel (Wizard® SV Gel and PCR Clean-Up System) was cut with HindIII and BstE2, the insert was isolated from agarose gel. Insert and vector were mixed in 2:1 ratio and ligated by T4 ligase overnight at 16°C.

3.1.8 Marker swap

YEp-Ssa3-LacZ plasmid contain *URA3* selection marker. To prepare strain for the experiments, YEp-Ssa3-LacZ was transformed in YPH499. Cells containing the plasmid were transformed according to standard protocol with pUL9 (Cross, 1997). Prior the transformation, plasmid was digested with Sma1 (NEB). After the transformation cells were distributed on CM without *LEU2* selection marker. After 4 days in 30°Cincubator, plate replica was done on CM plate without uracil. This plate was incubated for two days at 30°C. Clones which are growing on CM without leucine but not growing on CM without uracil were selected.

3.1.9 Antibodies

First antibodies.

Antibody	Animal	1st dilution	2nd dilution	Reference
CPY	mouse	1/5000	1/1000	Invitrogen
Dsk2	rabbit	1/5000	1/5000	Abcam
FBPase	rabbit	1/5000	1/5000	Gift from D.H. Wolf

GFP	mouse	1/1000	1/1000	Roche
HA	rat	1/1000	1/1000	Roche high affinity
Luciferase	goat	1/2000	1/5000	Promega
Myc	mouse	1/250	1/1000	Santa Cruz
PGK	mouse	1/2000	1/1000	Invitrogen
Rad23	Goat	1/1000	1/5000	Santa Cruz
Sis1	rabbit	1/5000	1/5000	Cosmo Bio Co., Ltd
Ssa1	rabbit	1/10000	1/5000	Gift from E.A. Craig
Sse1 1484	rabbit	1/10000	1/5000	Gift from A. Bracher
Ydj1 1326	rabbit	1/2000	1/5000	Gift from E.A. Craig
Flag	mouse	1/1000	1/1000	Sigma

Secondary antibodies

Secondary antibodies	Host	Reference
anti-mouse-IgG-HRP	goat	Sigma A4416
anti-rabbit-IgG-HRP	goat	Sigma A9169
anti-goat-IgG-HRP	rabbit	Sigma A5420
anti-rat-IgG-HRP	goat	Pierce 31476
anti-rabbit-CY3	goat	Dianova
anti-mouse-CY3	goat	Dianova
anti-rabbit-FITC	goat	Dianova
anti-mouse-FITC	goat	Dianova

3.2   Methods

3.2.1 DNA

Overnight bacterial cultures with the plasmid of interest were grown at 37°C at 240 rpm in LB media. Plasmid preparations were performed with Promegas's Mini-Prep or Midi-Prep Kits according to supplier's instructions.

The concentration was determined by a photometer at 260 nm (Beckman DU640 Spectrophotomer) or with Nanodrop (Thermo scientific). Constructs were verified by DNA sequencing (Sequiserve, Germany or in-house facility).

Restriction and cloning enzymes

The restriction enzymes were purchased from New England Biolabs (NEB). Plasmids, primers and PCR products were digested according to instructions from supplier. T4 ligase was produced in the in-house facility.

3.2.2 Biochemical methods

Agarose gel electrophoresis

1% agarose gel was prepared with 1X TAE buffer. 1/10000 SYBR Safe DNA Gel Stain (Life Technologies) was added to the gel. 6 x Loading Dye Solution (Fermentas) was added to the samples. 1X TAE buffer was added to the tank and was run at 110V for 20-45 minutes, depending on the size of the products. The *Gene Ruler 1 kb-DNA-Ladder* (Fermentas) was used as size marker. The DNA in the gel was visualized using UV light. Isolation form the gel (if needed) was performed with Wizard SV Gel and PCR Clean-Up System.

Polymerase chain reaction (PCR)

Polymerase chain reaction was performed in a Thermocycler (Biometra) according to a standard protocol with minor changes or modifications. Annealing temperature or extension time varied according to primer composition and template length. Taq-polymerase (Promega) or Pfu- polymerase (Promega) were used. Typical PCR running conditions shown below:

DNA template - final concentration 25 ng – 50a ng
Primer - 20 pm
dNTPs - 1 mM
Polymerase buffer 1 x
Polymerase 2.5 to 5 U
Final volume 25µl or 50 µl

Typical PCR cycle profile:
94°C 4 minutes

94°C 1 minute
55°C 1 minute
72°C 2 minutes
=> 30-35 cycles

72°C 10 minutes

PCR product was purified with Wizard SV Gel and PCR Clean-Up System.

DNA ligation

DNA Vector and DNA insert were cut with proper restrictive endonucleases. They have been isolated form the gel with Wizard SV Gel and PCR Clean-Up System and mixed at a ratio of 1:7 with total volume of 15µl with addition of ligase buffer. 0.4 µl of T4-DNA ligase (100U) was added. Ligation mixture was incubated in ligase buffer at 16°C overnight and transformed into chemically competent cells.

SDS-PAGE

SDS-PAGE was performed according to original paper in mini-Protean 3 system (BioRad) (Laemmli, 1970). Electrophoresis chambers were supplied by BioRad. Polyacrylamide gels were prepared according to the following protocol:

Chemicals	Separating gel			Stacking gel
	8%	10%	12%	5%
H20	23.2 ml	19.8 ml	16.5 ml	6.8 ml
30% Acrylamide/ 0.8%	13.3 ml	16.7 ml	20 ml	1.7 ml
1.5M Tris-HCl pH8.8	12.5 ml	12.5 ml	12.5 ml	
1 M Tris-HCL pH6.8				1.25 ml
10% SDS	0.5 ml	0.5 ml	0.5 ml	1.7 ml
10% freshly prepared APS	0.5 ml	0.5 ml	0.5 ml	0.1 ml
TEMED	0.03 ml	0.02 ml	0.02 ml	0.01 ml
Total Volume	*50 ml*	*50 ml*	*50 ml*	*10 ml*

4M or 8M UREA loading buffer (4M or 8M urea, 5% SDS, 200 mM Tris-HCl [pH 6.8], 1 mM EDTA 0.1% bromphenol blue, 1.5% 2-mercaptoethanol) was added to protein samples. 95°C. Samples were centrifuged before loading. Gel electrophoresis was carried out at a voltage 120V when samples are in the stacking gel and 200V when they are in separating gel.

Prestained Protein Marker (Fermentas) used as a molecular weight marker.

Western Blotting and immunodetection

After SDS-PAGE, proteins in the polyacrylamide gels were transferred to nitrocellulose membranes (Protran, GE Healthcare) in a liquid western blotting unit (GE Healthcare) at a constant current of 300mA for 45 minutes. Nitrocellulose membranes were blocked with TBST with 5% skim milk for 10 minutes. Membranes were incubated with primary antibody (1-3 hours), washed and incubated with secondary antibody (1 hour). Washed 3 times with TBSt and developed with ECL (Millipore luminata solution). Exposure was done on the Image Reader LAS 3000 (Fujifilm).

Western blot membrane stripping and reproving with different antibodies

For removal of primary and secondary antibodies membrane was incubated in stripping buffer at 55°C for 5-10 minutes with mild shaking. After that, membrane was extensively washed with distilled H_2O and 5 times with PBS solution on the shaker.

Stripping buffer composition:

For preparation of 100 ml:

20 ml SDS 10%
12.5 ml 0.5M Tris HCl pH 6.8
67.5 ml ultra-pure water
Add 0.8 ml ß-mercaptoethanol (under the fume hood)
Fill the volume with H_2O

Filter retardation assay

Glass beads lysis was performed but samples were not mixed with sample buffer. Instead, 0.5µl benzonase (40U, Merck) was added per 100µl of supernatant. These samples were incubated 1hr at 4°C. Equal amount of 4% SDS / 100mM DTT was added to benzonase treated lysates. Probes were incubated in 96°Cfor 5 minutes. These samples were loaded on a cellulose acetate membrane (Schleicher&Schuell). Membrane had been soaked in 0.1% SDS for 10 minutes. Slot blot machine (Hoefer) was washed with 0.1% SDS solution 3 times. Serial dilutions of samples were loaded in a slot blot machine. Membrane with

SDS insoluble aggregates was blocked with 5% milk solution in TBST and immunodetection of the signal was performed (Scherzinger at al. 1997).

Trichloroacetic acid (TCA)-precipitation

TCA precipitation was performed to concentrate protein samples. Protein samples were mixed at 1:1 ratio with a 20% TCA. Solution was incubated for 10 minutes on ice and centrifuged at 20,000 g for 15 minutes at 4°C. Pellets were washed with 1 ml of acetone (preincubated at -20°C) three times. Pellets were dried and stored or used for SDS-PAGE. For SDS-PAGE, UREA buffer (8 M urea, 5% SDS, 200 mM Tris-HCl [pH 6.8], 1 mM EDTA 0.1% bromphenol blue, 1.5% 2-mercaptoethanol) was added to the pellet. Pellet was vortexed for 30 seconds and heated with UREA buffer if required.

Immunoprecipitation

Glass beads lysis was performed and yeast cell lysate was obtained. Lysates were cleared by fast speed centrifugation at 20,000g for 10 minutes at 4°C. Supernatant fractions containing 2 mg of protein incubated with 50 µl of anti-myc MicroBeads (Miltenyi Biotech) for 2 hours at 4°C. Part of the supernatant was taken as an input control for the experiment. Beads were washed 4 times with lysis buffer; bound proteins were analyzed by immunoblotting.

SILAC labelling.

Stable isotope labeling by amino acids in cell culture (SILAC) is a mass spectrometry based quantitative proteomics. In our work, we used it to identify interactors of the certain protein. Yeast cells were grown over night in CM with glucose without uracil and histidine. CM contained 100mg/l heavy L-lysine-$^{13}C_6$, $^{15}N_2$ (Heavy) or with 100mg/l unlabeled L-Lysine (Light)(Ong and Mann, 2006). PolyQ and CG* were co-expressed in CM with 2% raffinose and 2% galactose instead of glucose. OD of the cells should be 0.8. Yeast cells were lysed by glass beads with lysis buffer composition: (25 mM Tris-HCl [pH 7.5], 50 mM KCl, 10 mM MgCl2, 1 mM EDTA, 5% glycerol, 0.5% Triton X-100, complete protease inhibitors [Roche]). Cell lysates were cleared by centrifugation at high speed: 10 minutes at 20,000g at 4°C. Myc tagged proteins were immunoprecipitated for 2 hours at

4°C with anti-myc Microbeads (Miltenyi Biotech). After 3 washes with lysis buffer bound proteins were eluted with UREA buffer (8M urea, 5% SDS, 200 mM Tris-HCl [pH 6.8], 1 mM EDTA 0.1% bromphenol blue, 1.5% 2-mercaptoethanol)). Heavy and light eluates were mixed with 1 to 1 ratio and followed by SDS-PAGE, in-gel digestion and with LC-MS.

Liquid chromatography-tandem mass spectrometry (LC-MS/MS)

After SDS-PAGE and in-gel digestion, peptides were eluted from OMIX tips with 50 µl of 80% acetonitrile/0.1% TFA. Elution was dried in a vacuum centrifuge at 35°C and resuspended in 6 µl 0.1% formic acid (FA). Lysate fractions and solutions were also digested and directly suspended in 6 µl of 0.5µl/min in 0.1% FA onto a 15 cm long capillary column with 75 µm inner diameter with a pre-pulled capillary tip (New Objective) with Reprosil-Pur 1.9 µm C18 material (Dr. Maisch). Peptides were eluted at 0.3 µl/min with a 120 min gradient (pull-down eluate), or a 220 min gradient (lysate fractionation of samples) from 2 to 80 % acetonitrile, in 0.1 % FA. Peptides were directly injected into a Thermo LTQ-FT Ultra using a nano-electrospray ion source (Proxeon) with electrospray voltages ranging from 1.5 to 2.5 kV. FT scans from m/z 330-1700 were taken at 100,000 resolution for LTQ-FT Ultra, followed by collision induced dissociation (CID) scans in the LTQ of the 8 or 10 most intense ions with signal greater 2000 counts, and charge state larger than one. Dynamic exclusion of parent masses already fragmented was enabled. CID settings were as follows: isolation width 1, normalized collision energy 35 V, activation Q 0.250, and activation time 30 ms.

Determination of SILAC Ratios

Mass spectrometry data was analyzed with MaxQuant 1.0.13.13 software (Cox and Mann, 2008). Program was used with parameters: Quant; SILAC Triplets, Medium Labels: Lys4, Heavy Labels: Lys8. Maximum labeled amino acids: 3. Variable modifications: Oxidation (M), Acetyl (Protein N-terminus). Fixed modifications: Carbamidomethyl (C). Database used for analysis: Yeast translated orf from *Saccharomyces* Genome Database (www.yeastgenome.org), published in 2012. Enzyme: LysC/P. MS/MS tolerance: 0.5 Da. Maximum missed cleavages: 2. Top MS/MS peaks/100 Da: 6. Mascot version 2.2 (Matrix Sciences, www.matrixsciences.com) was used to generate search results for MaxQuant. Identify; Peptide FDR: 0.01. Protein FDR: 0.01. Maximum PEP: 1. Minimum unique peptides: 1. Minimum peptide length: 6. Minimum peptides: 1. Protein Quantitation

based on Razor and Unique peptides. Minimum Ratio count: 2. 'Re-quantify' and 'Keep low-scoring versions of identified peptides' were both enabled. Normalized or non-normalized ratios were used as specified below for every experimental set-up.

Determination of 96Q Interactions

SILAC was performed with swapped labeling: 96QmCh/CG* (H) versus 20QmCh/CG* (L) or 96QmCh/CG* (L) versus 20QmCh/CG* (H). 96Q interactors have been selected if they have been enriched in at least 2 experiments out of 3 by at least 2 fold in the pull down of 96QmCh over 20QmCh. All experiments were done independently. Correction of protein concentration was done (which could happen due to 96Q expression), normalized H/L and L/H ratios measured for the proteins in pull downs were corrected for significant differences in protein abundance in the respective protein lysates (Significance B calculated by MaxQuant < 0.05).

3.2.3 Preparation of competent *E.coli* cells

One colony from LB-plate was incubated in 3 ml LB medium overnight. Culture was incubated in 50 ml LB with initial OD600 = 0.05. Culture was grown for 2-3 hours at 30°C until OD600 reached 0.45-0.5. Cells were transferred on Ice and resuspended in sterile TfB I. Cells were pelleted at 4,000 g and resuspended in TfB II. 50-100 µl were frozen in liquid nitrogen. Chemically competent cells were stored at -80°C.

TfB1	Chemical	Concentration
3.0g	RbCl	100 mM
2.48g	MnCl2 X 4H2O	50 mM
7.5 mL	1M Kac pH 7.5	30mM
0.38g	CaCl2 X 2H2O	10mM
37.5g	Glycerin	15%
Add 250mL	ddH2O	

TfB2	Chemical	Concentration
0.3g	RbCl	10 mM
5.0 mL	0.5M MOPS, pH 6.8	10 mM
2.75g	CaCl2 X 2H2O	75 mM
37.5g	Glycerin	15%

Add 250 mL	ddH2O	

Transformation

Competent cells were thawed on ice for 7 minutes. Cells were mixed with 0.5-1 µl plasmid DNA or 5-10 µl of ligation mixture. Samples were incubated for 30 minutes on ice and shocked with heat at 42°C for 70 seconds and immediately transferred on ice. 1 ml of LB was added to the cells and incubated at 37°C for 1-2 hours. Afterwards cells were pelleted and transferred on LB plates with antibiotics.

3.2.4 Yeast

Alkaline lysis of yeast.

Yeast culture was collected after 15-18 hours of incubation in a selective galactose/raffinose containing CM media. 3 OD of the cells was used per sample and washed with ice-cold water. Then 1 ml of water was added to each sample. Probes vortexed for 15 seconds and 150µl of lysis buffer added per to cells. Resulting solution was vortexed 3 times and incubated on ice for 20 minutes. Lysis buffer consist of 925 µl 2M NaOH and 75 β-Me. After the incubation 150µl of 50% TCA (trichloroacetic acid) was added and vortexed. Samples were left on ice for 15-30 minutes. As a next step, lysates were centrifuged on maximum speed for 10 minutes (20,000g) and supernatant was discarded. Pellets were washed with ice-cold acetone and sedimented by centrifugation with maximum speed for 5 minutes. Supernatant was again discarded. 100 µl of 8M UREA sample buffer (8M UREA; 5% SDS; 0.1 mM EDTA; 0.075mM bromphenol blue; 1.5 DTT) was added. Probes were shaken in Eppendorf Thermomixer Comfort at 1200 rpm for 15 minutes at 37°C. As a last step of preparation of lysate – it was incubated at 96°Cfor 5 minutes and sample sedimented by centrifugation for 3 minutes at maximum speed. 10-15 µl of extract was taken per well of the gel for SDS-PAGE.

Glass beads lysis of yeast.

Yeast culture was collected after 15-18 hours of incubation in a selective galactose/raffinose containing CM media. Starting OD for the culture was 0.1-0.2OD/ml and total volume 50ml. Approximately 10-20OD was collected and was pelleted at 2000rpm. 400µl of 1X lysis buffer was added to the sample and equal amount of glass beads. Probes were vortexed 2 times for 1minute. As a next step, samples were centrifuged 2,000rpm for 5minutes at 4°C. Supernatants were transferred in a new tube and protein concentration was measured by Bradford assay (Bio Rad). Concentration in the samples was adjusted with lysis buffer according to respective protein levels. Lysates were mixed with 1/5 amount of 5X sample buffer. The same amount of protein loaded per well for SDS-PAGE.

1X lysis buffer composition: 25mM Tris-Cl pH 7.5; 50mM KCl; 10mM $MgCl_2$; 1mM EDTA; 5% glycerol; 1mM DTT and 1 mM PMSF (added freshly); 1x protease inhibitor cocktail (from 25X stock: 1 tablet of protease inhibitor from Roche/2mLH_2O, freshly made)

Depending on the experiment, +1% of Triton X-100 could be added for dissolving membranes.

Cycloheximide chase.

After 15-18 hours of incubation of yeast cultures in a selective galactose/raffinose SC cells were collected in a 50ml falcon tube (cells were in the middle of log phase). Supernatant was discarded and 2ml of glucose CM media was added. Pelleted cells were redistributed in a media by pipetting or vortexing. 100µlof cycloheximide solution (10mg /ml) was added. Probes were incubated at 30°Cin the incubator. 500µl of the cells were collected per sample. Eppendorf tubes for sample collection had contained 500µl of 0.03M sodium azide (NaN_3). Collected samples were pelleted by maximum speed centrifugation for 30 sec and were frozen in liquid nitrogen. Samples were stored in -80°C.

Time points for the samples collection depended on the level of expression of the protein. Typical time points used in this work were 0h, 1h, 2h, 3h; 0, 45 min, 90 min, 135 min; 0, 40 min, 80min, 120min.

Drop test

Cells were diluted in a 96 well plate. Cells were diluted in water or in respective CM without sugars in 1:6 or 1:10 ratios. Starting OD600 for dilutions were 0.1 OD. After dilutions are done 96 well replicator (created in core facility of MPI) used for making a plate replicas by dipping it in the wells and by pressing it on the selective plate with or without induction. Cells were grown in the incubator at indicated temperature (30°C if not stated otherwise).

Yeast transformation

Yeast cells were grown overnight and 0.5ml of culture was spun down in a centrifuge for 10 sec, 10, 000g. Supernatant was discarded and 10µl of carrier DNA was added plus 1µl of DNA for transformation. Solution was vortexed well. 0.5ml of PLATE solution was added. Mixture was vortexed 2 times for 20 sec. 57 µl DMSO was added and transformation mixture was vortexed briefly. Solution was incubated at 30°C for 30 minutes. Heat shock was done for 15 minutes at 42°C. Cells were pelleted at 6,000 g for 30 seconds. Most of the supernatant was removed and the rest was used to spread cells on the selective CM plates.

Plate solution: 40% PEG 3350

                      0.1 M Lithium acetate

                      10mM Tris/HCl pH 7.5

                      1 mM EDTA

Fluorescence microscopy

10 ml of yeast culture was fixed by addition of 1.2 ml formaldehyde addition and 1 ml of 1M potassium phosphate (pH 6.5). Mixture was incubated at room temperature for 1 hour. 1 ml of ice-cold SP buffer (composition?) was added and cells were sedimented at 4°C at 800 g. Cells were again resuspended in ice cold SP buffer and washed with it 5 times. Later cells were resuspended in 900 µl of SPβ buffer (composition) and 100µl of zymolyase (100T) solution (6 mg/ml) was added. Cells were incubated for 0.5-1 hour at 30°C and were incubated 5 minutes on ice. Generated spheroplasts were washed 5 times

as described before and were resuspended in 150µl of cold SP buffer. Polylysine covered slides were prepared (20 µl of 0.5mg/ml polylysine solution per well) with 15 minutes incubation. Wells were washed 5 times with buffer. 20µl of spheroplasts were applied per well followed by an incubation for 10 minutes at room temperature. The spheroplasts were washed with PBS. The slides were immersed in ice cold methanol for 3 minutes and ice cold acetone for 30 sec. Slides were dried on air, 20 µl of PBST/4%BSA was added to each well for 50 minutes of incubation at room temperature. The wells were washed twice with PBST and 20 µl of primary antibody were added. Slides were incubated in the wet chamber for 1 hour and washes 5 times with PBST. Secondary antibodies were applied and procedure was repeated as before. Slides were air-dried and later DAPI mounting medium (1µg/ml) (or its analogs) was added for the nuclear staining. Slides were covered by coverslips and sealed by nail polish on its sides. Microscopy observation was done with Zeiss Axiovert 200M.

Live cell fluorescence imaging

Hoechst 33342 or DAPI stains were used for nuclear staining of the yeast cells. Fluorescence imaging of live yeast cells was performed using a Zeiss Axiovert 200M inverted microscope. Program for image analysis AxioVision 4.7.1 or ImageJ with additional extended scripts for working with .zvi files.

B-Galactosidase assay

Original protocol for β Galactosidase assay was used with some modifications (Guarente, 1983). Cells were grown overnight and diluted at the morning to 0.01 OD. Cells were grown up to 0.5OD, centrifuged and supernatant was discarded. Pellet was resuspended in 1 ml of Z buffer. 3 drops of chloroform and 2 drops of 0.1% SDS were added. Mixture was vortexed and preincubated at 28°C for 5 minutes. 0.2ml of ONPG was added (4mg/ml). After the color develops 0.5 ml of Na_2CO_3 solution was added. OD was measured at 420 nm after removal of cell debris (measurements were done against blank which did not contain any cells but all previous steps were applied).

Z buffer:

Chemical	Concentration
$Na_2HPO_4\ 7H_2O$	60mM

NaH$_2$PO$_4$ 1H$_2$O   40mM

KCL   10mM

MgSO$_4$ ·7H$_2$O   1mM

dH$_2$0 till the final volume

pH 7, stored at 4°C

Before using 50mM of 2-Mercaptoethanol was added.

ONPG (o -nitrophenyl- β -D-galactoside) stock solution:

4 mg/ml in Z buffer. Stored at –20°C.

Na$_2$CO$_3$ stock solution used - 1M in H$_2$O

3.3   Contribution of other people to this work

Results presented in this work were done in parts in a collaboration with Sae-Hun Park and Tao-Tao Chen. These results were published (Park et al., 2013).

3.4   Aim of the study

PolyQ interference with protein quality control in the cell has been a subject of considerable debate (Díaz-Hernández et al., 2006;Ortega et al., 2010;Juenemann et al., 2013). Recent studies revealed that polyQ expansion proteins impair the normal function of the UPS and diminish the proteolytic activity of the proteasome(Michalik and Van Broeckhoven, 2004; Wang et al., 2008; Maynard et al., 2009). In contrast, other studies demonstrated no significant reduction in proteolytic activity in the presence of polyQ expansion proteins(Jana et al., 2001; Seo et al., 2004; Seo et al., 2007). Moreover, polyQ proteins did not have an effect on purified proteasomes; however, polyQ proteins indirectly interfered with the ubiquitin proteasome system (Bennett et al., 2005; Hipp et al., 2012). Therefore, whether polyQ expansion proteins inhibit the UPS remains unclear. If they actually inhibit the UPS, what is the mechanism underlying polyQ-dependent interference with protein quality control?

The first goal of the present study was to systematically analyze whether pathogenically expanded polyQ proteins affect proteasome function and protein quality control in the cell. Well-studied eukaryotic, terminally misfolded proteins based on CPY* were used as the model proteins for UPS activity in this study (Taxis et al., 2003). Degradation of these proteins by the proteasome was monitored using a cycloheximide chase assay. To accomplish the goal of this study, we examined the fate of the terminally misfolded proteins in the presence of the first exon of the huntingtin protein. Moreover, we observed whether quality control interference differed in various compartments of the cell. We determined whether the proteasome function changed in the presence of polyQ-expanded protein. We also addressed whether polyQ expression altered the ubiquitination of misfolded proteins.

To address the mechanism of polyQ protein affecting protein quality control in the cell, we performed proteomic analyses by SILAC. These experiments were expected to provide us with quantitative data and a list of interactors with the polyQ-expanded proteins. Some of the proteins identified would be involved in the mechanism through which polyQ interferes with the protein quality control system in the cell. Using SILAC we anticipated to obtain sufficient data to unravel the mechanism through which polyQ affects the ubiquitin proteasome system and protein quality control.

The second goal of this study was to study the exact mechanism of polyQ interference with the terminally misfolded protein CG*. We hoped to overcome the negative effects of polyQ

expression by overexpression of polyQ-interacting proteins. Understanding the exact mechanism of polyQ interference should provide insight into how polyQ expression affects protein quality control and how the normal degradation of misfolded proteins in presence of polyQ can be restored.

4   Results

4.1   General approach and model proteins

Proteins are only marginally stable and are at risk of misfolding and aggregating. Cells have evolved extensive protein quality control machinery, in particular molecular chaperones, to maintain proteostasis and to prevent the accumulation of potentially toxic aggregate protein species. Failure of these protective systems is associated with degenerative diseases such as Alzheimer's, Parkinson's and Huntington's diseases (Douglas and Dillin, 2010).

A major goal of this study was to investigate the effects of pathologically expanded polyQ proteins on overall proteostasis. The yeast *S. cerevisiae* is a well-established model organism for studying polyQ protein aggregation and toxicity, which underlie Huntington's disease (Cohen et al., 2012). In this work, we overexpressed the N-terminal exon1 fragment of huntingtin with a non-pathogenic length of the polyQ tract (20Q) and a pathogenically expanded polyQ tract (96Q) in yeast. Overexpression of the exon1 fragment with the expanded polyQ tract is sufficient to cause HD-like pathology in different organisms (Mangiarini et al., 1996; Li et al., 1999). Exon1 of huntingtin contains the polyQ tract and surrounding sequences, which may play important roles in the disease pathology. The flanking sequences of huntingtin protein appear to have a profound effect on polyQ toxicity and aggregation propensity (Duennwald et al., 2006; Robertson et al., 2011). Moreover, the proline-rich region following the polyQ tract mitigates toxicity (Dehay and Bertolotti, 2006). In this work, we used the entire exon1 sequence including the proline-rich segment and varied only the polyQ length (Figure 8). The proteins were overexpressed under a galactose-inducible (*GAL1*) promoter (Krobitsch and Lindquist, 2000).To visualize the polyQ proteins in cells, we also generated C-terminal fusion constructs with fluorescent mCherry (20QmCh and 96QmCh).
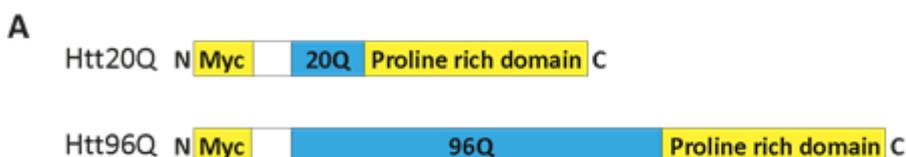
B
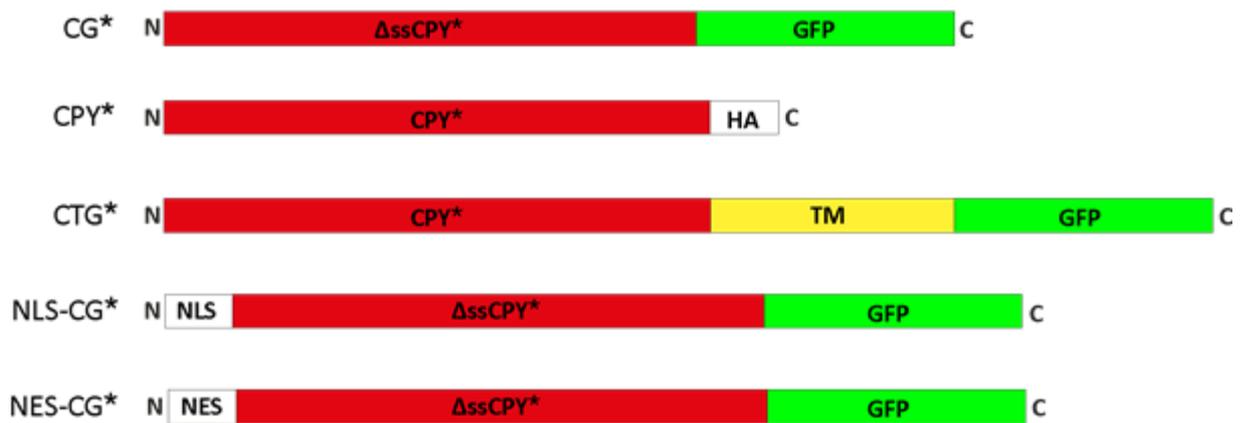
Figure 8. Schematic picture of the constructs used in this study.

The polyQ proteins and terminally misfolded proteins based on mutated carboxypeptidase Y (CPY*) used in this work are shown. Both polyQ proteins carry a myc-tag at the N-terminus for detection. These proteins also contain a poly-proline sequence after the 20Q or 96Q.

To measure the effects of polyQ expansion proteins on proteostasis, we analyzed the ability of yeast cells to degrade misfolded proteins. The following terminally misfolded proteins were used: CG*, a mutant version of the secretory protein carboxypeptidase Y lacking the signal sequence (ΔssCPY*) and fused to GFP, and CG*, which is unable to fold in the reducing environment of the cytosol and undergoes rapid degradation via the UPS in a manner dependent on cytosolic Hsp70 (Ssa1) and Hsp40 (Ydj1) (Park et al., 2007). We also created two other constructs based on CG*. A nuclear localization signal (NLS) or a nuclear export signal (NES) was attached to the N-terminus of CG* (NLS-CG* and NES-CG*, respectively) to create versions of the protein that exclusively localized to the nucleus or to the cytosol. CPY* is a misfolded protein that resided in the ER lumen, and CTG* consists of CPY* linked to the ER membrane via a single transmembrane domain followed by a GFP domain, which is exposed to the cytosol. CPY* and CTG* are topologically different misfolded proteins that are degraded via ERAD.

4.1.1 Expression of CG* and polyQ proteins in yeast

We co-expressed CG* and 96Q or 96Q alone in wild-type cells (YPH499). CG* was expressed under the *CPY* promoter, whereas 96Q was expressed under a galactose-inducible (*GAL1*) promoter. Chronic overexpression of toxic proteins can lead to the selection of yeast that

produce lower yields of the proteins (Romanos et al., 1992). Therefore, we used a galactose-inducible promoter for 20Q and 96Q. These experiments were performed under otherwise non-stress growth conditions at 30°C. After 9 hr of induction, SDS-insoluble 96Qaggregates were detectable by immunoblotting (Figure 9).
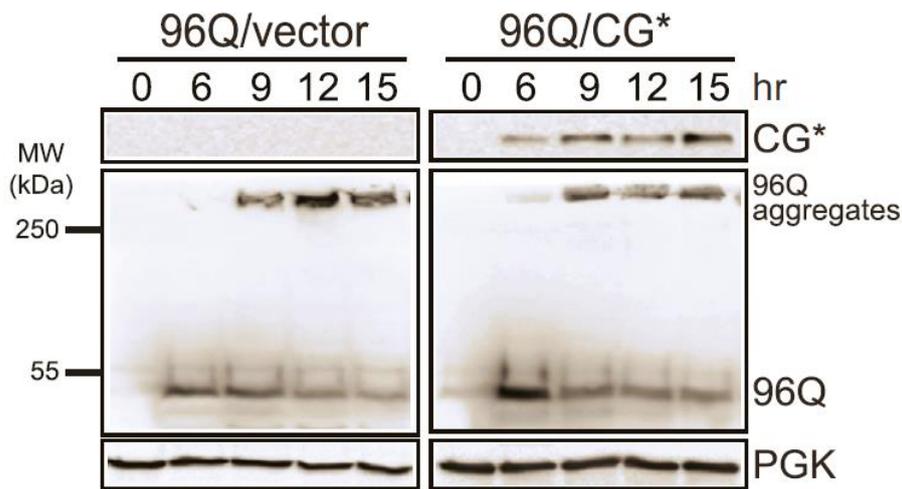

Figure 9. 96Q forms detergent-insoluble aggregates.

Cells expressing 96Q alone or co-expressing 96Q and CG* were induced with galactose. Samples were collected at 0, 6, 9, 12 and 15 hours post-induction, and then were subjected to immunoblotting analysis using anti-GFP, myc and anti-PGK antibodies. SDS-insoluble and SDS-soluble forms of 96Q are clearly visible on the blot. The SDS-insoluble fraction does not enter the stacking gel and thus remains at the top of the membrane (Heiser et al., 2000). The SDS-soluble fraction of 96Q is situated at the bottom of the membrane.

4.2 Global impairment of the ubiquitin-proteasome system by polyQ aggregation

Aggregation-prone polyQ-expanded proteins may interfere with the protein quality control mechanisms of proteostasis. Studies have shown the expression of polyQ-expanded proteins result in the disruption of cellular protein folding in the *C. elegans* nematode model and the decline in cellular proteostasis capacity in a cell culture model (Gidalevitz et al., 2006; Gupta et al., 2011). Moreover, UPS components appear to be included in polyQ aggregates (Ciechanover and Brundin, 2003; Cummings et al., 1998; DiFiglia et al., 1997). However, whether and how polyQ-expanded proteins interfere with cellular chaperone capacity and the UPS remain unclear. In previous studies, short-lived degron signal-containing proteins or small peptides

were used to explore the relationship between proteasome activity and polyQ-expanded protein aggregation (Bennett et al., 2007; Bett et al., 2009; Hipp et al., 2012; Maynard et al., 2009). However, these approaches are limited in their ability to explain whether polyQ-expanded proteins interfere with the ubiquitination process, inhibit proteasome function directly or both. Moreover, the use of small fluorogenic peptides to assess the functionality of the proteasome cannot address the question of whether polyQ-expanded proteins interfere with upstream reactions involved in proteasomal degradation, which includes ubiquitin modification and chaperone requirements. In this study, to analyze the interference of proteasomal degradation by polyQ-expanded proteins, we tested the degradation of several compartment-specific misfolded proteins in cells co-expressing polyQ proteins.

4.2.1 96Q interferes with the degradation of misfolded proteins in different compartments

Protein quality control in the cytosol

To evaluate the degree of interference of polyQ-expanded proteins in UPS functions, we co-expressed 96QmCh with CG* or 20QmCh with CG* in *S. cerevisiae* strain YPH499. Expression of CG* and polyQ proteins were induced with galactose for 15 hours. After induction, cells were collected, and the degradation of CG* was analyzed by a cycloheximide (CHX) chase assay. The addition of cycloheximide inhibits protein synthesis in the cell by blocking the movement of peptidyl-tRNA from the acceptor site to the donor site within ribosomes(McKeehan and Hardesty, 1969). This technique allows us to determine the degradation kinetics of a protein and estimate its half-life. Cells expressing 96QmCh exhibited strong stabilization of CG*. After a 3-hour CHX chase, approximately 80% of CG*remained. Cells expressing 20QmCh did not exhibit stabilization of CG*, and after a 3-hour CHX chase, only approximately 25% of CG* remained. The construct 96QmCh had a profound effect on the degradation of CG*, whereas 20QmCh did not appreciably interfere with CG* degradation. These results are shown in Figure 10.

A

B
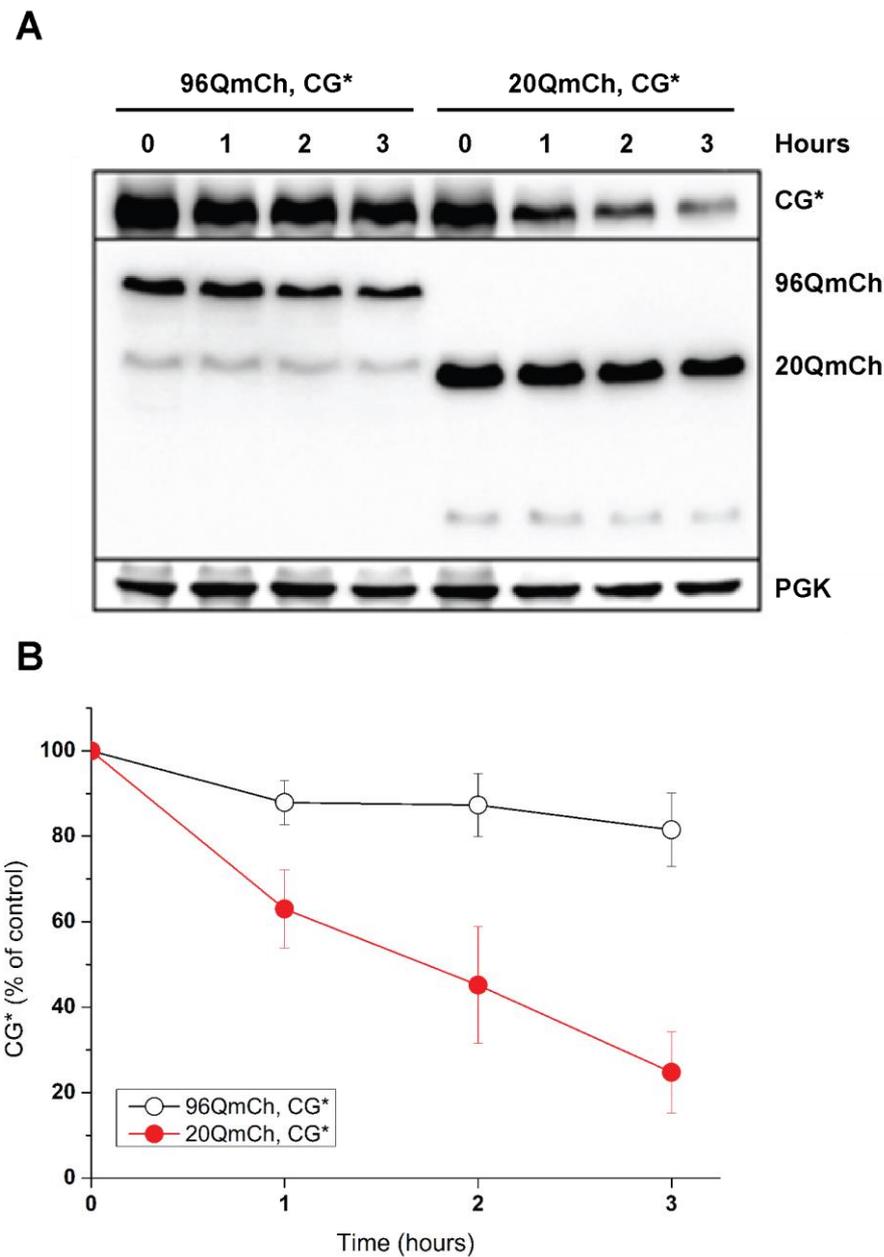
Figure 10. 96QmCh stabilizes CG*.

(A) The degradation of CG* was analyzed at several time points after the addition of CHX in wild-type cells expressing polyQ proteins and CG* expressed under the *GAL1* promoter. CG* and polyQ proteins were detected using anti-GFP and anti-myc antibodies, respectively. PGK was used as a loading control. (B) CG* was quantified by densitometry analysis. Averages and the standard deviation (SD) from three independent experiments are shown.

Interestingly, the observed effects on CG* stabilization were dependent on time. We did not observe CG* accumulation when CG* and 96Q were co-expressed for 6 hours (Figure 11).
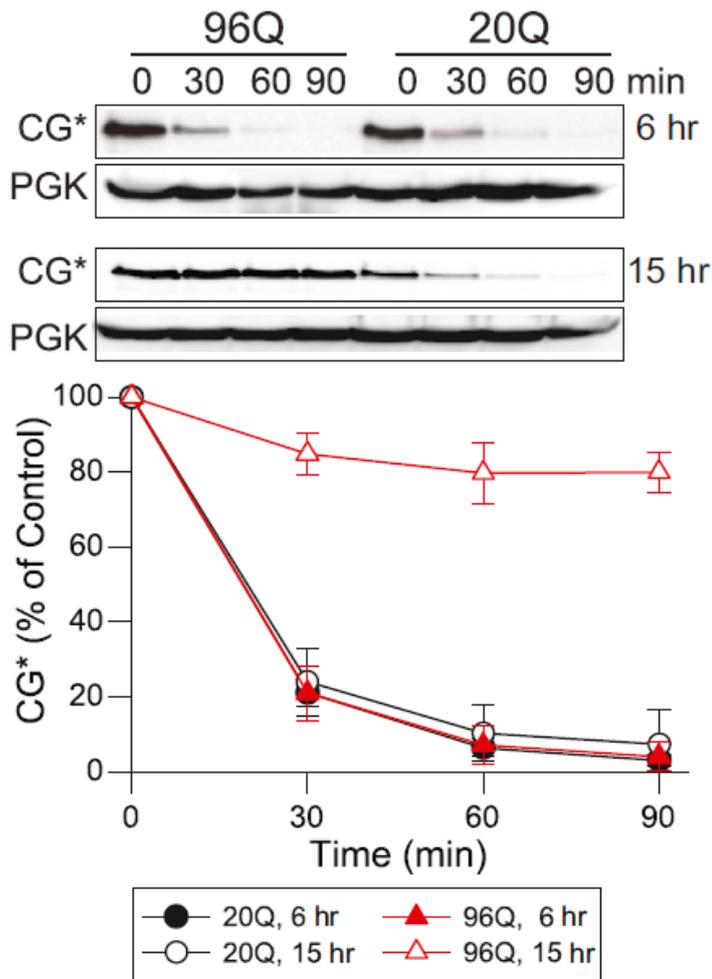
Figure 11. Turnover of CG* by CHX chase assay.

96Q or 20Q constructs were co-expressed with CG* for 6 hr or 15 hr. CHX was added to inhibit protein synthesis. Samples were collected at the indicated time points and were analyzed for CG* by anti-GFP immunoblotting. CG* was quantified by densitometry analysis. Averages and the SD from three independent experiments are shown.

Protein quality control in the nucleus

Next, we determined whether 96QmCh interfered with the degradation of misfolded proteins in the nucleus. To do this, we analyzed the degradation of NLS-CG* in cells co-expressing polyQ proteins. Interestingly, 96QmCh also interfered with NLS-CG* degradation. After a 3-hour CHX chase, approximately 53% of NLS-CG* remained. In cells expressing 20QmCh, only 22% of NLS-CG* protein remained after the experiment. NLS-CG* degraded at a much faster rate in the presence of 96QmCh when compared with CG*. Thus, our results suggest that

96QmCh strongly interferes with the degradation of misfolded proteins in the nucleus. These results are presented in Figure 12.
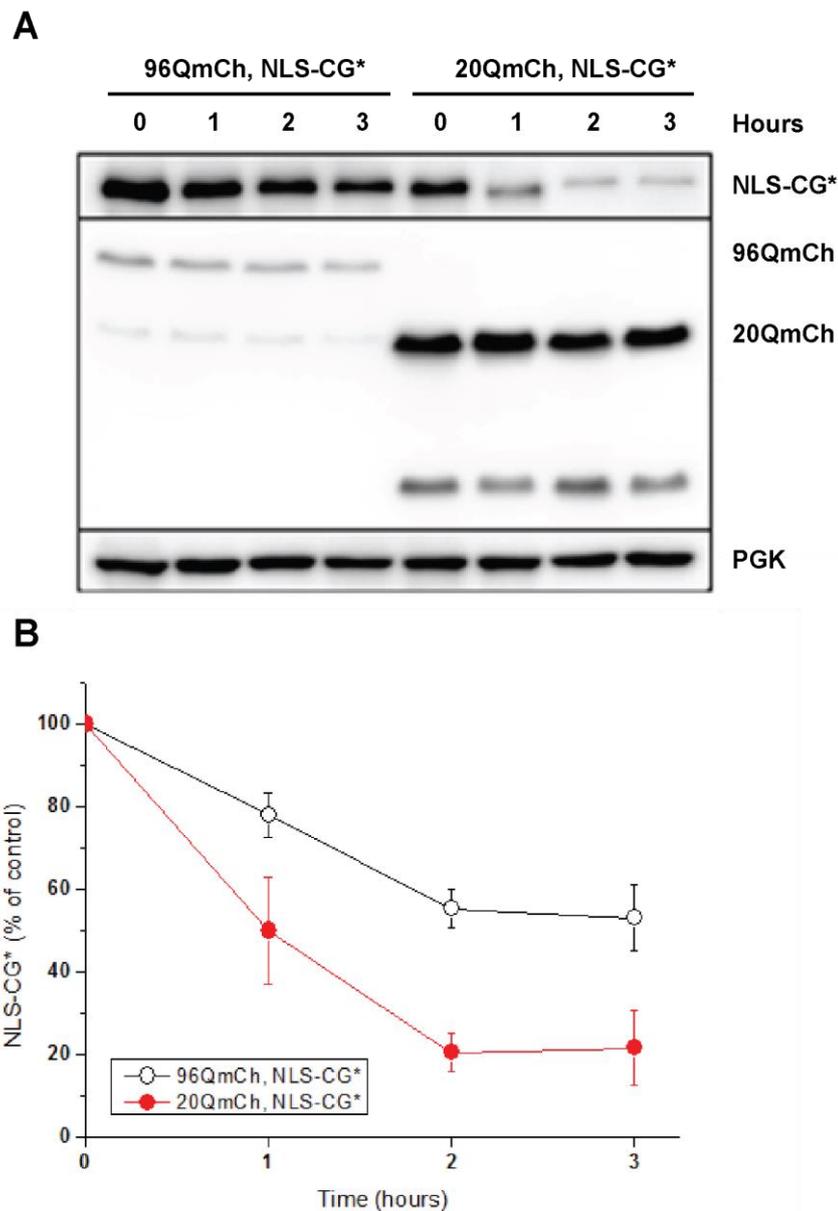
Figure 12. 96QmCh stabilizes NLS-CG*.

(A) The degradation of NLS-CG* was analyzed in the presence of CHX in wild-type cells expressing polyQ proteins and NLS-CG* expressed under the *GAL1* promoter. NLS-CG* and polyQ proteins were detected using anti-GFP and anti-myc antibodies, respectively. PGK was used as a loading control. (B) NLS-CG* was quantified by densitometry analysis. Averages and the SD from three independent experiments are shown.

Protein quality control in the ER

Expression of the polyQ-expanded protein 96QmCh inhibited the degradation of misfolded proteins in two different compartments, the cytosol and the nucleus. Next, we tested whether 96QmCh disturbed protein quality control in the ER. To this end, we took advantage of topologically distinct misfolded proteins based on CPY* (Figure 13).
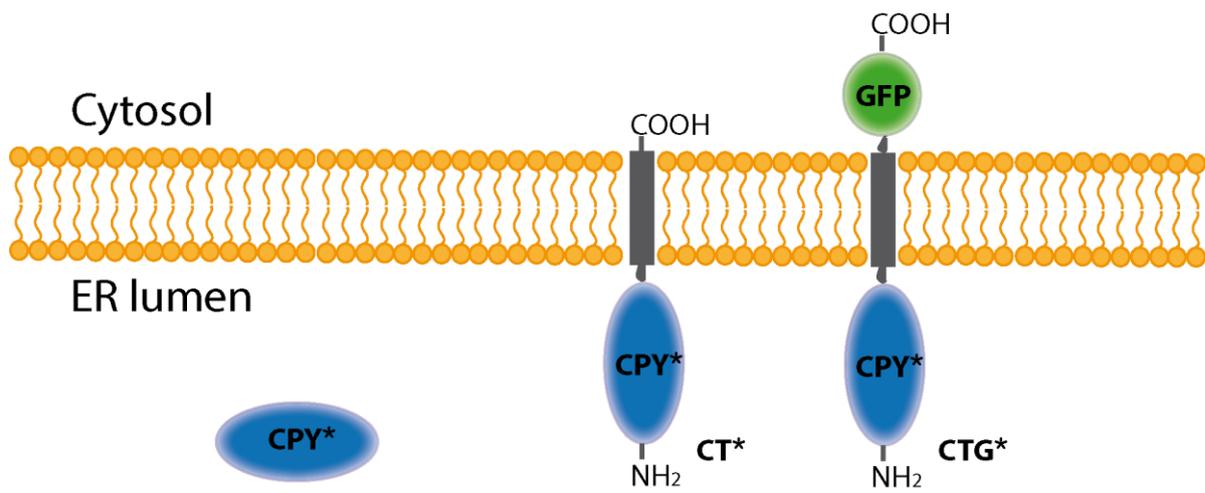
Figure 13. Topology of ERAD substrates used in this study.

The ability of 96QmCh to affect ER luminal misfolded protein degradation was tested using a CPY* reporter protein. PolyQ proteins and CPY* were co-expressed, and the CHX chase assay was performed as described in the preceding sections. 96QmCh substantially inhibited the degradation of CPY*. After 135 minutes of CHX treatment, 65% of CPY* remained. In the control sample co-expressing 20QmCh, only 33% of the reporter protein was present. These results suggest that 96QmCh interferes with the degradation of ER lumen-specific CPY* (Figure 14).

A

B
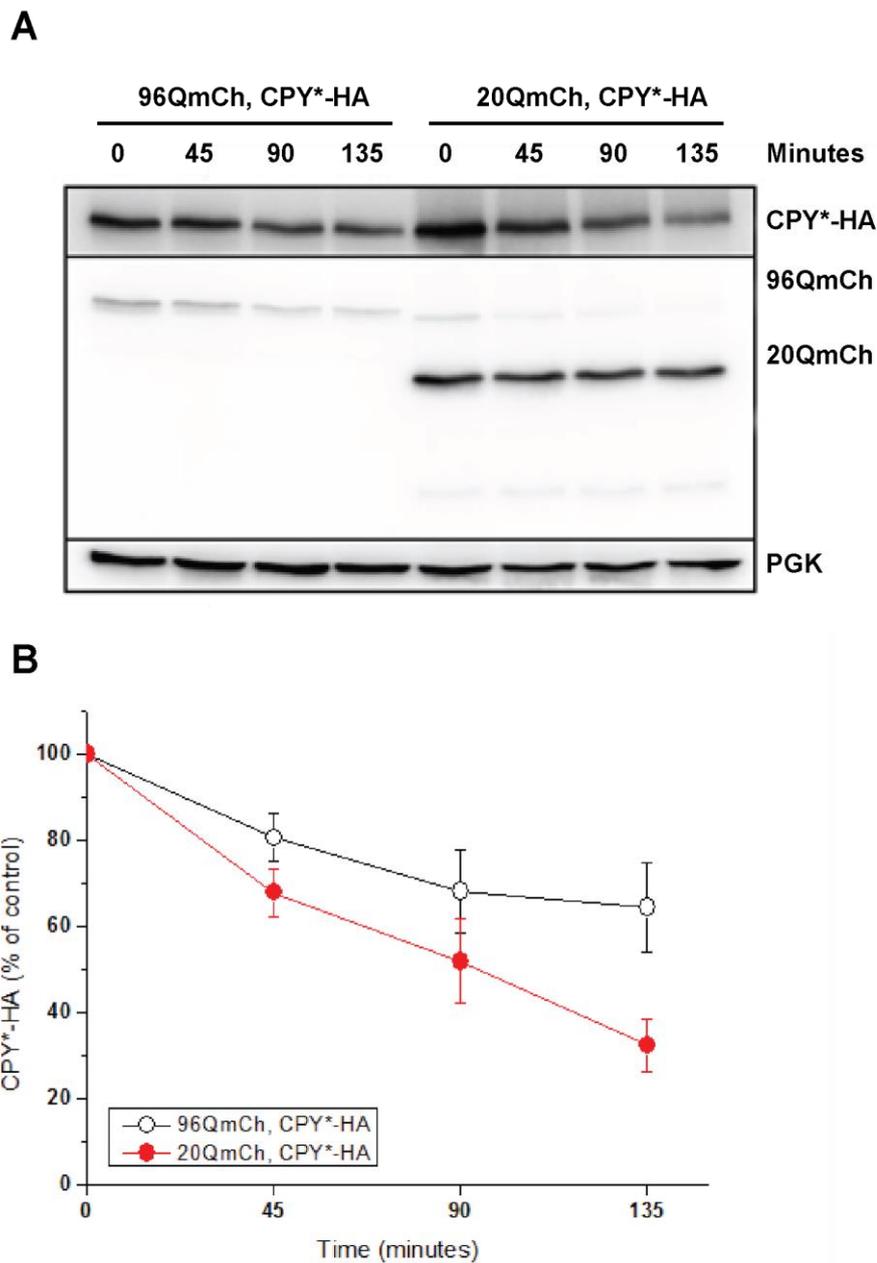
Figure 14. 96QmCh stabilizes CPY*.

(A) Degradation of CPY*-HA was analyzed upon the addition of CHX in wild-type cells expressing polyQ proteins. CPY*-HA was expressed under the *TDH3* promoter. CPY*-HA* and polyQ proteins were detected using anti-HA, myc and PGK antibodies, respectively. PGK was used as a loading control. (B) CPY*-HA was quantified by densitometry analysis. Averages and the SD from three independent experiments are shown.

96QmCh or 20QmCh was co-expressed with CTG* to determine whether polyQ-expanded proteins could affect the degradation of ER membrane-localized misfolded protein. 96QmCh interferes with CTG* degradation. After 135 minutes of CHX treatment, 64% of the CTG* was observed, whereas in cells expressing non-pathogenic polyQ protein (20QmCh), only 20% of CTG*remained. These results are shown in Figure 15.

A

B
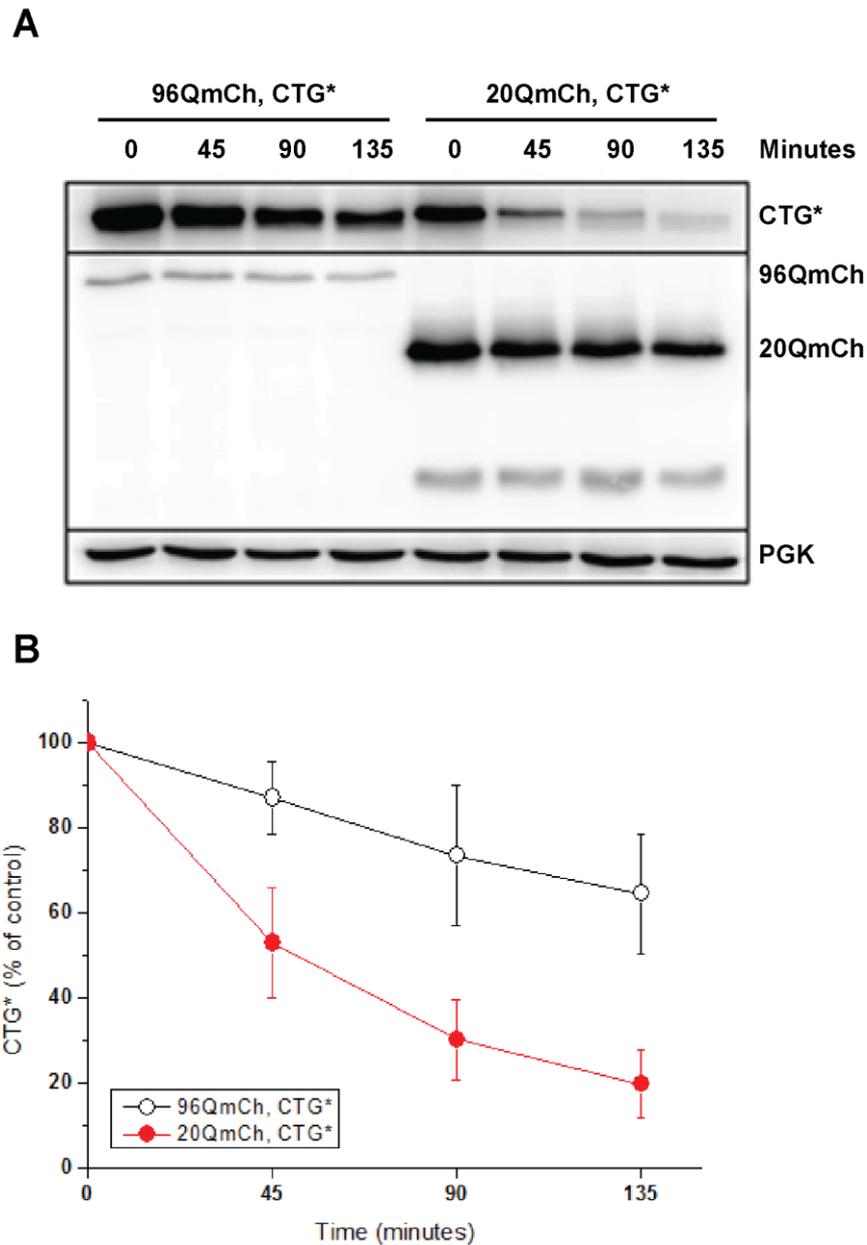
Figure 15. 96QmCh stabilizes CTG*.

 (A) The degradation of CTG* was analyzed upon the addition of CHX in wild-type cells expressing polyQ proteins. CTG* was expressed under the *TDH3* promoter. CTG* and polyQ proteins were detected using anti-GFP and anti-myc antibodies, respectively. PGK was used as a loading control. (B) CTG* was quantified by densitometry analysis. Averages and the SD from three independent experiments are shown.

4.3   Accumulation of misfolded proteins by 96Q leads to proteostasis collapse

4.3.1 The co-expression of 96Q with CG*, NLS-CG* and CTG* results in growth inhibition

Next, we tested whether the co-expression of polyQ-expanded proteins with misfolded proteins compromises proteostasis capacity. As we observed, co-expression of 96QmCh with various forms of misfolded proteins significantly inhibited the elimination of misfolded proteins, including CG*, NLS-CG*, CTG* and CPY*. To test the consequences of this effect, we analyzed the growth of cells co-expressing polyQ proteins with misfolded proteins. A cell growth assay was performed for strains expressing polyQ proteins alone or in a co-expressed manner with CG*, NLS-CG*, CTG* or CPY*. The co-expression of 96QmCh with CG*, NLS-CG*, or CTG* resulted in substantial growth inhibition (Figure 16). Interestingly, co-expression of 96QmCh with CPY* did not result in a growth defect in yeast cells, and co-expression of 20QmCh with any of the misfolded proteins did not result in any noticeable toxicity.
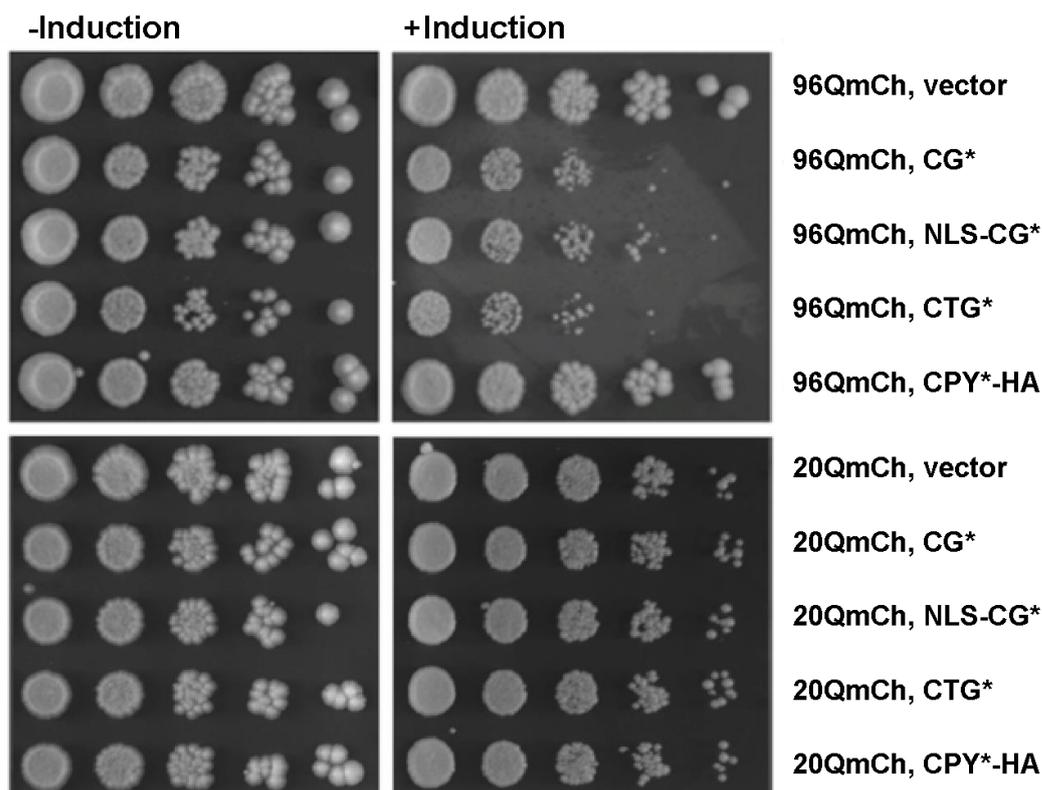
Figure 16. Growth of cells co-expressing polyQ-expanded proteins and misfolded proteins.

Six-fold serial dilutions of cells were spotted on agar plates containing glucose (- induction) or galactose (+ induction) to induce the expression of polyQ proteins and misfolded proteins. The plates were incubated for 4 days at 30°C.

The observed proteotoxic effectswere also dependent on the expression levels of the misfolded protein CG*. Three different levels of CG* expression were assessed: low, average and high. High expression corresponds to the CG* construct used in the experiments described in the preceding sections. 96QmCh or 20QmCh was co-expressed with CG* constructs expressing at low, average and high levels. Co-expression of 96QmCh with CG* was toxic, and cytotoxicity increased according to CG*expression levels (Figure 17).
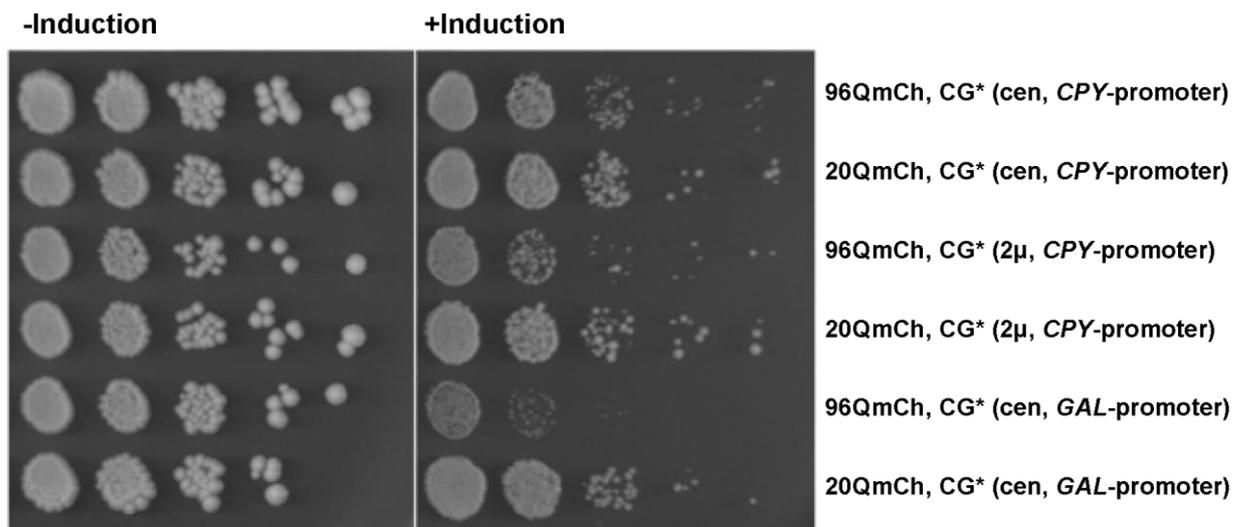
Figure 17. 96Q and CG* toxicity correlates with the expression level of CG*.

Growth of cells co-expressing 20Q or 96Q with CG*. Six-fold serial dilutions of cells were spotted on agar plates containing glucose or galactose. Plates were incubated for 4 days at 30°C. CG* expressed on a centromeric plasmid demonstrated low expression, CG* expressed on a multicopy plasmid demonstrated average expression, and CG* expressed under theGAL1 promoter on a centromeric plasmid expressed at the highest level.

4.3.2 Overexpression of the 96Q protein results in toxicity

Chronic accumulation of misfolded proteins can overwhelm the capacity of the protein quality control system, even though cells have a network of components to protect the proteome integrity and maintain proteostasis. (Finkbeiner, 2011;Hartl et al., 2011). Although the single expression of the polyQ-expanded proteins used in this study was not toxic for the yeast cells (Behrends et al., 2006; Krobitsch and Lindquist, 2000), we tested whether the overexpression of polyQ-expanded proteins alone could cause growth retardation.

To test this hypothesis, we overexpressed non-toxic versions of polyQ-expanded proteins (96QmCh and HA-96Q) from two plasmids, which resulted in cells expressing higher yields of the polyQ-expanded proteins. Both proteins were identical except for the expression of different epitope tags (HA and myc), which were used for their identification. The growth of cells overexpressing polyQ-expanded proteins was compared with cells co-expressing 96QmCh with CG*. Indicated combinations of cells overexpressing the polyQ proteins were analyzed by 6-fold serial dilution spotting. Overexpression of 96Q from two plasmids was toxic in the same manner as CG* co-expression to the cells. Co-expression of 20QmCh with HA-96Q or HA-96Q alone was not toxic (Figure 18).
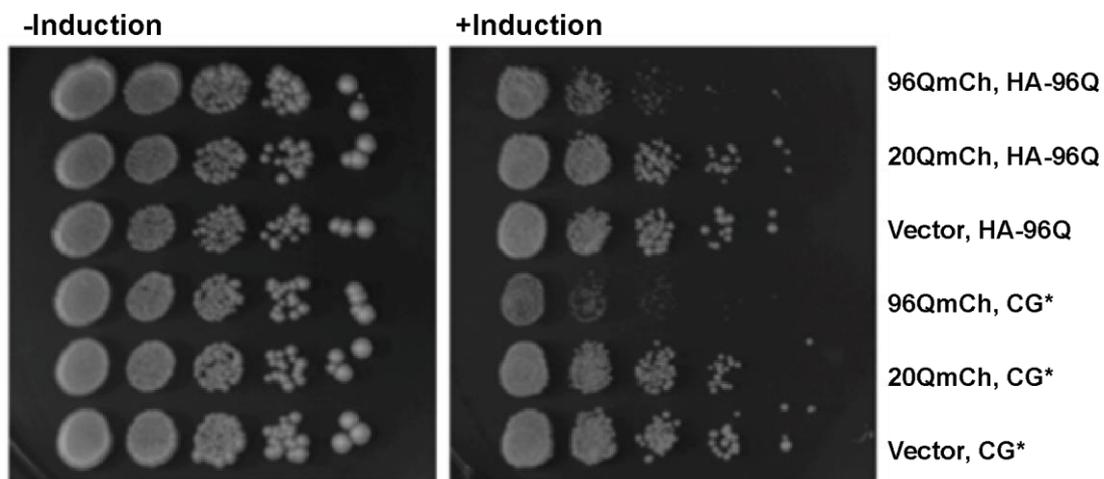
Figure 18. Overexpression of non-toxic polyQ proteins causes cytotoxicity.

Six-fold serial dilutions of cells were spotted on agar plates containing glucose (- induction) or galactose (+ induction) to induce the expression of polyQ proteins and misfolded proteins. The plates were incubated for 4 days at 30°C.

In addition, we examined whether the overexpression of terminally misfolded proteins caused toxicity in yeast cells. To address this question, we overexpressed CG*under the*GAL1* promoter with a multicopy plasmid backbone (2μ). As a result, CG* expression levels were significantly higher relative to CG* expressed on a centromeric plasmid. The viability of the cells overexpressing CG* (2μ) with ΔssCPY*-Cherry (CmCh*) was analyzed by 6-fold serial dilution cultures. Overexpression of CG*(2μ) with CmCh* was toxic to the cells. Surprisingly, overexpression of CG* with a multicopy plasmid was sufficient to induce cytotoxicity, which is likely due to the perturbation of proteostasis control attributable to the elevated levels of terminally misfolded proteins (Figure 19).
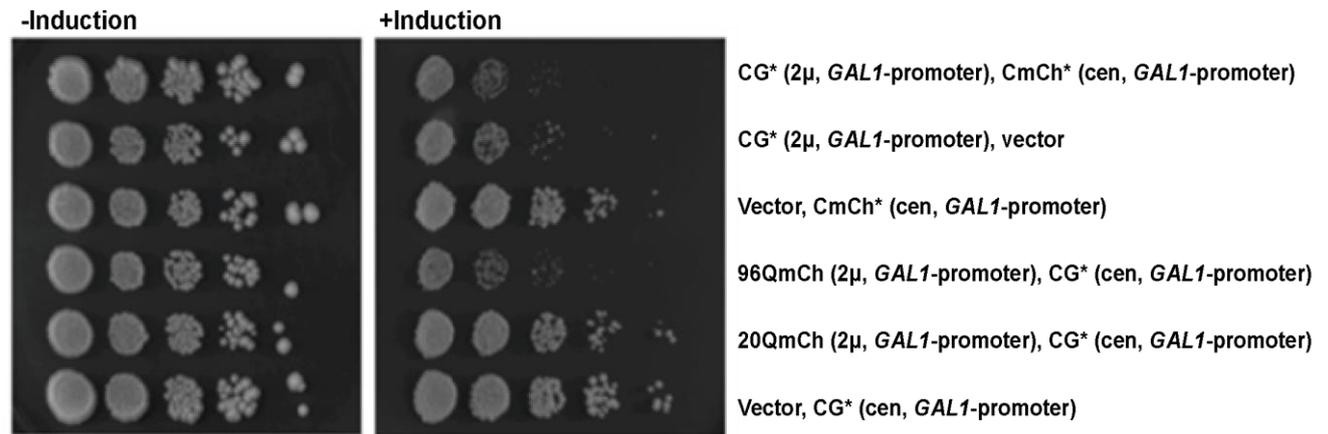
Figure 19. Overexpression of misfolded proteins does not cause significant growth inhibition.

The growth of cells overexpressing terminally misfolded proteins was assessed by 6-fold serial dilutions of the cells. Cells co-expressing 96QmCh with CG* and 20QmCh with CG* were used as controls. Six-fold serial dilutions of were spotted on agar plates containing glucose or galactose. The plates were incubated for 4 days at 30°C.

4.4   Inactivation of the heat shock response by polyQ proteins

96Q is a misfolded protein that is potentially harmful to the cell. Our data have shown that in combination with CG* expression, 96Q expression results in yeast cell growth inhibition. In what other ways do cells respond to the expression of polyQ-expanded proteins? Does co-expression of polyQ-expanded proteins with terminally misfolded proteins inhibit the cellular stress response? To address these questions, we determined whether polyQ-expanded proteins expressed alone or co-expressed with misfolded proteins elicits a cytosolic stress response using a reporter construct consisting of the β-galactosidase gene under the control of the heat-shock promoter element (HSE) of the stress-inducible Hsp70 gene *SSA3* (Boorstein and Craig, 1990a). Because the *SSA3* promoter is activated only under stress, we used this promoter to measure how cells react to stress (Boorstein and Craig, 1990b).

The spontaneous expression of LacZ was measured in cells expressing polyQ proteins alone or in combination with CG* under non-stress growth conditions at 30°C (Figure 18A). Under normal conditions, cells expressing 96QmCh alone or in combination with CG* exhibited a limited cytosolic stress response relative to control cells (Figure 20A). Furthermore, additional thermal stress consisting of 1 hour of heat shock at 37°C revealed that cells co-expressing 96QmCh and CG* remained insensitive to the induction of a cytosolic stress response to heat

shock when compared with cells expressing no proteotoxic proteins (Figure 20 B). Interestingly, cells expressing CG* alone or in combination with 20QmCh also exhibited a substantial reduction in the cytosolic stress response, although cells expressing 96QmCh or 20QmCh alone induced a level of stress response similar to the control cells (Figure 20B). The comparison of the cytosolic stress response under normal (A) and heat-shock conditions (B) is plotted in Figure 20C. Cells co-expressing the misfolded proteins 96QmCh and CG* demonstrated a limited ability to react to additional thermal stress. In this sample, cells were able to produce a thermal stress response that was only 2.2-fold higher than non-stress growth conditions at 30°C.Cells expressing 96QmCh alone produced a 6.1-fold increased stress response higher than non-stressed sample. Co-expression of 20QmCh with CG* or single expression of CG* resulted in 7.5- and 7.6-fold increases in stress activation, respectively. 20QmCh co-expressed with empty vector (p423Gal) or two empty vectors (pYES and p423Gal) responded to heat shock conditions with increases in LacZ activity by 14.5- and 13.1-fold, respectively. Moreover, the limited cytosolic stress response in cells co-expressing 96QmCh with CG* suggested that the cellular proteostasis system is impaired under these conditions.

A
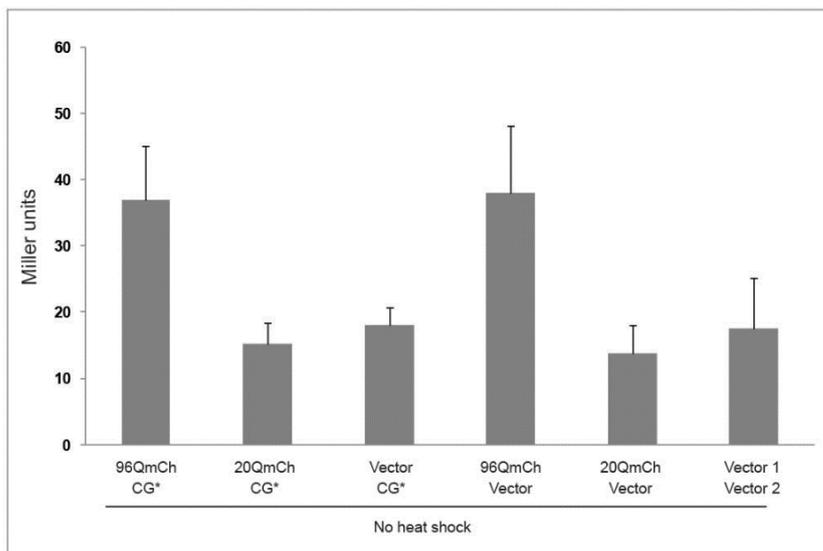
B
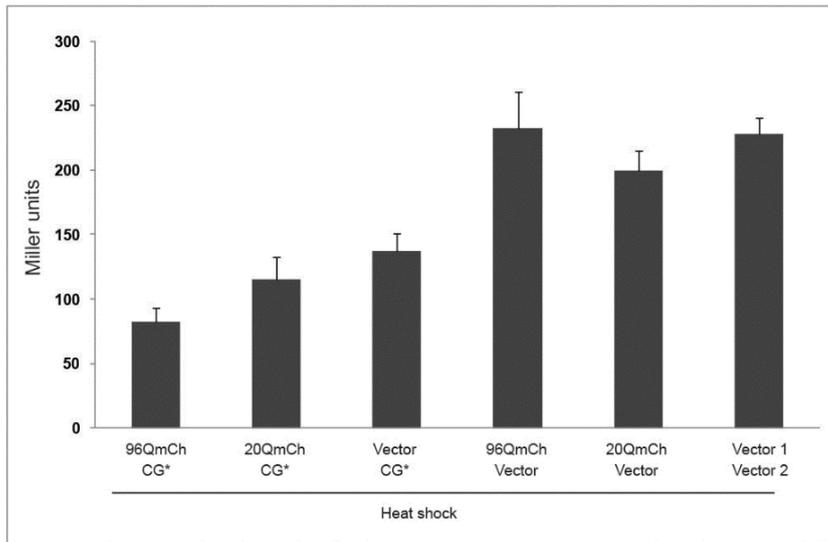
C
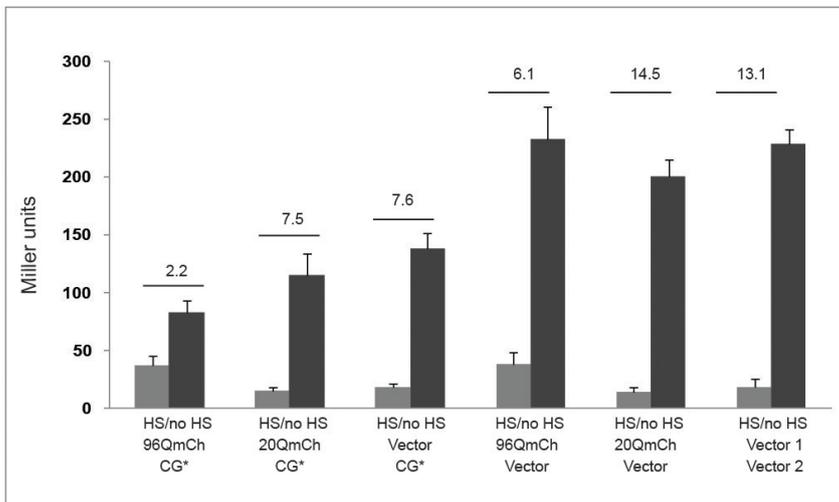
Figure 20. Co-expression of 96QmCh and CG* inhibits the cytosolic stress response.

The expression of LacZ was measured in cells expressing polyQ proteins alone or in combination with CG* under the conditions described in the Materials and Methods section. (A) A cytosolic stress response under normal growth conditions at 30°C (no heat shock). (B) A cytosolic stress response under heat-shock conditions at 37°C. Cells were subjected to heat shock at 37°C for 1 hour prior to the experiment. (C) Comparison of the cytosolic stress response under normal (A) and heat shock conditions (B). Averages and the SD from three independent experiments are shown.

4.5 CG* as a model protein for UPS impairment by polyQ-expanded proteins

We tested several UPS reporters that were stabilized in presence of the polyQ-expanded protein 96QmCh. These reporter proteins are associated with different compartments and are degraded via distinct mechanisms. We chose CG* as a primary UPS reporter to study its mechanism of degradation for several reasons. First, CG* is a cytosolic protein, and almost half of the proteins in the yeast cell are cytosolic (Kumar et al., 2002). Therefore, a cytosolic protein represents the largest fraction of proteins in yeast, which would allow us to extrapolate our findings to many other misfolded or incorrectly assembled cytosolic proteins. Second,the degradation pathway for CG* and the required UPS components involved are well known (Park et al., 2007; Heck, et al., 2010; Prasad, et al., 2010). For example, CG* degradation requires Hsp70 Ssa1-Ydj1 chaperone machinery. An understanding of how the UPS is impaired in CG* degradation by 96QmCh is important for elucidating the basic cellular mechanisms of polyQ protein aggregation.

4.5.1 96QmCh does not co-aggregate with CG*

How do polyQ expansion proteins inhibit the degradation of the misfolded cytosolic protein CG* via the UPS? Proteins that form SDS-insoluble aggregates or inclusion bodies often co-aggregate with other proteins. For example, chaperones co-localize with amyloid beta (Vattemi et al., 2004). Moreover, unrelated misfolded proteins tend to co-localize, but not to co-aggregate (Rajan et al., 2001). The co-localization of misfolded proteins could be explained by the accumulation of proteins in the juxta nuclear quality control compartment (JUNQ) or in insoluble protein deposits (IPODs) (Kaganovich et al., 2008). If CG* is sequestered by 96Q aggregates, then CG* would be less accessible to the UPS machinery. This could potentially explain CG* accumulation in the presence of 96Q.

To examine whether the inhibition of CG* degradation was due to co-aggregation of CG* and 96Q, we analyzed the subcellular distribution of 96QmCh and CG* in living cells. CG* was expressed under the control of the *GAL1* promoter in these experiments, which resulted in higher expression levels than when under the control of the *PRC1* promoter. In general, CG* was almost undetectable by fluorescence microscopy, which is likely because it is degraded relatively quickly, and 20QmCh was diffusely distributed and did not form any aggregates. Expression of 96QmCh led to the accumulation of multiple aggregates, and CG* formed cytosolic inclusions. However, the CG* inclusions did not overlap with the inclusions formed by 96QmCh (Figure 21). Therefore, we concluded that CG* stabilization was not due to co-aggregation of CG* with 96Q but is due to other reasons.

Hoechst	CG*	PolyQ	Merge	
				20QmCh/CG*
				96QmCh/CG*
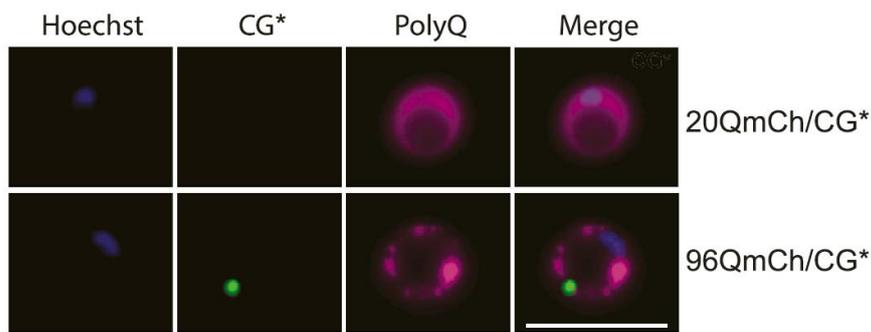
Figure 21. Formation of CG* inclusions upon co-expression with 96Q.

Cells co-expressing 20QmCherry (20QmCh) or 96QmCh in combination with CG* for 18 hours at 30°Cwere analyzed by live cell fluorescence microscopy. Nuclei were counterstained with Hoechst 33342. Scale bar, 10 mm. 96QmCh and CG* did not co-aggregate.

4.6 Proteasome function and ubiquitination are not affected by 96Q

4.6.1 96Q does not inhibit Ub^{G76V}-GFP degradation

We observed that the expression of 96Q interfered with the degradation of several misfolded proteins. However, how this interference occurs is not clear. One hypothesis that could explain this observation is that pathogenically expanded polyQ directly inhibits the proteasome because the proteasome cannot digest SDS-insoluble fibrils and/or because soluble 96Q contains a long polyQ tract that cannot be digested (Venkatraman et al., 2004; Raspe et al., 2009). The proteasome may become clogged with the polyQ domain. We tested the possibility of general inhibition of proteasome function using 96QmCh. If polyQ-expanded proteins inhibited the general function of the proteasome, then the degradation of all or most proteasomal substrates would be affected.

To test the ability of the proteasome to degrade other proteins, we used the short-lived UPS reporter Ub^{G76V}-GFP,which is exclusively degraded by the proteasome (Johnson et al., 1995;Dantuma et al., 2000). Ub^{G76V}-GFPconsists of a single ubiquitin molecule fused with GFP. Deubiquitination of the GFP fusion is completely inhibited because the C-terminal Gly^{76} of the ubiquitin moiety is substituted with Val^{76}(Johnson et al., 1995). Ub^{G76V}-GFP represents a normally folded but short-lived protein (due to ubiquitination). Under normal conditions, Ub^{G76V}-GFP is rapidly degraded via the UPS but accumulates in the cells upon proteasomal inhibition (Dantuma et al., 2000). Ub^{G76V}-GFP was co-expressed with 96QmCh or 20QmCh. Interestingly, Ub^{G76V}-GFP was not stabilized when co-expressed with 96QmCh. Moreover, the degradation kinetics of Ub^{G76V}-GFP in cells co-expressing 96QmCh were similar to control cells co-expressing Ub^{G76V}-GFP and 20QmCh.

A

B
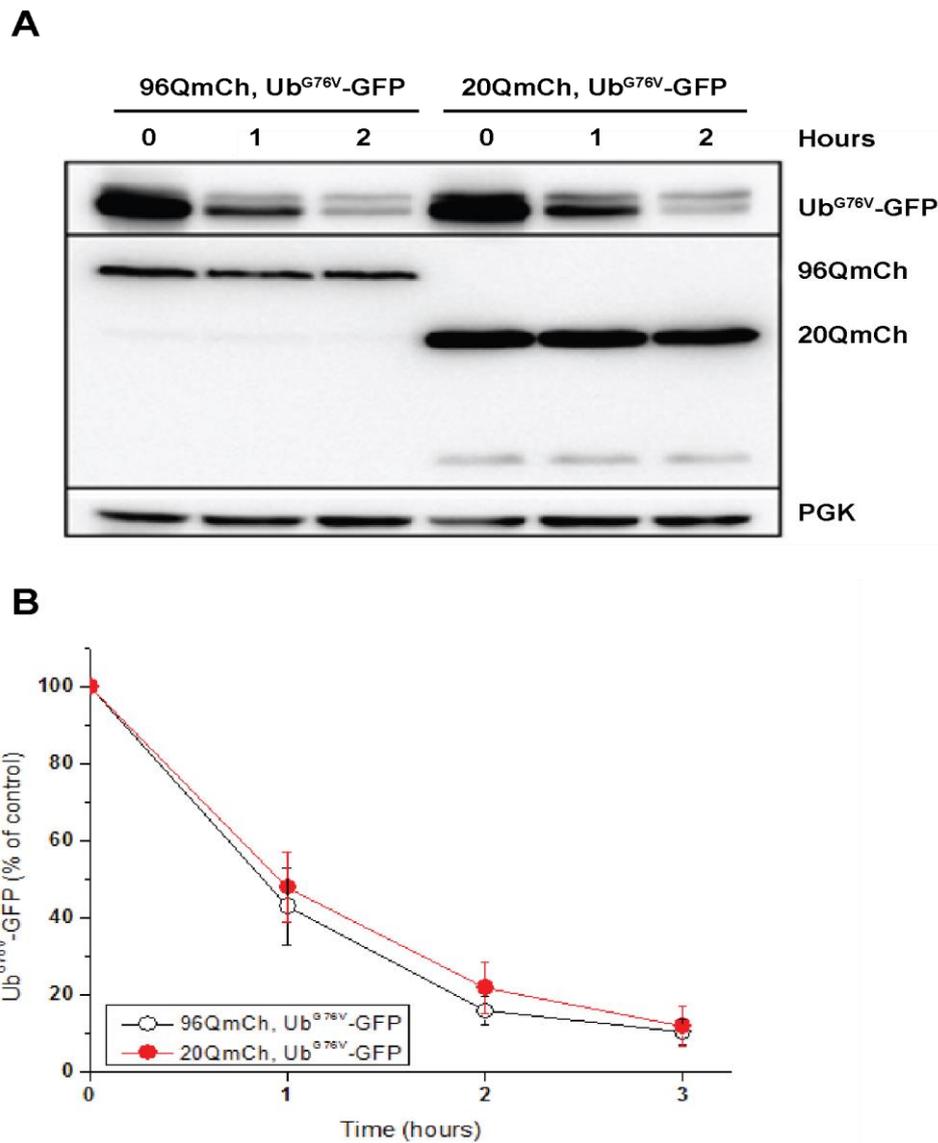
Figure 22. 96QmCh does not interfere with Ub^{G76V}-GFP degradation.

(A) The degradation of Ub^{G76V}-GFP was analyzed upon the addition of CHX in wild-type cells expressing polyQ proteins. Ub^{G76V}-GFPand polyQ proteins were detected using anti-GFP, myc and PGK antibodies, respectively. PGK was used as a loading control. (B) Ub^{G76V}-GFP was quantified by densitometry analysis. Averages and the SD from three independent experiments are shown.

4.6.2 Inhibition of CG* degradation occurs upstream of the proteasome

To obtain more evidence that 96QmCh does not inhibit the proteasome directly, we used GFPcODC in addition to the reporter. GFPcODC is a C-terminally GFP-tagged construct containing the 37-amino acid degron found in ornithine decarboxylase (cODC). This degron sequence targets GFPcODC to the 26S proteasome in a ubiquitin-independent manner (Zhang et al., 2003; Takeuchi et al., 2007;Takeuchi et al., 2008).We co-expressed CG* and GFPcODC in

the presence of polyQ proteins. This experiment would allow us to determine whether the proteasome remained functional under conditions where CG* degradation is inhibited by 96Q. As expected, in the presence of 96QmCh, degradation of CG* was inhibited, but interestingly, non-ubiquitin-dependent GFPcODC degradation occurred rapidly even in the presence of 96QmCh (Figure 23). Therefore, our findings that the degradation ofUb^{G76V}-GFP and GFPcODC remain unimpaired in yeast indicate that 96Q does not interfere with UPS function by blocking the proteasome core directly. Furthermore, these results suggest that the proteasome remains functional in the presence of 96Q (Figure 23).
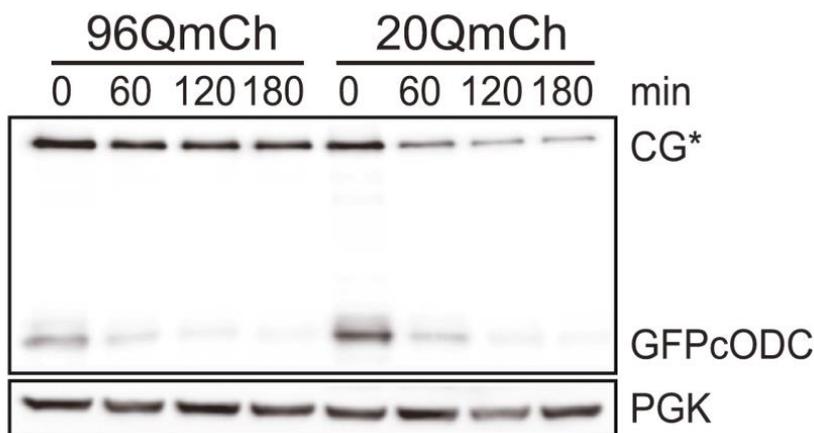
Figure 23. The proteasome remains functional in the presence of 96QmCherry.

CG* and GFPcODC were co-expressed in yeast with either 96QmCh or 20QmCh. After induction for 18 hr, CHX was added to follow the decay of CG* and GFPcODC as shown in Figure 12. PGK was included as a loading control.

4.6.3 The proteasome is capable of degrading polyQ proteins

To determine whether a long polyQ tract could be degraded by the proteasome, the C-terminal 37-aminoacid ornithine decarboxylase (cODC) degron was fused to the C-terminus of the polyQ-expanded proteins. When cODC was fused to the C-terminus of 96Q (96QcODC), the resulting fusion protein was effectively degraded, and blockage of CG* degradation was partially relieved (Figure 24). In contrast, 96Q fused with a mutated cODC (C441A) degron (96QcODC*) (Zhang et al.,2003) was stabilized and interfered with CG* degradation (Figure 24). In addition, SDS-soluble 96QcODC was degraded with kinetics similar to 20QcODC (Figure 25). These results exclude direct proteasome inhibition by 96Q. Therefore, we concluded that the proteasome remains functional in cells expressing 96QmCh, and inhibition of CG* and other

reporters by 96QmCh is not attributable to the direct inhibition of the proteasome (Figure 22, 23, 24 and 25).
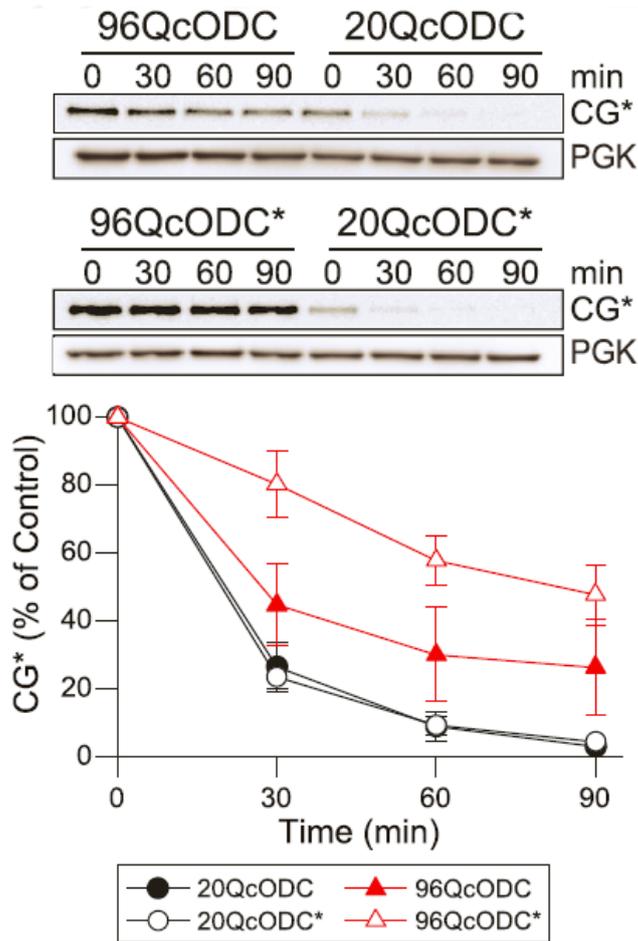
Figure 24. Targeting 96Q to the proteasome relieves the inhibition of CG* degradation.

CG* was co-expressed with 96QcODC or 20QcODC for 15 hours at 30°C. Cells expressing 96QcODC* or 20QcODC* (containing a mutated cODC degron) served as controls. The degradation kinetics of CG* were analyzed after the addition of CHX. Subsequently, SDS-PAGE and immunoblotting using anti-GFP and PGK antibodies were performed. Averages and the SD from three independent experiments are shown.
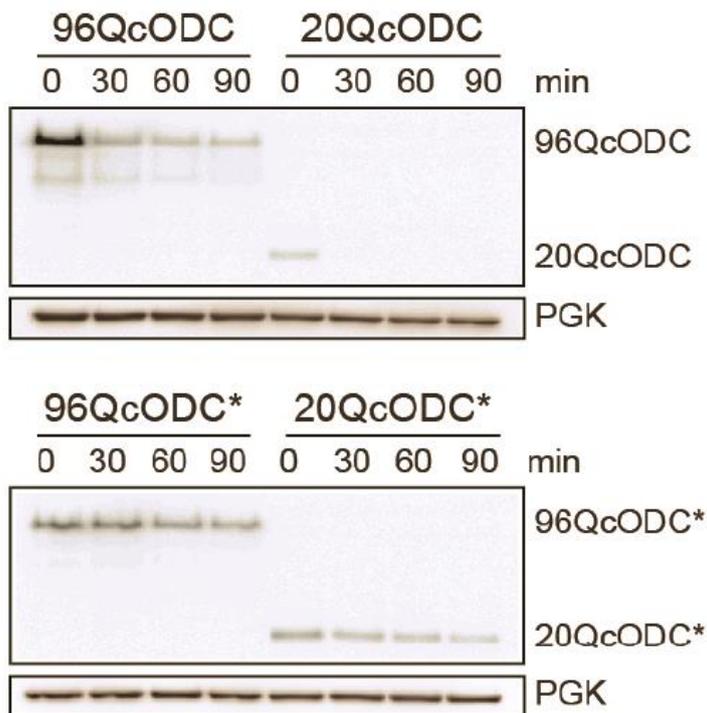
Figure 25. Targeting the polyQ protein to the proteasome.

Targeting the polyQ protein to the proteasome. The turnover of 96QcODC and 20QcODC was analyzed upon the addition of CHX. 96QcODC* and 20QcODC* were used as controls. PGK was included as a loading control.

4.7   Ubiquitination of CG* and Ubr1 overexpression

4.7.1 CG* ubiquitination is not affected by polyQ proteins

Protein poly-ubiquitination is a hallmark of proteasomal degradation by the UPS, and poly-ubiquitination is mediated by reactions catalyzed by the enzymes from the families E1, E2 and E3 ligases (Dennissen et al., 2012; Valera et al., 2005). Therefore, we tested whether CG* was efficiently ubiquitinated in the presence of 96QmCh. These experiments were performed in cells expressing His_6-ubiquitin (His_6-Ub). His_6-ubiquitin-conjugated proteins were isolated from cell extracts using TALON magnetic beads under denaturing conditions. When CG* was expressed either alone or in combination with 20QmCh or 96QmCh, ubiquitinated CG* was detected in pull-down assays by immunoblotting with an anti-CPY antibody (Figure 26, lanes 5–7). Co-expression with 96QmCh did not reduce the amount of ubiquitinated CG* (Figure 26, lane 7).
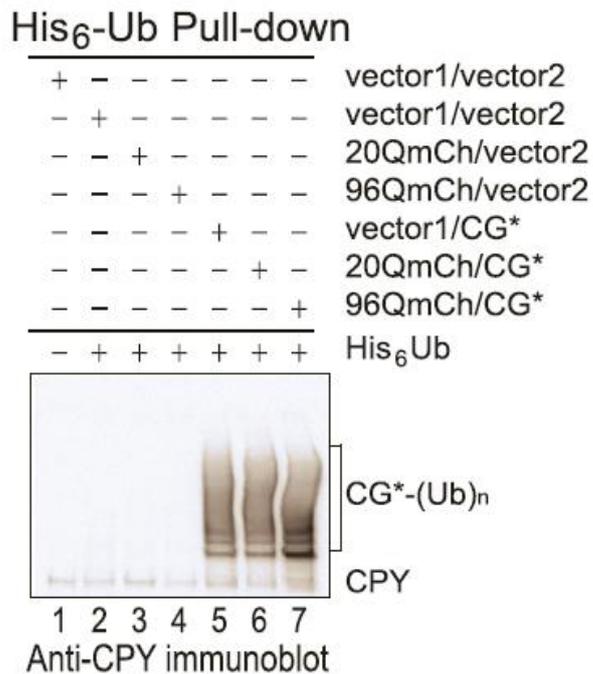
Figure 26. 96QmCh does not interfere with CG* ubiquitination.

His$_6$-Ub-conjugated proteins were isolated from cells expressing the indicated constructs (20QmCh or 96QmCh, CG* or vector control and His$_6$-Ub), followed by 4–12% gradient SDS-PAGE and immunoblotting using an anti-CPY antibody to detect ubiquitinated CG*. CPY marks the position of the endogenous CPY protein.

4.7.2 Overexpression of Ubr1 does not improve CG*degradation

To test whether the ubiquitination of CG* was a rate-limiting step for degradation, we overexpressed the E3 ubiquitin ligase Ubr1, which is involved in the ''N-end rule'' degradation pathway and is also required for efficient CG* degradation (Eisele and Wolf, 2008; Hecket al., 2010; Varshavsky, 2012). Ubr1 overexpression did not rescue CG* degradation in the presence of 96QmCh but stimulated CG* degradation in 20QmCh-expressing cells (Figure 27). These results suggest that Ubr1 is not a limiting factor for CG* degradation.
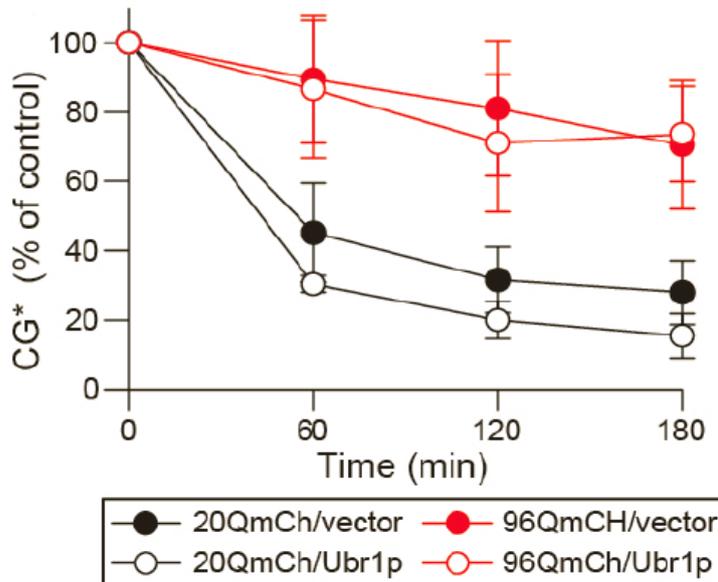
Figure 27. Ubr1 is not a limiting factor for CG* degradation in the presence of polyQ proteins.

Ubr1 was overexpressed under the control of the *ADH1* promoter in cells co-expressing 96QmCh or 20QmCh and CG*. After 18 h of polyQ induction, CG* degradation was analyzed upon the addition of CHX. CG* levels were quantified. Averages and the SD from three independent experiments are shown.

4.7.3 Disruption of Ubr1 in 96Q and CG*-expressing cells results in increased toxicity

Despite the fact that overexpression of Ubr1 does not accelerate CG* degradation in the presence of 96QmCh, Ubr1 plays an important role in the clearance of misfolded proteins. We co-expressed 96Q with CG* or 20Q with CG* in Δ*Ubr1* cells. As controls, we used wild-type cells co-expressing 96Q with CG* or 20Q with CG*. We analyzed the survival rates of the cells grown on agar plates containing glucose or galactose (Figure 28).
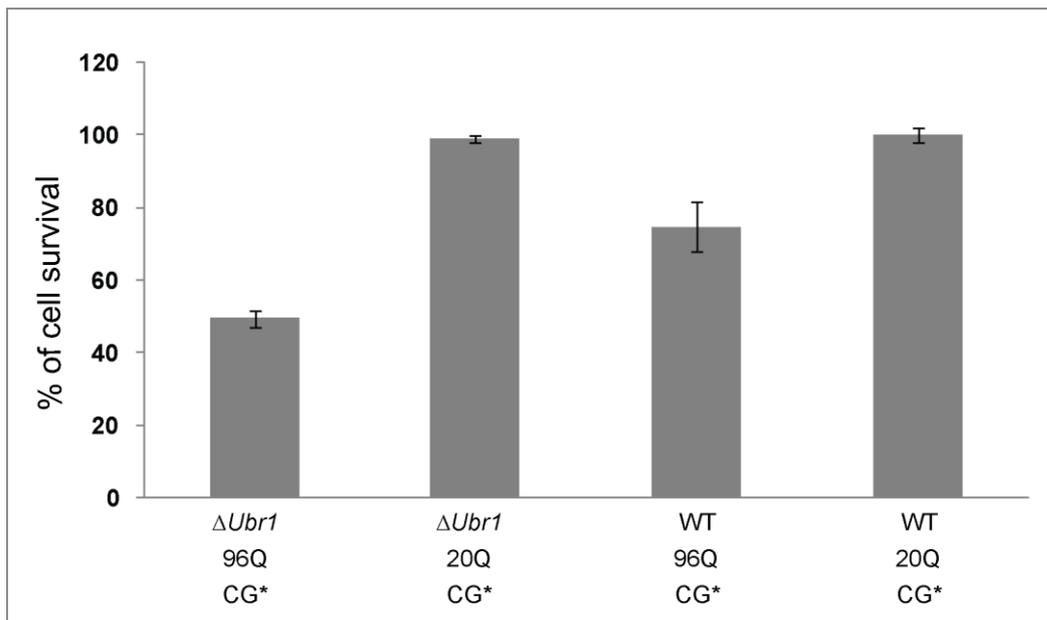
Figure 28. Co-expression of 96Q with CG* in *ΔUbr1* cells results in enhanced cytotoxicity.

The percent cell survival in *ΔUbr1* cells co-expressing polyQ proteins with CG* was assessed by counting the number of colonies on agar plates containing glucose or galactose after 4 days of culture at 30°C. WT refers to the BY4741 strain. Averages and the SD from three independent experiments are shown.

4.8   Interactome of 96Q by quantitative proteomic analysis

Misfolded proteins are involved in many aberrant interactions. For example, artificial β-sheet proteins sequester endogenous proteins into aggregates and cause cytotoxicity. Particularly vulnerable proteins for these interactions are the components of the metastable subproteome in the cell (Olzscha et al., 2011). The first line of defense against misfolded proteins with exposed hydrophobic residues consists of chaperones. Molecular chaperones are well known for their ability to modulate polyQ-dependent toxicity (Barral et al., 2004). Proteasomes and other components also play obvious roles in this interaction because misfolded protein must be degraded; however, these components would be involved in the later stages (Kim et al., 2013). 96Q likely interacts with chaperones, components of the proteasome and other proteins. 96Q interactions could inactivate or occupy proteins required for the efficient degradation of the misfolded substrates used in our study. To identify interacting proteins, we tested the interactome of 96Q versus the non-pathogenic 20Q protein. Among the interactors, we expected to find protein(s)that are required for CG* degradation and potentially for the degradation of the other misfolded proteins included in our study. If 96Q-interacting proteins are required for CG* degradation, then these proteins could be identified in a straightforward manner.

4.8.1 Identification of 96Q-interacting proteins

The results described above suggest that 96QmCh inhibits CG*degradation by sequestering one or more factors that act upstream of the proteasome in addition to ubiquitination. To identify proteins that preferentially interact with 96QmCh relative to 20QmCh, we performed a quantitative interactome analysis using SILAC (stable isotope labeling with amino acids in cell culture)(Ong and Mann, 2006). Cells co-expressing 96QmCh and CG*were labeled for 20 hr with a heavy lysine isotope, while cells co-expressing 20QmCh and CG* were grown in light medium to serve as the control sample. Using anti-myc antibody, 96QmCh and 20QmCh were isolated from cell extracts that had been clarified by centrifugation to remove polyQ inclusions. The isolated fractions were mixed in a 1:1 ratio and were separated by SDS-PAGE followed by in-gel digestion and LC-MS/MS analysis. Approximately 100proteins were enriched over 2-fold (and up to 100-fold) upon 96QmCh immunoprecipitation when compared with 20QmCh immunoprecipitation in at least two of three independent experiments. A list of the protein interactors that were increased in the presence of 96QmCh relative to 20QmCh is presented in Table 2.

Highly enriched proteins can be divided into several groups according to their function:

- Chaperones
- Glutamine-rich proteins
- Yeast prion proteins
- UPS components
- Nuclear pore complex proteins
- Vesicle transport

Interestingly, many 96QmCh-interacting proteins localized to the nucleus. We found 76 proteins with nuclear or nuclear/cytosolic localization that interacted with96QmCh. As we have shown before, 96QmCh was located primarily in the cytosol and not in the nucleus. However, we are unable to completely rule out partial nuclear 96QmCh localization that cannot be detected due to degradation or other reasons, which could explain the enrichment of interactions observed with nuclear proteins in our experiment. Furthermore, PolyQ proteins have been reported to localize to the nucleus, supporting partial localization of 96QmCh in the nucleus(Havel et al., 2009). To address this question, experiments with MG132 or other proteasome inhibitors should be performed; however, these experiments are beyond the scope of our study.

UPS components

Some UPS components were enriched in the 96QmCh fraction when compared with the 20QmCh fraction. We observed a 20-fold increase in Dsk2 in the 96QmCh fraction when compared with the 20QmCh fraction. Dsk2 is a ubiquitin-binding protein that plays a role in many processes such as the degradation of other proteins and spindle pole body duplication (Biggins et al., 1996). Three proteins that were enriched were Rpn5, Rpn1 and Rpn11. These proteins, which are components of the 26S proteasome, were enriched in the 96QmCh fraction by 4-, 3- and 3-fold increases, respectively.

Chaperones

Chaperones and co-chaperones were strongly enriched in the 96QmCh fraction. We observed a 29-fold increase in Sis1 co-immunoprecipitation in the 96QmCh fraction. We also observed an 8-fold increase in Ssa2 co-immunoprecipitation in the 96QmCh fraction. Ssa1 and Ssa4 were both enriched 4-fold, and Ydj1 was enriched 3-fold in the 96QmCh fraction when compared with the 20QmCh fraction. Cytosolic Hsp70 and Hsp40 members also strongly interacted with pathogenically expanded polyQ, which is consistent with observations made from our immunoprecipitation data that will be discussed later.

Q-rich proteins

Another category of polyQ interactors is glutamine-rich (Q-rich) proteins. Pathogenic polyQ proteins are known to co-aggregate with other proteins that are Q-rich (Steffan et al., 2000; Nucifora et al., 2001). Pub1 was 104.3-fold enriched in the 96QmCh fraction relative to the 20QmCh fraction. Pub1 is a poly(A)+ RNA-binding protein, an abundant mRNP component protein, that binds mRNA and is required for mRNA stability. Another protein that was highly enriched in the 96QmCh fraction is Sgt2. Sgt2 was enriched 50-fold in the 96QmCh fraction. Sgt2 is a cytoplasmic co-chaperone that is required for the complex formation of Get4, Get5 and other TRC complex members(Chang et al., 2010).This complex mediates the posttranslational insertion of tail-anchored proteins into the ER membrane. Def1 is another polyQ-containing chaperone that was enriched 39-fold in the 96QmCh fraction. Def1 is an RNAPII degradation factor that functions in a complex with the Rad26 protein (Woudstra et al., 2002).

Yeast prions

Many yeast prions were enriched in the 96QmCh fraction relative to the 20QmCh fraction. Cyc8 was enriched 87-fold in the 96QmCh fraction. Cyc8 is a transcriptional co-repressor and a part of the transcriptional co-activator complex that recruits the SWI/SNF and SAGA complexes to

promoters. Yeast prion Rnq1 was enriched 7-fold in the 96QmCh fraction. Rnq1 is an infectious prion protein that results in the [PIN+] phenotype in yeast. Sup35 was enriched 6-fold. The Sup35 protein functions as the translation termination factor eRF3. In prion form,Sup35 expression results in the [PSI+] phenotype (Lindquist et al., 2001;Derkatch et al., 2004). Pin3 was 4-fold enriched in the 96QmCh fraction. Pin3 is a negative regulator of actin nucleation-promoting activity. Pin3 also induces the appearance of [PIN+] when overproduced (Derkatch et al., 2001).

Nuclear pore complex

We observed a 34-fold enrichment of Nup100 protein in the 96QmCh fraction relative to the 20QmCh fraction. Nup100 is an FG-nucleoporin component of the central core of the nuclear pore complex (Rout et al., 2000). A 10-fold enrichment of Nup116 was also observed in the 96QmCh fraction. Nup116 is a paralog of Nup100. Nsp1 was 4-fold enriched in the 96QmCh fraction. Nsp1 is a part of the nuclear pore complex and is an FG-nucleoporin component.

Vesicle transport

Two proteins involved in vesicle transport were enriched in the 96QmCh fraction relative to the 20QmCh fraction. Pan1 and Ent1 were enriched 24 and 18 times, respectively. Pan1 is a part of the actin cytoskeleton-regulatory complex Pan1-Sla1-End3 (Wendland et al., 1996). Ent1 is an epsin-like protein that takes part in endocytosis and actin patch assembly.

Table 2. List of 96Q interactors.

The SILAC labeling experiment was repeated in triplicate with swapped SILAC labeling patterns: 96QmCh, CG* (H) versus 20QmCh, CG* (L) or 96QmCh, CG* (L) versus 20QmCh, CG* (H). 96Q interacting proteins were enriched by at least 2-fold in the immunoprecipitation of 96QmCh when compared with the immunoprecipitation of 20QmCh in at least 2 out of 3 independent experiments. Interacting proteins were sorted from high to low according to their degree of enrichment in the 96QmCh fraction (based on a ratio of 96QmCh/20QmCh). The background value is a median for three independent SILAC experiments. Labeling in the table: gene ID, systematic name in the Saccharomyces Genome Database (SGD); standard name, gene name in SGD; description, protein information; 96QmCh/20QmCh ratio, enrichment of 96QmCh co-immunoprecipitation over the 20QmCh fraction; MW, molecular weight; E, essentiality; localization, subcellular localization by pSORT (cyto, cytosol; cysk, cytoskeletal; nucl, nucleus).

	Gene ID	Gene name	Description	96QmCh/20QmCh Ratio	MW (kDa)	E	Localization
1	YNL016W	PUB1	Nuclear and cytoplasmic polyadenylated RNA-	104.3	50.8		cyto/nucl

			binding protein				
2	YER162C	RAD4	DNA repair protein RAD4	87.5	87.2		nucl
3	YBR112C	CYC8	General transcriptional corepressor CYC8	87.1	107.2		nucl
4	YOR007C	SGT2	Small glutamine-rich tetratricopeptide repeat-containing	50.2	37.2		cyto/nucl
5	YNL084C	END3	Actin cytoskeleton-regulatory complex protein	44.2	40.3		nucl
6	YKL054C	DEF1	RNAPII degradation factor	39.2	84.0		nucl
7	YKL068W	NUP100	Nucleoporin NUP100	34.3	100.0		nucl
8	YGR136W	LSB1	LAS seventeen-binding protein 1	32.6	26.1		nucl
9	YDR099W	BMH2	Protein BMH2	31.7	31.1		nucl
10	YNL007C	SIS1	Protein SIS1	29.4	37.6	E	cyto
11	YIR006C	PAN1	Actin cytoskeleton-regulatory complex protein PAN1	23.9	160.3	E	nucl
12	YMR276W	DSK2	Ubiquitin domain-containing protein	20.5	39.3		nucl
13	YDL161W	ENT1	Epsin-1	18.2	52.4		nucl
14	YER177W	BMH1	Protein BMH1	14.5	30.1		nucl
15	YNL208W	YNL208W	Uncharacterized protein	13.9	20.2		nucl
16	YOR265W	RBL2	Tubulin-specific chaperone A	12.9	12.4		nucl
17	YMR047C	NUP116	Nucleoporin NUP116	10.1	116.2	E	nucl
18	YPR181C	SEC23	Protein transport protein SEC23	9.7	85.4	E	cyto/nucl
19	YDR505C	PSP1	Growth inhibitory protein 5	8.3	95.3		nucl
20	YLL024C	SSA2	Heat-shock protein SSA2	7.6	69.5		cyto
21	YGR250C	YGR250C	Uncharacterized RNA-binding protein	7.6	89.5		nucl

22	YOL111C	MDY2	Ubiquitin-like protein MDY2	7.5	23.7		nucl
23	YOR197W	MCA1	Metacaspase-1	7.2	48.0		nucl
24	YDR405W	MRP20	54S ribosomal protein L41	7.0	30.6		mito
25	YCL028W	RNQ1	[PIN+] prion protein RNQ1	7.0	42.6		nucl
26	YCR093W	NOT1	General negative regulator of transcription subunit 1	7.0	240.3	E	plas
27	YPR088C	SRP54	Signal recognition particle subunit SRP54	6.2	59.6	E	cyto
28	YHR030C	SLT2	Mitogen-activated protein kinase SLT2	6.2	55.6		nucl
29	YGL014W	PUF4	Pumilio homology domain family member 4	6.1	97.8		nucl
30	YBR018C	GAL7	Galactose-1-phosphate uridylyltransferase	6.0	42.4		nucl
31	YDR172W	SUP35	Translation release factor 3	5.8	76.6 E		nucl
32	YPL243W	SRP68	Signal recognition particle subunit SRP68	5.1	69.0	E	nucl
33	YPL210C	SRP72	Signal recognition particle subunit SRP72	5.0	73.5	E	nucl
34	YPL190C	NAB3	Nuclear polyadenylated RNA-binding protein 3	4.9	90.4	E	nucl
35	YIL033C	BCY1	cAMP-dependent protein kinase regulatory subunit	4.5	47.2		nucl
36	YKL032C	IXR1	Intrastrand cross-link recognition protein	4.5	67.9		nucl
37	YDL226C	GCS1	ADP-ribosylation factor GTPase-activating protein	4.4	39.3		nucl
38	YGR178C	PBP1	PAB1-binding protein 1	4.4	78.8		nucl
39	YNL091W	NST1	Stress response protein NST1	4.3	141.5		nucl

40	YOR164C	YOR164C	UPF0363 protein YOR164C	4.2	36.3		cyto
41	YJL041W	NSP1	Nucleoporin NSP1	4.2	86.5	E	mito
42	YAL005C	SSA1	Heat shock protein SSA1	4.2	69.7		cyto
43	YER103W	SSA4	Heat shock protein SSA4	4.1	69.7		cyto
44	YPR154W	PIN3	[PSI+] inducibility protein 3	4.0	23.5		nucl
45	YDL147W	RPN5	26S proteasome regulatory subunit RPN5	3.9	51.8	E	nucl
46	YGL112C	TAF6	Transcription initiation factor TFIID subunit 6	3.8	57.9	E	cyto/nucl
47	YIL036W	CST6	Chromosome stability protein CST 6	3.8	65.3		nucl
48	YJL066C	MPM1	Mitochondrial peculiar membrane protein 1	3.7	28.5		cyto
49	YKL173W	SNU114	Growth inhibitory protein 10	3.7	114.0	E	nucl
50	YGL234W	ADE5	Phosphoribosylamine-glycine ligase	3.6	86.1		cyto
51	YBL007C	SLA1	Actin cytoskeleton-regulatory complex protein SLA1	3.5	135.8		nucl
52	YMR124W	YMR124W	Uncharacterized protein YMR124W	3.3	105.9		nucl
53	YIR001C	SGN1	RNA-binding protein SGN 1	3.2	29.0		nucl
54	YML105C	SEC65	Signal recognition particle subunit SEC65	3.2	31.2	E	nucl
55	YHR027C	RPN1	26S proteasome regulatory subunit RPN1	3.2	109.5		nucl
56	YNL064C	YDJ1	Yeast dnaJ protein 1	3.0	44.7		cyto
57	YBR172C	SMY2	Suppressor of MYO2-66 protein	3.0	81.4		nucl

58	YDL053C	PBP4	Protein PBP4;PBP1-binding protein 4	3.0	19.9		nucl
59	YJR045C	SSC1	Heat shock protein SSC1	2.8	70.6	E	mito
60	YNL059C	ARP5	Actin-related protein 5	2.8	87.6		nucl
61	YIL115C	NUP159	Nucleoporin NUP159	2.8	158.9	E	cyto/nucl
62	YJL061W	NUP82	Nucleoporin NUP82	2.8	82.1	E	nucl
63	YMR214W	SCJ1	DnaJ-related protein SCJ1	2.8	41.5		cyto/nucl
64	YDR171W	HSP42	Heat shock protein 42	2.7	42.8		nucl
65	YIL109C	SEC24	Protein transport protein SEC24	2.7	103.6	E	nucl
66	YFR004W	RPN11	26S proteasome regulatory subunit RPN11	2.7	34.4	E	cyto
67	YGR264C	MES1	Methionyl-tRNA synthetase	2.7	85.7	E	cyto
68	YIL070C	MAM33	Mitochondrial acidic protein MAM33	2.6	30.1		mito
69	YLL013C	PUF3	mRNA-binding protein PUF3	2.5	98.1		nucl
70	YMR318C	ADH6	NADP-dependent alcohol dehydrogenase 6	2.5	39.6		cyto
71	YPL235W	RVB2	RuvB-like protein 2	2.5	51.6	E	cysk
72	YIL041W	GVP36	36 kDa Golgi vesicle protein	2.5	36.7		nucl
73	YBR019C	GAL10	Galactose mutarotase	2.4	78.2		cyto
74	YML008C	ERG6	Sterol 24-C-methyltransferase	2.4	43.4		cyto
75	YGR204W	ADE3	Methenyltetrahydrofolate cyclohydrolase	2.4	102.2		cyto
76	YHR121W	LSM12	Sm-like protein 12	2.4	21.3		cyto/nucl
77	YDR190C	RVB1	RuvB-like protein 1	2.3	50.5	E	cyto
78	YAL021C	CCR4	Glucose-repressible alcohol dehydrogenase transcriptional effector	2.3	94.7		nucl
79	YIL075C	RPN2	26S proteasome regulatory subunit RPN2	2.3	104.2	E	cyto
80	YFR002W	NIC96	Nucleoporin NIC96	2.3	96.2		nucl

81	YCL009C	ILV6	Acetolactate synthase small subunit	2.3	34.0		mito
82	YOR117W	RPT5	26S protease regulatory subunit 6A	2.3	48.3	E	nucl
83	YBR169C	SSE2	Heat shock protein homolog SSE2	2.3	77.6		cyto
84	YLR187W	SKG3	Suppressor of lethality of KEX2-GAS1 double null mutant protein 3	2.3	114.1		nucl
85	YJL081C	ARP4	Actin-related protein 4	2.2	54.8	E	nucl
86	YIL108W	YIL108W	Putative zinc metalloproteinase	2.2	77.4		cyto
87	YGL048C	RPT6	26S protease regulatory subunit 8 homolog	2.2	45.3	E	cysk
88	YPR108W	RPN7	26S proteasome regulatory subunit RPN7	2.2	49.0	E	nucl
89	YOR141C	ARP8	Actin-like protein ARP8	2.2	100.2		nucl
90	YMR033W	ARP9	Chromatin structure-remodeling complex protein ARP9	2.2	53.1	E	nucl
91	YPL106C	SSE1	Heat shock protein homolog SSE1	2.2	77.4		cyto
92	YLR025W	SNF7	Vacuolar-sorting protein SNF7	2.1	27.0		nucl
93	YNL088W	TOP2	DNA topoisomerase 2	2.1	164.2	E	nucl
94	YDL097C	RPN6	26S proteasome regulatory subunit RPN6	2.1	49.8	E	nucl
95	YDR394W	RPT3	26S protease regulatory subunit 6B homolog	2.1	47.9	E	nucl
96	YBR198C	TAF5	Transcription initiation factor TFIID subunit 5	2.1	89.0	E	nucl
97	YOR091W	TMA46	Translation machinery-associated protein 46	2.1	39.5		nucl
98	YKR001C	VPS1	Vacuolar protein sorting-associated protein 1	2.0	78.7		nucl

99	YFL024C	EPL1	Enhancer of polycomb-like protein 1	2.0	96.7	E	nucl
100	YBR160W	CDC28	Cell division control protein 28	2.0	34.1	E	cyto/nucl
101	YDR117C	TMA64	Translation machinery-associated protein 64	2.0	64.0		nucl
102	YGL150C	INO80	Putative DNA helicase INO80	2.0	171.5	E	nucl
103	YKL145W	RPT1	26S protease regulatory subunit 7 homolog	2.0	52.0	E	nucl
104	YHL034C	SBP1	Single-stranded nucleic acid-binding protein	2.0	33.0		cyto/nucl
105	YOL006C	TOP1	DNA topoisomerase 1	2.0	90.0		nucl
106	YFL039C	ACT1	Actin	2.0	41.7	E	cysk

4.8.2 CG* stabilization by 96Q depends on [PIN+] prion status of the cell

Our results show that 96QmCh interacts with yeast prions. Rnq1 was enriched 7-fold in the 96Q fraction relative to the 20Q fraction in our SILAC experiment. The Rnq1 protein can induce the [PIN+] phenotype, which is known to influence the aggregation of other polyQ-containing proteins in the cell (Derkatch et al., 2001;Derkatch et al., 2004). We tested whether CG* stabilization by 96Q was dependent on the [PIN+] status of the cells. Most yeast strains are [PIN+] (Manogaran et al., 2010). To generate the [pin-] phenotype, we incubated YPH499 in YPD medium containing 3mM GuCl (Jung and Masison, 2001). After overnight incubation, cells were transferred to YPD medium containing 3mM GuCl, and the incubation was repeated for two additional rounds. Cells were plated on agar plates containing YPD. Individual colonies were then tested for [pin-] status. Cells were transformed with Rnq-GFP, and [pin-] strains displayed diffuse GFP fluorescence throughout the cytosol (Figure 29).
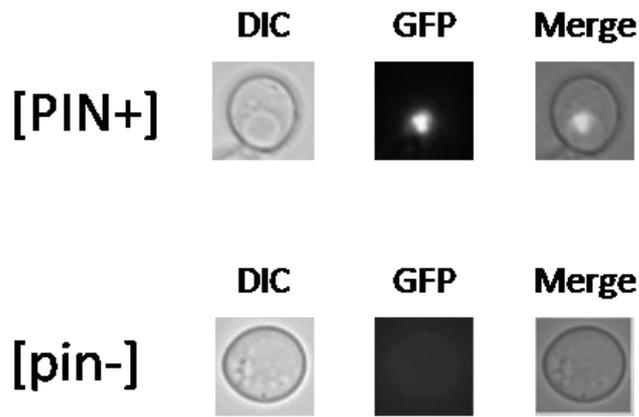
Figure 29. [PIN+] and [pin-] status of YPH499 cells expressing Rnq-GFP before and after incubation in 3mM GuCl YPD medium.

96Q expressed in the [pin-] background does not interfere with the degradation of CG*

96QmCh and CG* were co-expressed in [PIN+] or [pin-] cells. 96QmCh stabilization of CG* was observed only in [PIN+] cells, whereas CG* expressed in [pin-] cells was not stabilized by 96QmCh. The [PIN+] and [pin-] status of the cells had a profound impact on the ability of the cells to degrade misfolded proteins. These results are shown in Figure 30.

A

B

Figure 30. CG* is not stabilized by 96QmCh in [pin-] cells.

96QmCh and CG* were co-expressed in [PIN+] and [pin-] cells. CG* degradation was analyzed by CHX chase, SDS-PAGE and immunoblotting using anti-myc, GFP and PGK antibodies. PGK was included as a loading control. (B) CG* was quantified by densitometry analysis. Averages and the SD from three independent experiments are shown.

A similar effect was observed for the degradation of NLS-CG* in [pin-] cells. 96QmCh and NLS-CG* were co-expressed in [PIN+] and [pin-] cells. NLS-CG* stabilization was observed only in [PIN+] cells, whereas NLS-CG* was not stabilized by 96QmCh in [pin-] cells. These results are shown in Figure 31.

A

Figure 31. NLS-CG* is not stabilized by 96QmCh in [pin-] cells.

96QmCh and NLS-CG* were co-expressed in [PIN+] and [pin-] cells. NLS-CG* degradation was analyzed by CHX chase, SDS-PAGE and immunoblotting with anti-myc, GFP and PGK antibodies. PGK was included as a loading control. (B) NLS-CG* was quantified by densitometry analysis. Averages and the SD from three independent experiments are shown.

In addition, we studied the influence of the [PIN+] and [pin-] phenotypes on CTG* degradation in 96QmCh-expressing cells. 96QmCh and CTG* were co-expressed in [PIN+] and [pin-] cells. CTG* stabilization by 96QmCh was observed only in [PIN+] cells, whereas CTG* stabilization by 96QmCh was not observed in [pin-] cells. These results are shown in Figure 32. The [pin-] status of the cell appears to play a pivotal role in the degradation of misfolded proteins in the presence of 96QmCh.
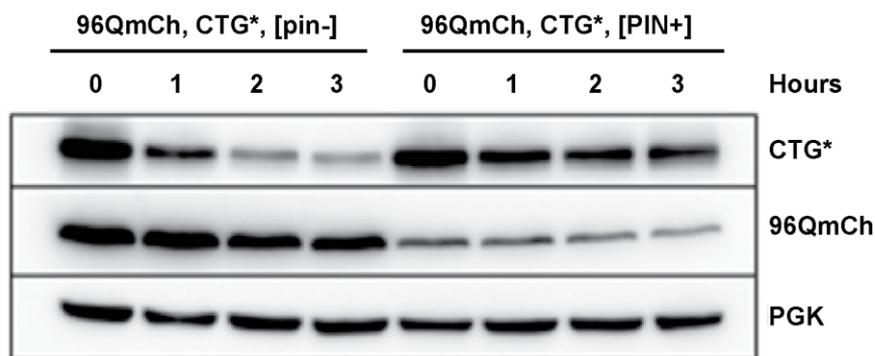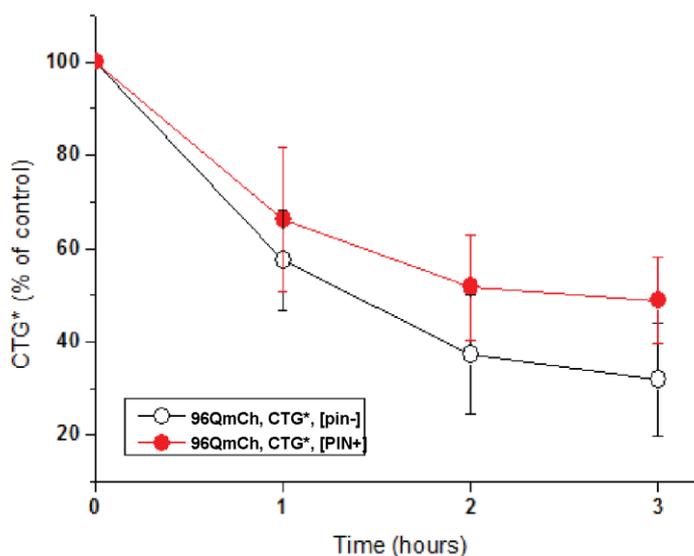
Figure 32. CTG* is not stabilized by 96QmCh in [pin-] cells.
96QmCh and CTG* were co-expressed in [PIN+] and [pin-] cells. CTG* degradation was analyzed by CHX chase, SDS-PAGE and immunoblotting with anti-myc, GFP and PGK antibodies. PGK was included as a loading control. (B) CTG* was quantified by densitometry analysis. Averages and the SD from two independent experiments are shown.

As shown in the preceding figures, several combinations of co-expressed misfolded proteins were toxic. To follow up on these observations, we determined whether the cytotoxicity observed previously was dependent on [PIN+] status. 96QmCh and CG*, 96QmCh and NLS-CG* or 96QmCh and CTG* were co-transformed into [PIN+] or [pin-] cells. Interestingly, [pin-] cells expressing the combinations of 96QmCh and CG*, 96QmCh and NLS-CG* or 96QmCh and CTG* did not demonstrate detectable growth inhibition, whereas the expression of any of these combinations in [PIN+] cells resulted in growth inhibition (Figure 33). We suspect that [pin-]

status affects certain important properties of polyQ proteins rendering polyQ proteins less prone to aggregation, thereby alleviating their cytotoxic effects.

[PIN+]

[pin-]
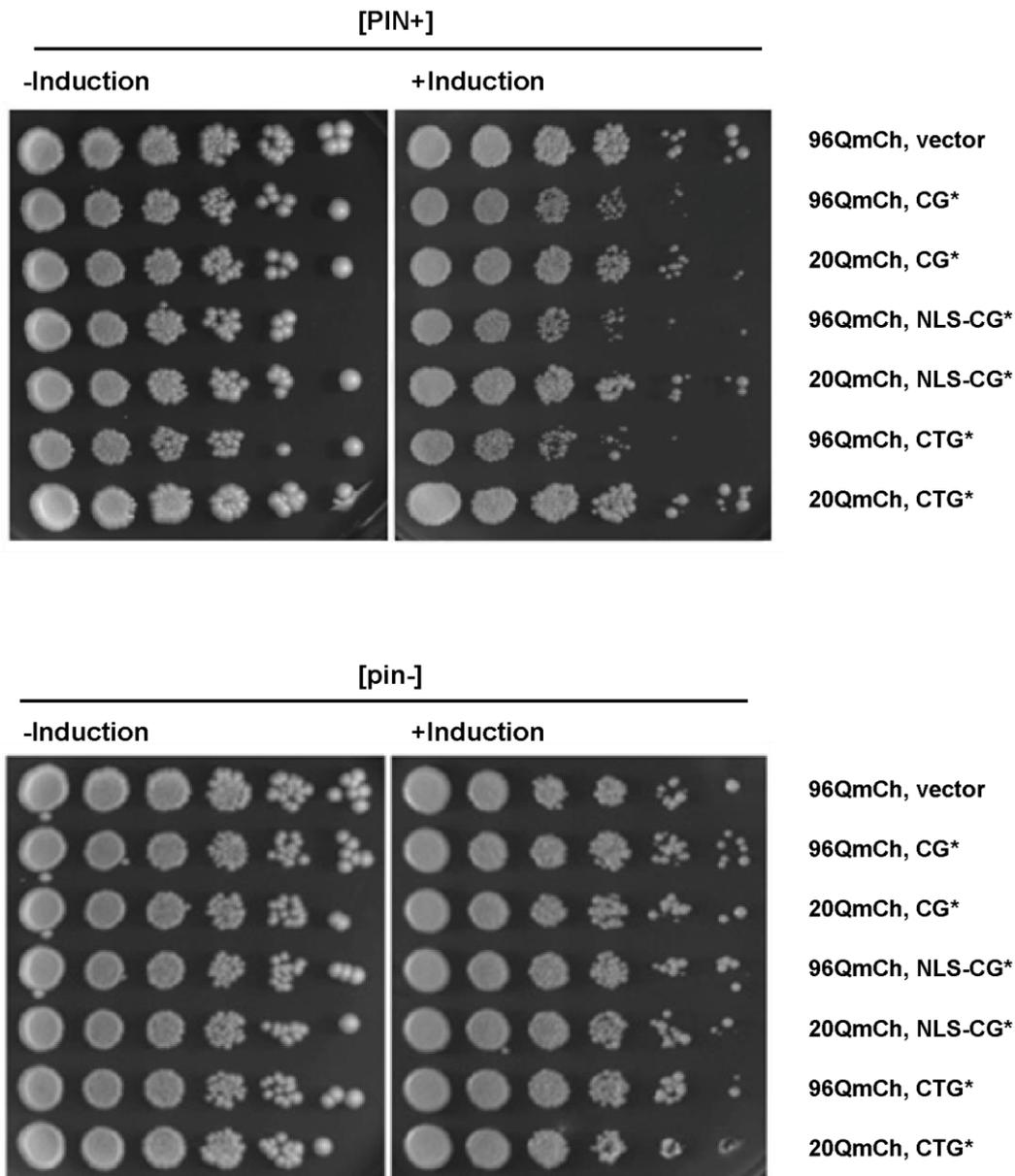
Figure 33. Growth of [pin-] and [PIN+] cells on plates.

Growth of cells was assessed as described for Figure 16. Plates were incubated for 4 days at 30°C.

Chaperone capacity is increased in [pin-] cells

96QmCh did not inhibit protein degradation in [pin-] cells. Moreover, we observed no growth inhibition caused by the co-expression of 96QmCh and CG*. This could occur because 96QmCh

interacted differently with chaperones and other proteins due to conformational changes. To determine the status of the most important interactors of misfolded proteins (i.e., chaperones), we co-expressed 96QmCh with CG* and 20QmCh with CG* in [PIN+] and [pin-] cells. Immunoprecipitation (IP), SDS-PAGE and immunoblotting were performed, and the results are presented in Figure 34. 96QmCh expressed in [PIN+] cells strongly interacted with Sis1, Ssa1 and Ydj1. In contrast, 96QmCh expressed in [pin-] cells exhibited reduced interactions with all chaperones tested. These data suggest that in [pin-] cells expressing 96QmCh, cellular chaperone capacity was increased due to fewer interactions between 96QmCh and the chaperones. Chaperones interacted to a lesser extent with 96QmCh in [pin-] cells and thus could execute their customary chaperone functions. The pool of available chaperones had more access to Sis1, Ssa1 and Ydj1, which indicates that total chaperone capacity was increased. Because of the increase in chaperone capacity, co-expression of 96QmCh and CG* was not cytotoxic at least in part because the available pool of chaperones was able to handle their normal housekeeping tasks.
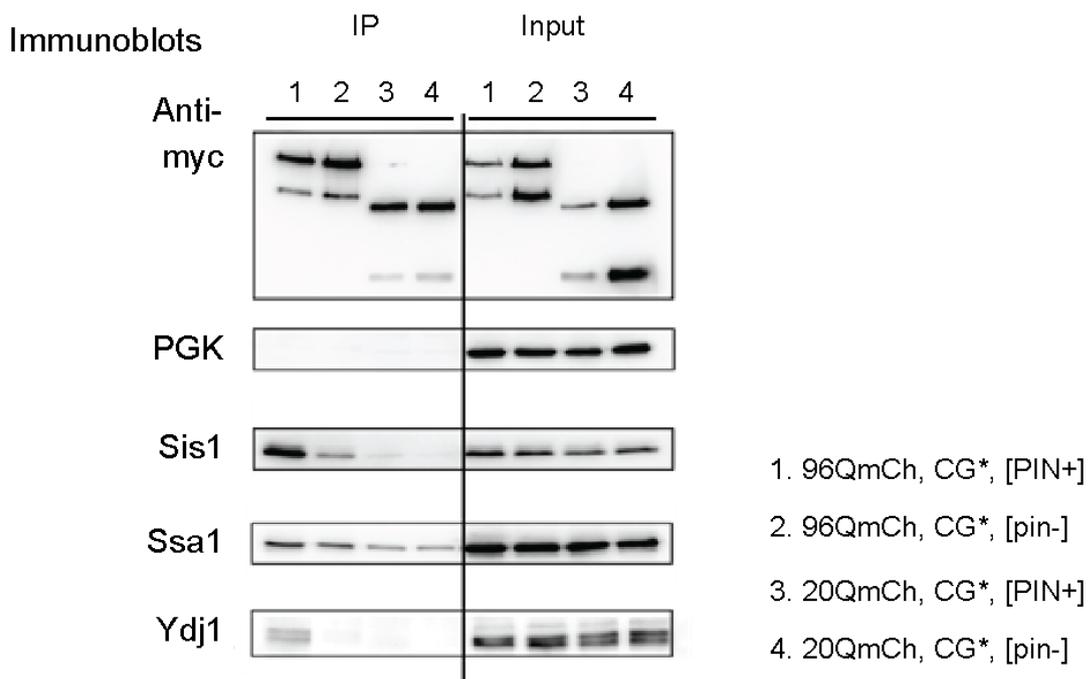

Figure 34. Interaction of 96QmCh with chaperones in [pin-] cells.

96QmCh and 20QmCh were immunoprecipitated from the indicated cells with an anti-myc antibody. The association of polyQ proteins with chaperones was analyzed using anti-Sis1, Ssa1 and Ydj antibodies. PGK was included as a control for loading (in the input fraction) and as a specificity marker (in the IP fraction) because PGK should not interact with the 96QmCh and 20QmCh proteins.

Ssa1 and Ydj1 overexpression do not promote CG* degradation

As observed in Figure 34, Ssa1 and Ydj1 interacted with 96QmCh. CG* degradation depends on the assistance of these proteins for its proteasomal degradation(Park et al., 2007). Therefore, the aberrant interaction of 96QmCh with Ssa1 and Ydj1 could be a rate-limiting factor for the degradation of the reporter proteins used in this work. The depletion of cellular levels of Ssa1 and Ydj1 by 96QmCh for CG* degradation could represent an underlying reason for CG* stabilization under these conditions.

To test this hypothesis, we co-expressed 96QmCh and CG* together with Ssa1 under the control of the *GAL1* promoter and then analyzed the rate of degradation of CG*. Overexpression of Ssa1 did not improve the clearance of CG* in the presence of 96QmCh. Interestingly, Ssa1 overexpression partially stabilized CG* degradation in cells expressing 20QmCh. These results are shown in Figure 35.
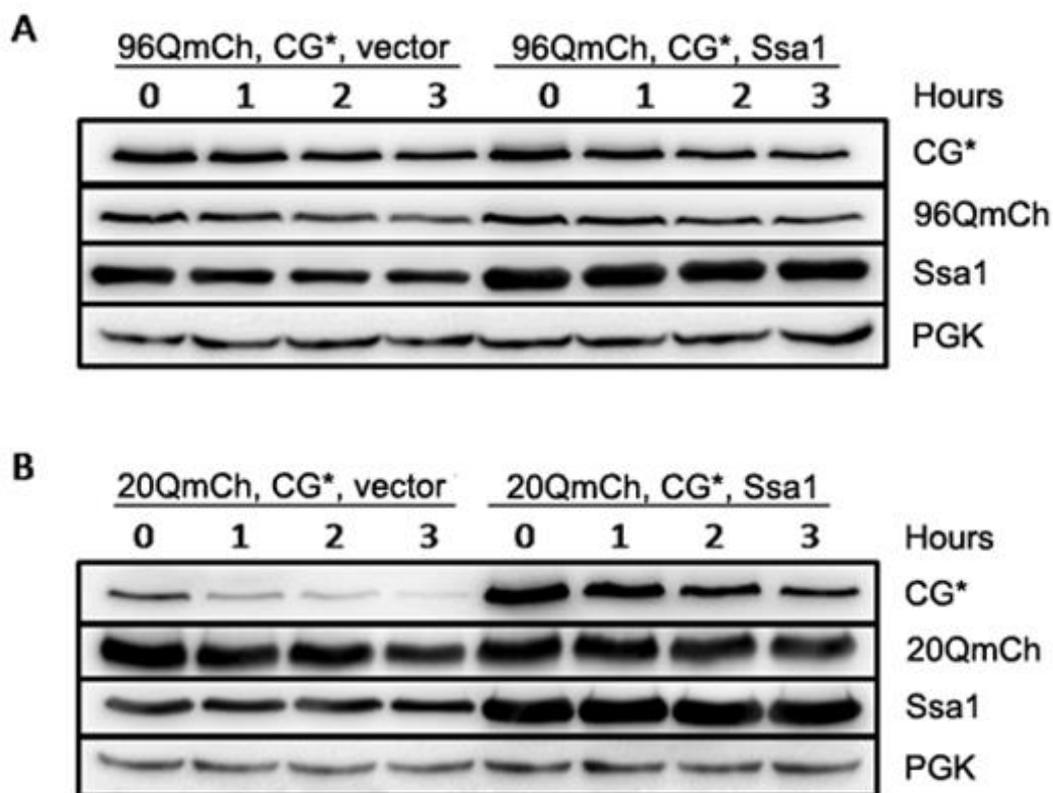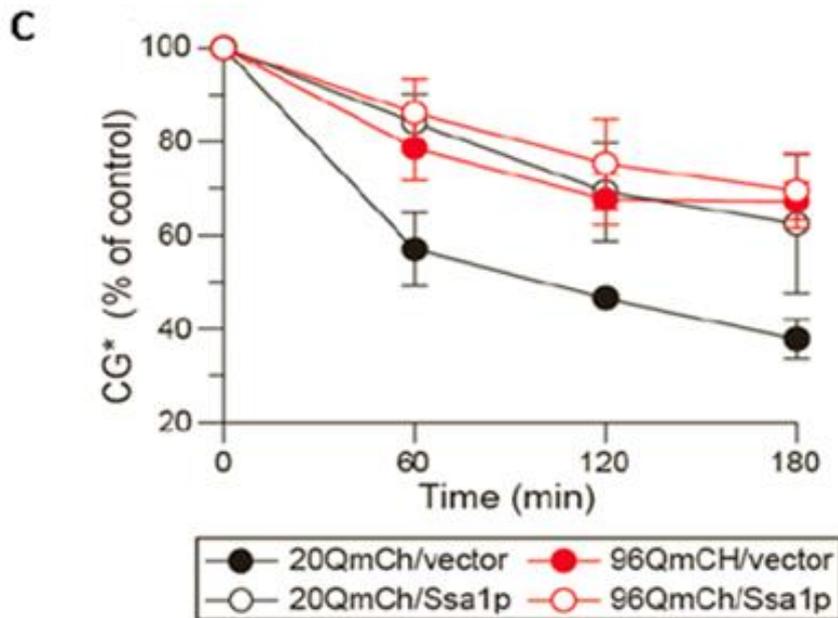
Figure 35. Overexpression of Ssa1 does not restore CG* degradation in the presence of 96Q.

(A and B) Ssa1p was overexpressed under the control of the *GAL1* promoter in cells co-expressing CG* with 20QmCh or 96QmCh. CG*, polyQ proteins and Ssa1 were detected by immunoblot analysis of cell lysates using anti-GFP, myc and Ssa antibodies, respectively. PGK antibody was included as a loading control (C) CG* was quantified.

Ydj1 was also tested as a possible rate limiting factor for CG* degradation by 96QmCh. When Ydj1 was overexpressed in combination with 96QmCh, CG* degradation did not increase. Similarly, Ydj1 was overexpressed in combination with CG* in the presence of non-pathogenic 20QmCh, which resulted in the stabilization of CG*. These results are shown in Figure 36.
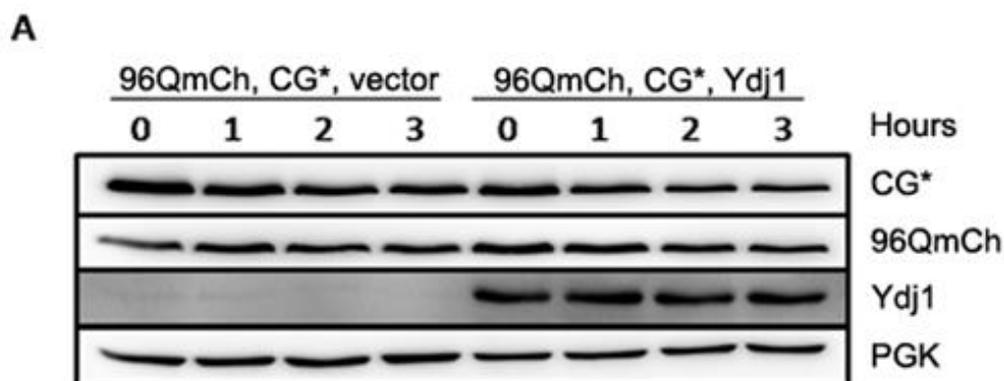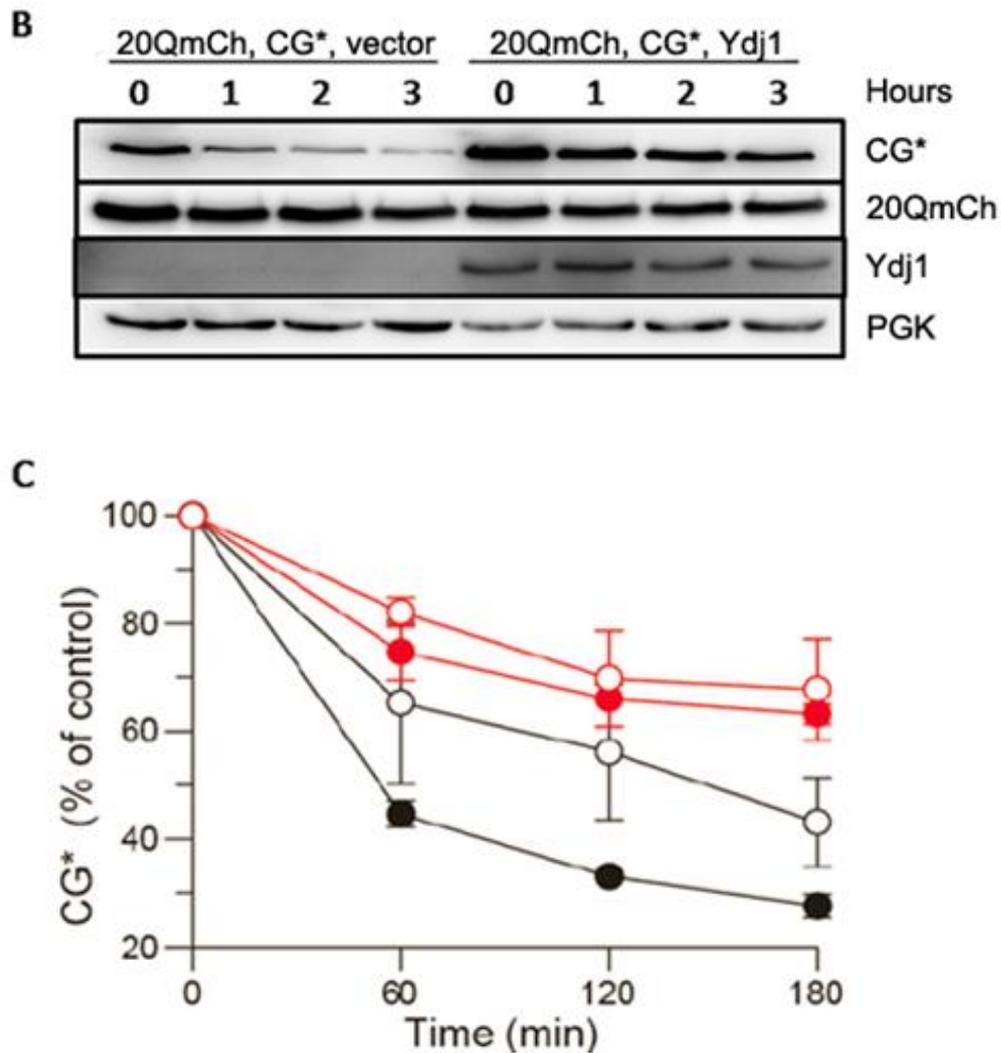
Figure 36. Ydj1 overexpression inhibits CG* degradation.

(A and B) Ydj1 was overexpressed under the control of the *GAL1* promoter in cells co-expressing CG* with 20QmCh or 96QmCh. CG*, polyQ proteins and Ydj1 were detected by immunoblot analysis of the cell lysates using anti-GFP, myc and Ydj antibodies, respectively. PGK antibody was included as a loading control (C) CG* was quantified.

Furthermore, overexpression of Ssa1 or Ydj1 in combination with 96QmCh reduced the formation of SDS-insoluble polyQ aggregates. These results are presented in Figure 37.
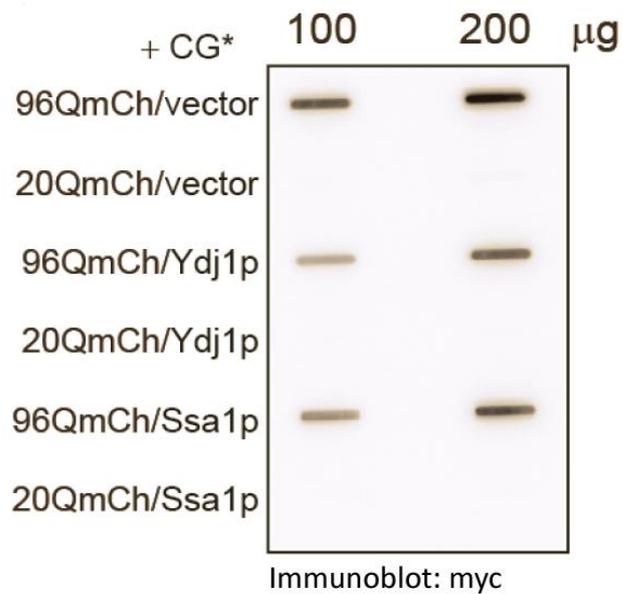
Figure 37. Ydj1 or Ssa1 overexpression reduces the amounts of SDS-insoluble polyQ aggregates.

Lysates of cells expressing the indicated proteins were analyzed in a filter-trap assay in the presence of SDS to visualize SDS-insoluble 96QmCh aggregates. PolyQ proteins were detected with an anti-myc antibody. One hundred micrograms and 200 µg of total protein was loaded onto the membrane to visualize the results.

To assess the effects of chaperones on cytotoxicity, we co-expressed Ssa1 or Ydj1 in cells containing 96QmCh and CG* or 20QmCh and CG*. As controls we used cells co-expressing 96QmCh, CG* and empty vector and cells co-expressing 20QmCh, CG* and empty vector. These strains were used to assess the effects of the chaperones and co-chaperones in a growth test. Ssa1 did not significantly affect the growth of cells expressing 96QmCh and CG*. In contrast, Ydj1 overexpression improved the growth of cells expressing 96QmCh and CG*. These results are shown in Figure 38.
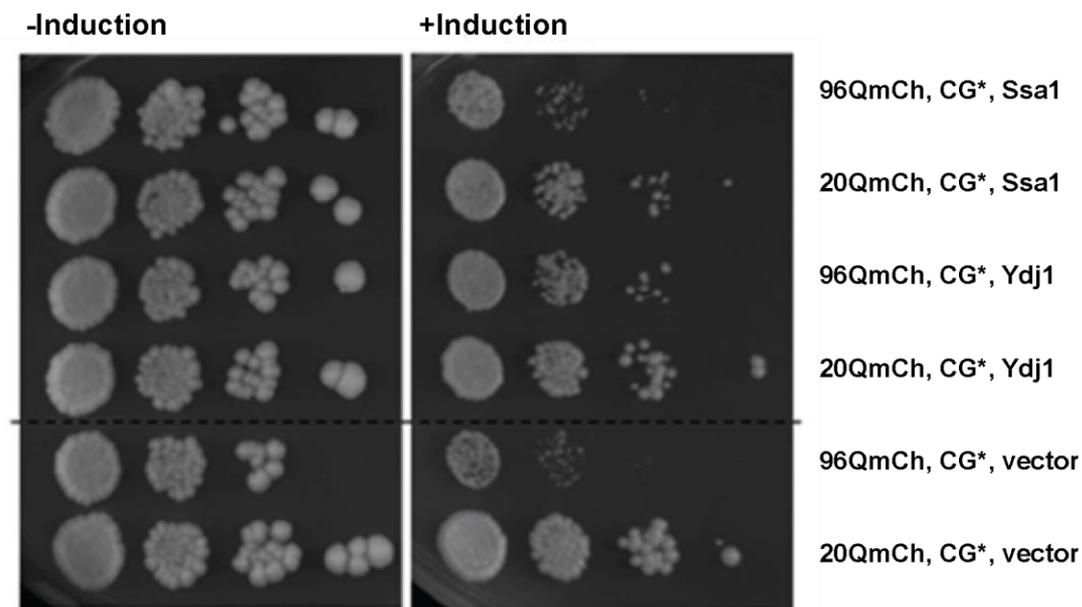
Figure 38. Ydj1 overexpression partially rescues the growth of cells expressing 96QmCh and CG*.

The cells indicated above were diluted six-fold and spotted on agar plates containing 2% glucose (-Induction) or 2% galactose (+Induction). CG* was expressed from a multi-copy plasmid under the control of the *CPY* promoter (average level of expression). Plates were incubated for 4 days at 30°C.

This result was confirmed by counting the number of cells grown under similar conditions. Cells co-expressing 96QmCh and CG* in the presence of Ydj1 demonstrated a higher percent cell survival (Figure 39).
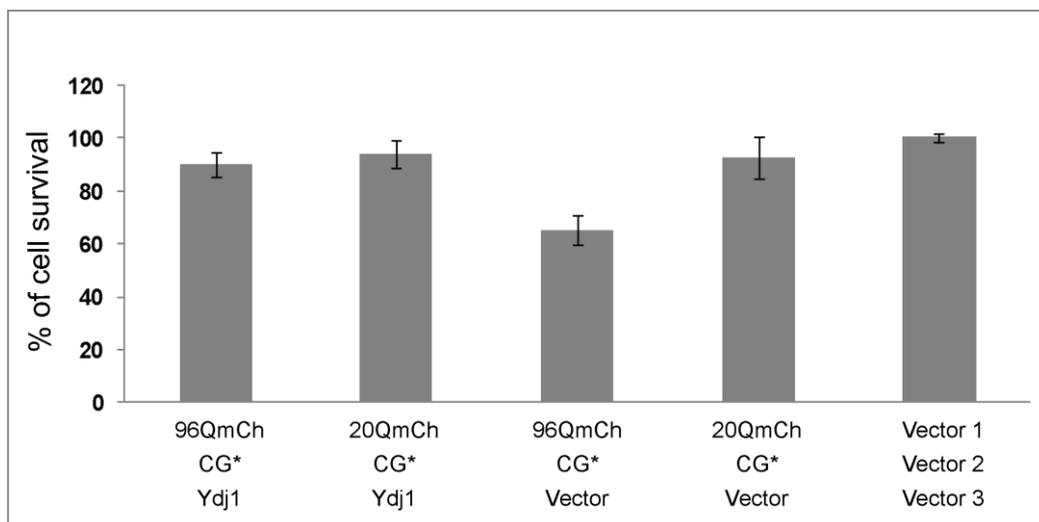

Figure 39. Ydj1 overexpression suppresses 96QmCh and CG* toxicity.

Percent cell survival was assessed by counting the number of colonies on agar plates containing glucose or galactose after growth for 4 days at 30°C.Averages and the SD from three independent experiments are shown.

4.8.3 Sis1 overexpression in the 96Q background restores the degradation of misfolded proteins

We identified 96Q interacting proteins in a systematic way. We hypothesized the existence of a factor X that is depleted due to its interaction with 96Q. This factor should be required for the degradation of CG*, NLS-CG*, CPY* and CTG*. Thus, if factor X binds to polyQ proteins, it cannot assist in the degradation of other misfolded proteins. Furthermore, if this factor is present in the cell in low abundance, then factor X could be subjected to depletion. Likewise, overexpression of factor X should be able to restore the degradation of misfolded proteins even in the presence of polyQ protein. The overexpression of factor X would hypothetically remove the excess pressure on the protein quality control systems in the cell thereby alleviating the cytotoxicity caused by the co-expression of 96Q and CG*.

Sis1 overexpression rescues CG, NLS-CG* and CTG* degradation in 96QmCh-expressing cells*

To identify factor X according to our hypothesis, we analyzed the list of 96QmCh interacting proteins obtained from our SILAC experiments. As discussed in previous sections, the Sis1 chaperone strongly interacted with 96QmCh to an extent that could result in the depletion of Sis1 from the pool of available chaperones in the cell. The abundance of different chaperones and co-chaperones in the cell is presented in the Table 3. Compared with other chaperones, Sis1 protein is in much lower abundance. Therefore, the strong association between Sis1and 96QmChwould likely impact the availability of this chaperone. Sis1 overexpression is a reasonable experiment that could demonstrate whether this proteinis a limiting factor for the degradation of misfolded proteins in the presence of 96QmCh.

Table 3. Chaperone and co-chaperone abundance in *S.cerevisiae*.

This table was prepared based on a study performed in the laboratory of Prof. Weissman (Ghaemmaghami et al., 2003; SGD, http://www.yeastgenome.org)**.**

Chaperone	Molecules/cell
Sis1	20,300
Ydj1	119,000
Ssa1	269,000
Ssb1	170,000

Cells co-expressing 96QmCh and CG* or 20QmCh and CG* with Sis1 overexpression or empty vector were generated. Cells were cultivated in glucose-containing medium overnight and then were shifted to 2% galactose/raffinose medium. After 15 hours of incubation in the galactose/raffinose medium, the cells were subjected to a CHX chase experiment. Then, SDS-PAGE and immunoblotting were performed. The overexpression of Sis1 strongly promoted CG* degradation in the presence of 96QmCh and removed the "degradation block" imposed by 96QmCh overexpression on CG*. These results are shown in Figure 40.
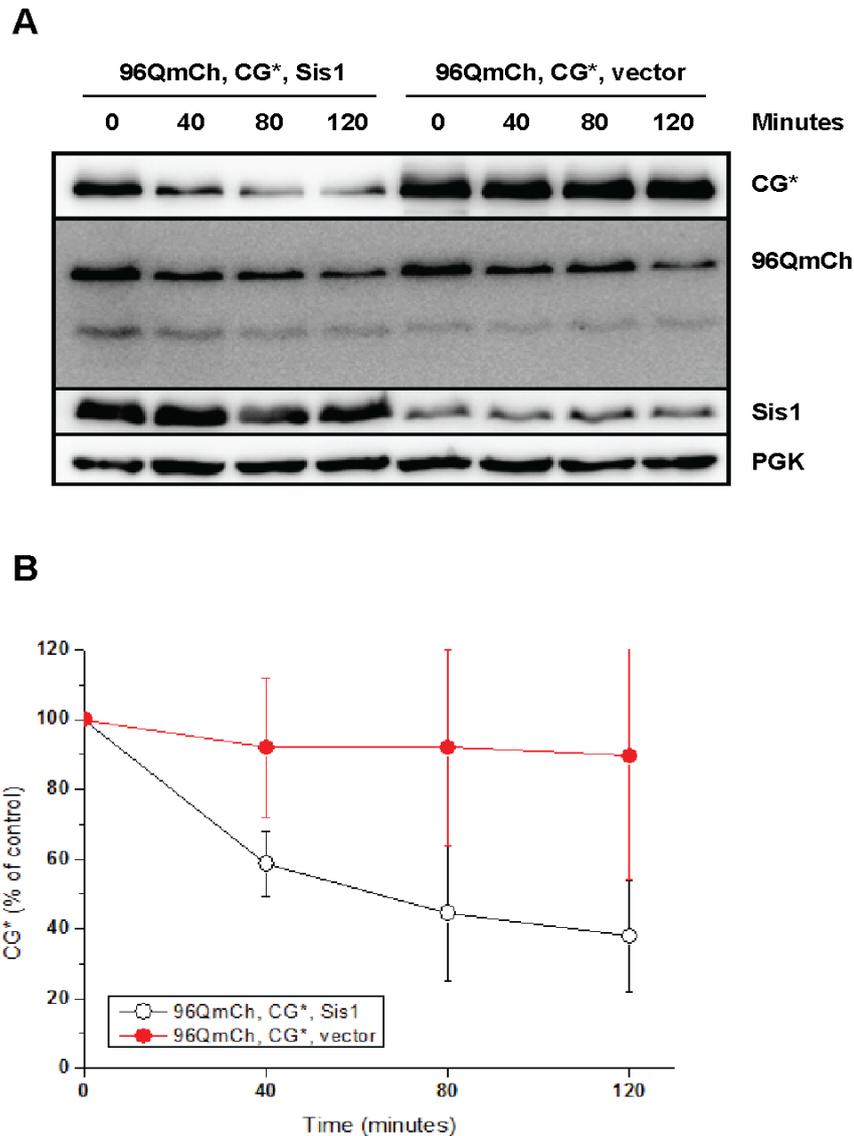

Figure 40. Sis1 overexpression accelerates CG* degradation in 96QmCh-expressing cells.

(A) A CHX chase assay was performed as described in the Materials and Methods section. Samples were collected every 40 minutes for 2 hours. Cells co-expressing 96QmCh, CG*, and Sis1 or 96QmCh, CG*, and empty vector were collected at the indicated time points and frozen in liquid nitrogen. Samples were subjected to SDS-PAGE and western blot analysis using anti-myc, GFP, Sis1 and PGK antibodies. (B) Densitometry analysis of CG* in the 96QmCh-expressing strain with or without overexpression of the Sis1 protein. Averages and the SD from three independent experiments are shown.

Sis1 overexpression also increased CG* degradation, even in the absence of a degradation block by 96QmCh. In the figure below, cells co-expressing 20QmCh and CG* with or without Sis1 overexpression were analyzed by the CHX chase assay. Overexpression of Sis1 increases the degradation speed of CG* in the presence of 20QmCh (Figure 41).
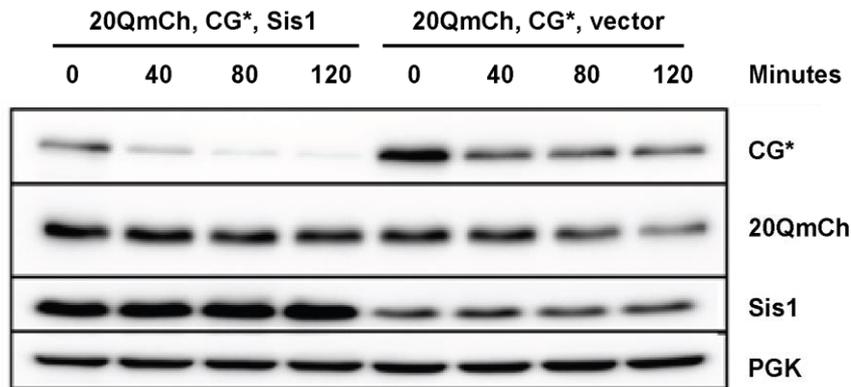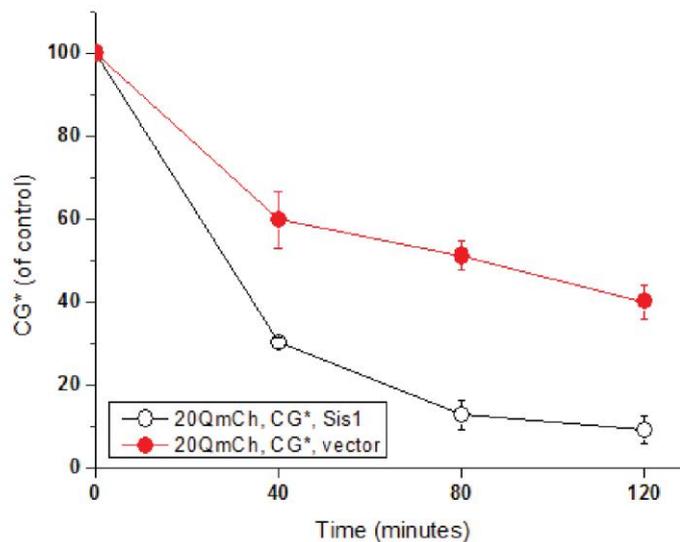

Figure 41. Sis1 overexpression accelerates CG* degradation in 20QmCh-expressing cells.

(A) A CHX chase assay was performed as described in the Materials and Methods section. Samples were collected every 40 minutes for 2 hours. Cells co-expressing 20QmCh, CG* and Sis1 or 20QmCh, CG* and empty vector were collected at the indicated time points and frozen in liquid nitrogen. Samples were subjected to SDS-PAGE and western blot analysis using anti-myc, GFP, Sis1 and PGK antibodies. (B) Densitometry analysis of CG* in the 20QmCh-expressing strain with or without overexpression of the Sis1 protein. Averages and the SD from three independent experiments are shown.

Sis1 overexpression also increased the degradation of NLS-CG* in cells expressing 96QmCh. This effect was not as strong when compared with the effect of Sis1 overexpression on CG* degradation in the same strain. These results are shown in Figure 42.
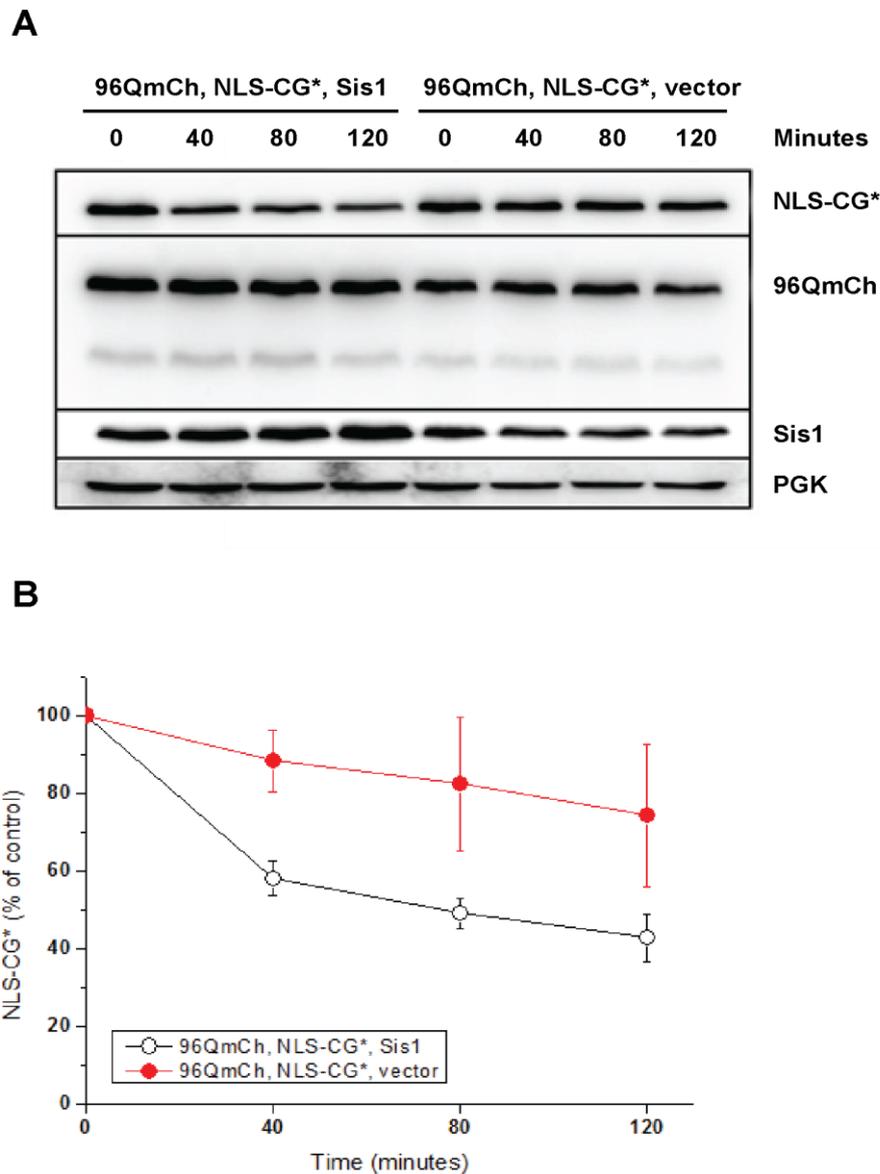
Figure 42. Sis1 overexpression accelerates NLS-CG* degradation in 96QmCh-expressing cells.

(A) A CHX chase assay was performed as described in the Materials and Methods section. Samples were collected every 40 minutes for 2 hours. Cells co-expressing 96QmCh, NLS-CG* and Sis1 or 96QmCh, NLS-CG* and empty vector were collected at the indicated time points and frozen in liquid nitrogen. Samples were subjected to SDS-PAGE and western blot analysis using anti-myc, GFP, Sis1 and PGK antibodies. (B) Densitometry analysis of NLS-CG* in the 96QmCh-expressing strain with or without overexpression of the Sis1 protein. Averages and the SD from three independent experiments are shown.

Sis1 overexpression slightly increased degradation of the NLS-CG* reporter in the 20Q-expressing cells. However, NLS-CG* co-expressed with 20QmCh showed rapid degradation kinetics; therefore, it was difficult to determine whether a significant increase in NLS-CG* occurred in the presence of Sis1 overexpression. However, we observed an increase in NLS-CG* degradation in Sis1-overexpressing cells. The results are shown in Figure 43.
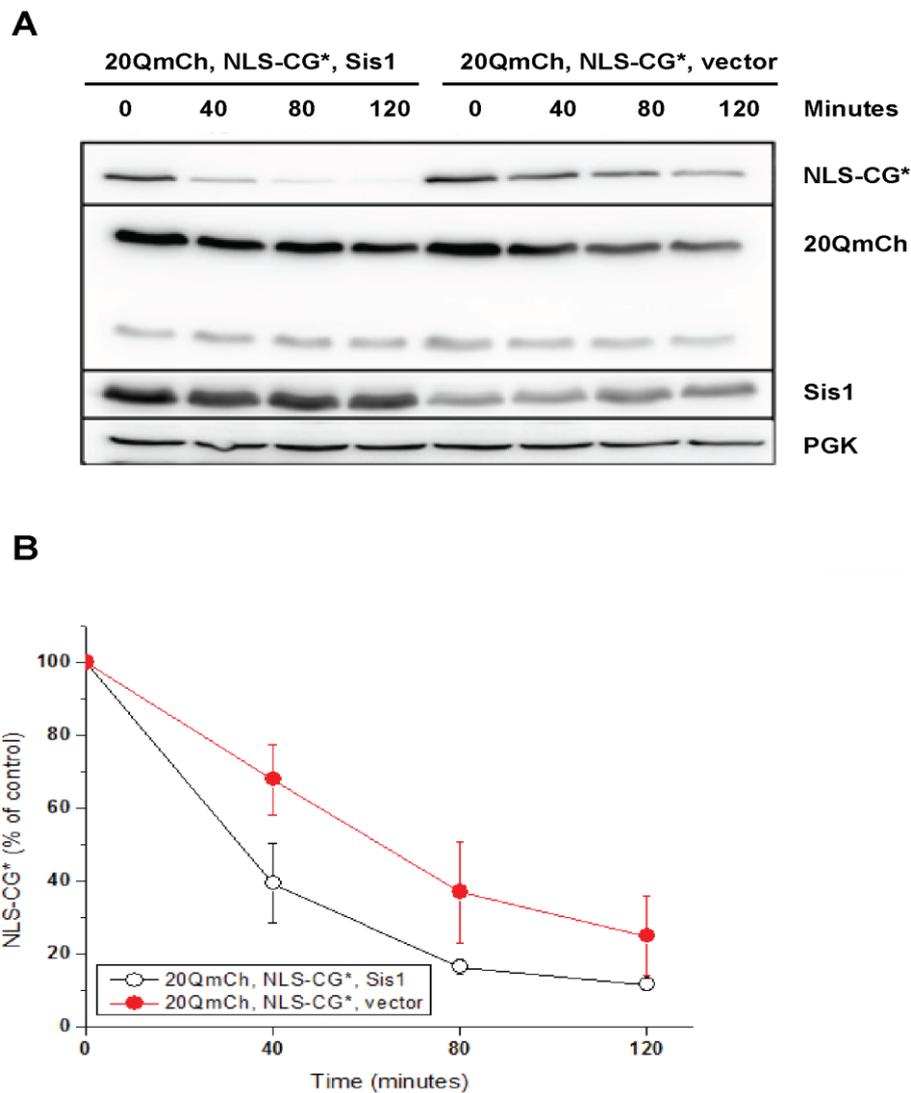

Figure 43. Sis1 overexpression accelerates NLS-CG* degradation in 20QmCh-expressing cells.

(A) A CHX chase assay was performed as described in the Materials and Methods section. Samples were collected every 40 minutes for 2 hours. Cells co-expressing 20QmCh, NLS-CG* and Sis1 or 20QmCh, NLS-CG* and empty vector were collected at the indicated time points and frozen in liquid nitrogen. Samples were subjected to SDS-PAGE and western blot analysis using anti-myc, GFP, Sis1 and PGK antibodies. (B) Densitometry analysis of NLS-CG* in the 20QmCh-expressing strain with or without overexpression of the Sis1 protein. Averages and the SD from three independent experiments are shown.

Sis1 overexpression did not rescue CPY*-HA degradation in the presence of 96QmCh. The degradation kinetics of CPY*-HA in Sis1-overexpressing and wild-type cells were similar. These results are shown in Figure 44.
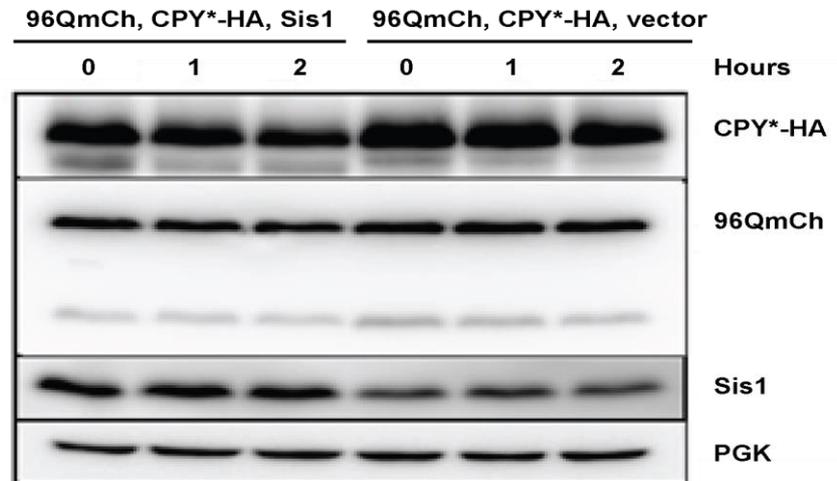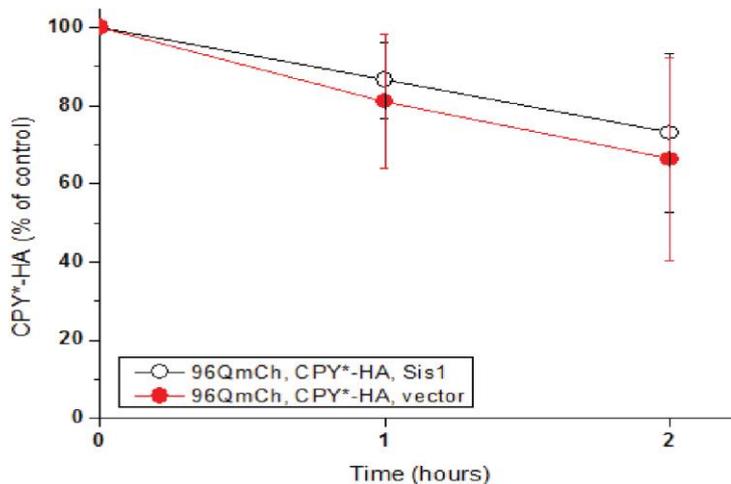

Figure 44. Sis1 overexpression does not accelerate CPY* degradation in 96QmCh-expressing cells.

(A) A CHX chase assay was performed as described in the Materials and Methods section. Samples were collected every 40 minutes for 2 hours. Cells co-expressing 96QmCh, CPY*-HA and Sis1 or 96QmCh, CPY*-HA and empty vector were collected at the indicated time points and frozen in liquid nitrogen. Samples were subjected to SDS-PAGE and western blot analysis using anti-myc, CPY, Sis1 and PGK antibodies. (B) Densitometry analysis of CPY*-HA in 96QmCh-expressing cells with or without the co-expression of Sis1 protein. Averages and the SD from three independent experiments are shown.

Similar results were observed for CPY*-HA expressed in the presence of 20QmCh. Sis1 did not increase the degradation kinetics of CPY*-HA in the presence of 20QmCh. These results are presented in Figure 45.
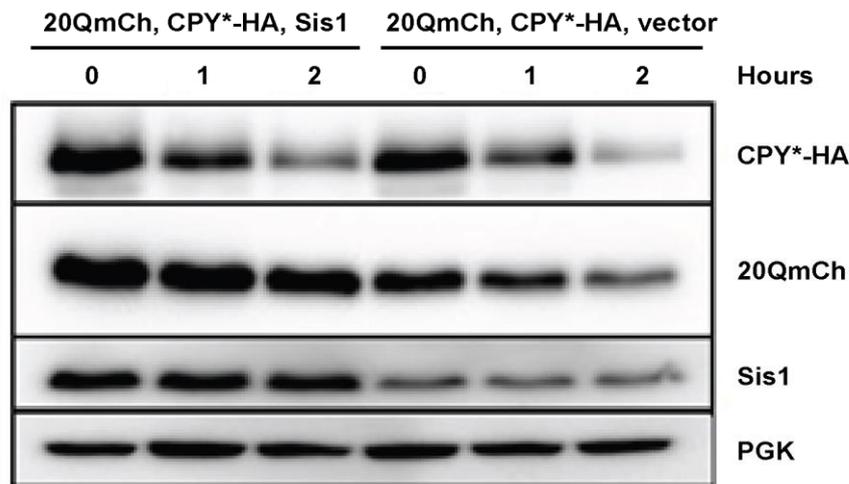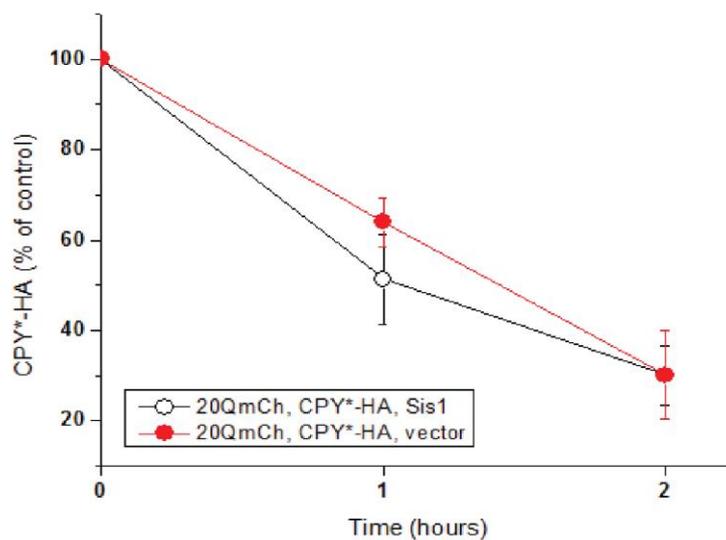

Figure 45. Sis1 overexpression does not accelerate CPY* degradation in 20QmCh-expressing cells.

(A) A CHX chase assay was performed as described in the Materials and Methods section. Samples were collected every 40 minutes for 2 hours. Cells co-expressing 20QmCh, CPY*-HA and Sis1 or 20QmCh, CPY*-HA and empty vector were collected at the indicated time points and frozen in liquid nitrogen. Samples were subjected to SDS-PAGE and western blot analysis using anti-CPY, myc, Sis1 and PGK antibodies. (B) Densitometry analysis of CPY*-HA in 20QmCh-expressing cells with or without overexpression of the Sis1 protein. Averages and the SD from three independent experiments are shown.

Sis1 overexpression did not rescue CTG* degradation in the presence of 96QmCh. The degradation kinetics of CTG* were similar in the presence or absence of Sis1 overexpression. These results are presented in Figure 46.

A

B
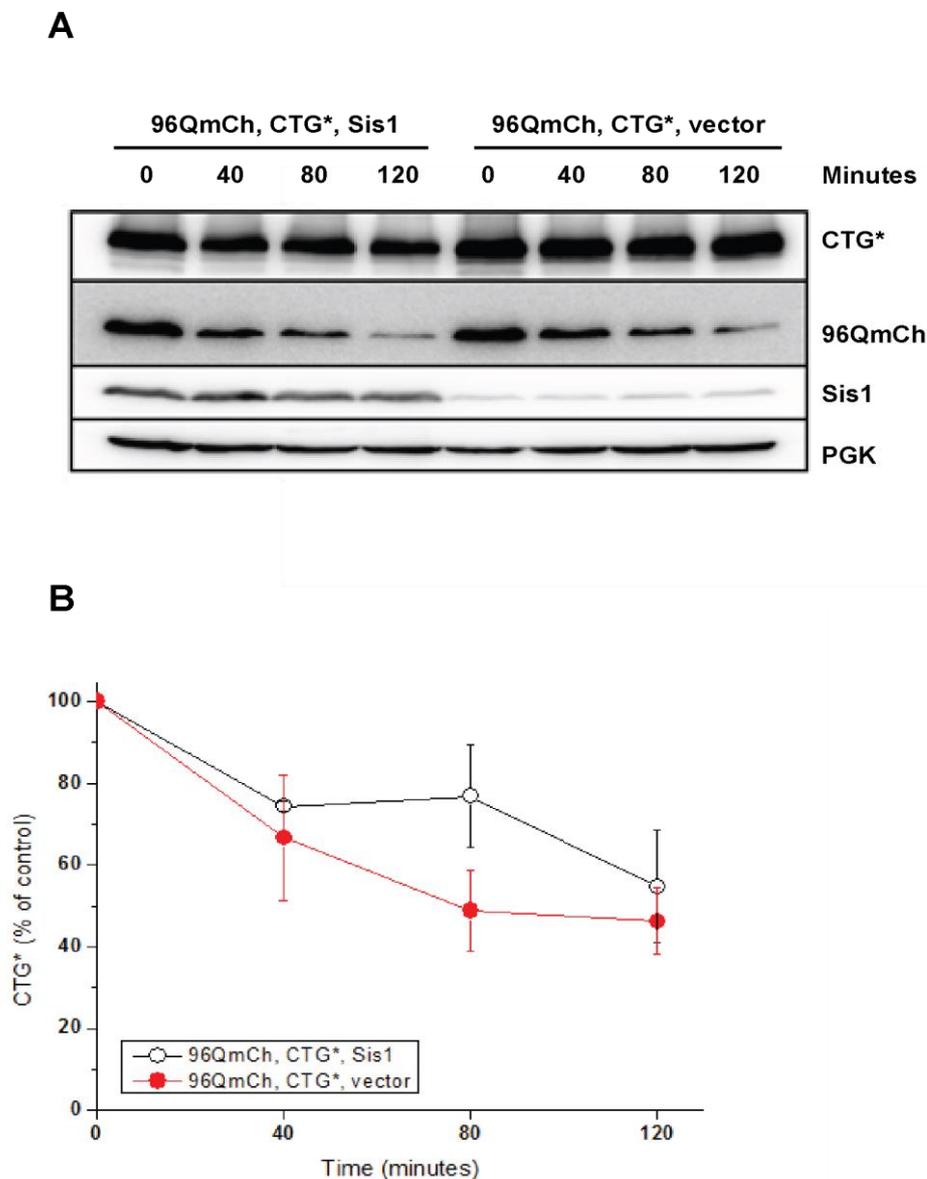
Figure 46. Sis1 overexpression does not accelerate CTG* degradation in 96QmCh-expressing cells.

(A) A CHX chase assay was performed as described in the Materials and Methods section. Samples were collected every 40 minutes for 2 hours. Cells co-expressing 96QmCh, CTG* and Sis1 or 96QmCh, CTG* and empty vector were collected at the indicated time points and frozen in liquid nitrogen. Samples were subjected to SDS-PAGE and western blot analysis using anti-GFP, myc, Sis1 and PGK antibodies. (B) Densitometry analysis of CTG* in the 96QmCh-expressing strain with or without overexpression of the Sis1 protein. Averages and the SD from three independent experiments are shown.

Similar results were observed when CTG* was overexpressed in the presence of 20QmCh. These results are shown in Figure 47.

A
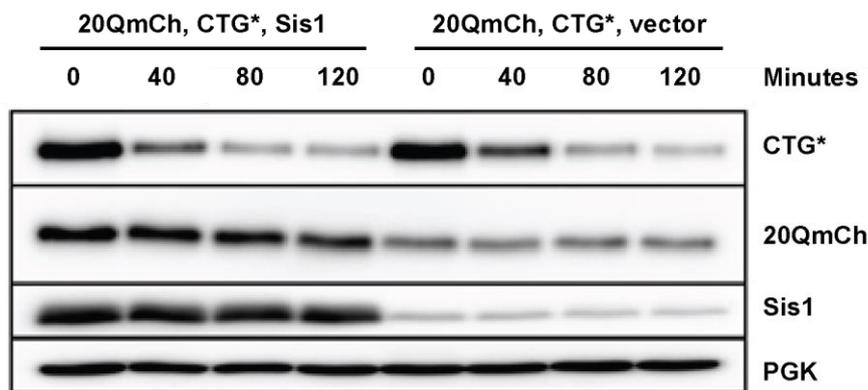
B
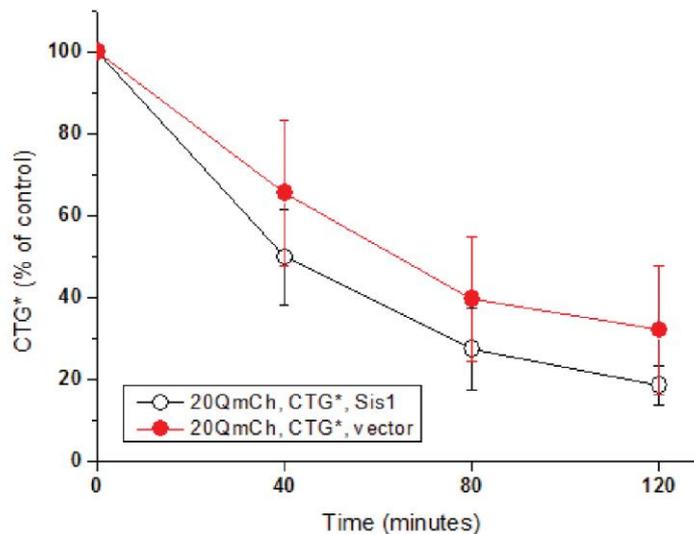
Figure 47. Sis1 overexpression does not accelerate CTG* degradation in 20QmCh-expressing cells.

(A) A CHX chase assay was performed as described in the Materials and Methods section. Samples were collected every 40 minutes for 2 hours. Cells co-expressing 20QmCh, CTG* and Sis1 or 20QmCh, CTG* and empty vector were collected at the indicated time points and frozen in liquid nitrogen. Samples were subjected to SDS-PAGE and western blot analysis using anti-myc, GFP, Sis1 and PGK antibodies. (B) Densitometry analysis of CTG* in 20QmCh-expressing cells with or without overexpression of the Sis1 protein. Averages and the SD from three independent experiments are shown.

Sis1 overexpression stimulates the stress response

Sis1 overexpression reversed the cytotoxicity observed in cells co-expressing 96QmCh and CG*. A possible explanation for this effect is that Sis1 promoted the degradation of CG*, and thus

misfolded proteins did not overburden the proteostasis capacity of the cell. However, another possibility is that Sis1 affected certain components of the proteostasis network consistent with an indirect effect of Sis1 on misfolded protein degradation.

Several combinations of the constructs 96QmCh, 20QmCh and empty vector were overexpressed in combination with Sis1 or with empty vector in yeast cells, after which the cells were subjected to a stress assay using the SSA3LacZ construct. Cells expressing Sis1 or empty vector were heat-shocked for 1 hour as control samples. Interestingly, Sis1 overexpression increased the expression of LacZ when compared with cells carrying empty vector under heat shock conditions. Furthermore, LacZ expression increased two-fold in cells co-expressing 96QmCh with Sis1 relative to cells expressing 96QmCh alone.Sis1-overexpressing cells produced a stronger stress response to pathogenic misfolded proteins. These data are shown in the Figure 48. The increased cytosolic stress response observed in cells expressing Sis1 under heat shock conditions could help explain how Sis1 stimulates the stress response to heat shock, but other possible explanations may exist. Sis1 overexpression may help maintain correct LacZ folding or could increase the mRNA levels of LacZ as a result of the stress response. These possibilities are partially controlled for by cells co-expressing 20QmCh, CG* and Sis1; however, other controls and experiments should also be considered to further validate our conclusions.
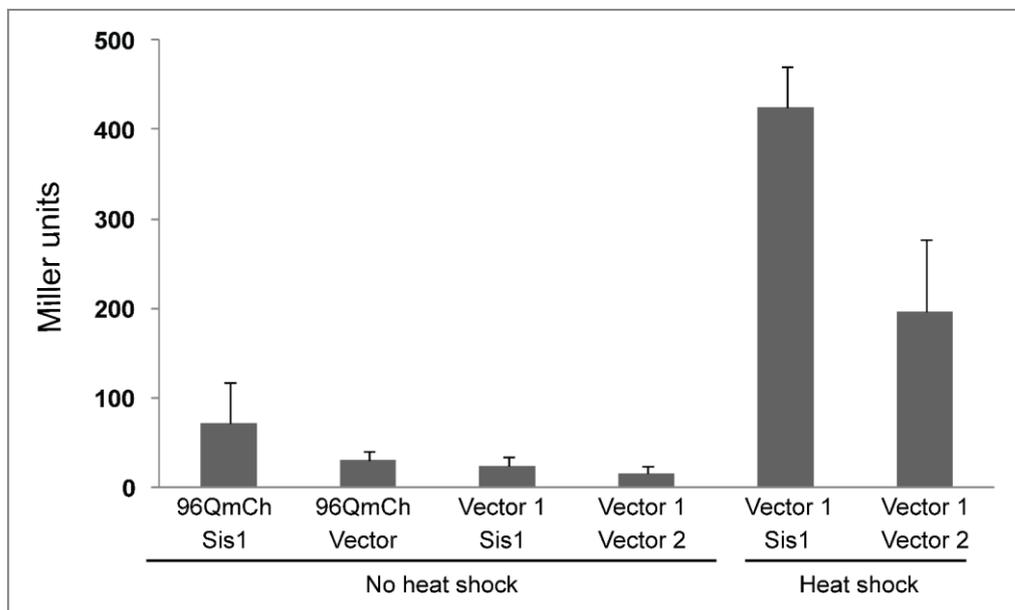
Figure 48. Cells overexpressing Sis1 mount a stronger heat shock response.

The expression of LacZ was measured in cells expressing 96QmCh alone or in combination with Sis1 at 30°C (no heat shock) and at 37°C (heat shock conditions). A LacZ activity test was performed as described in the Materials and Methods section, and the final values in Miller units were calculated. Averages and the SD from three independent experiments are shown.

4.9   The general requirement of Sis1 for terminally misfolded cytosolic proteins

4.9.1 Effects of Sis1 depletion on CG* degradation

To determine the extent of the involvement of Sis1 in the degradation of misfolded proteins independent of 96QmCh, Sis1 was depleted in cells. The original Sis1 promoter was replaced with a tetracycline-regulated promoter (Tet-Off). Sis1 promoter replacement resulted in a 20-25% reduction in Sis1protein levels when compared with the wild-type strain. In the Tet-Off SIS1 cells expressing CG*, significant stabilization of the reporter protein was observed in a CHX chase assay (Figure 49) even without the addition of doxycycline. The addition of doxycycline greatly reduced Sis1 expression levels and resulted in even stronger CG* stabilization. After 2 hours of CHX chase, 85% of misfolded protein remained (in the control, only 50% remained).
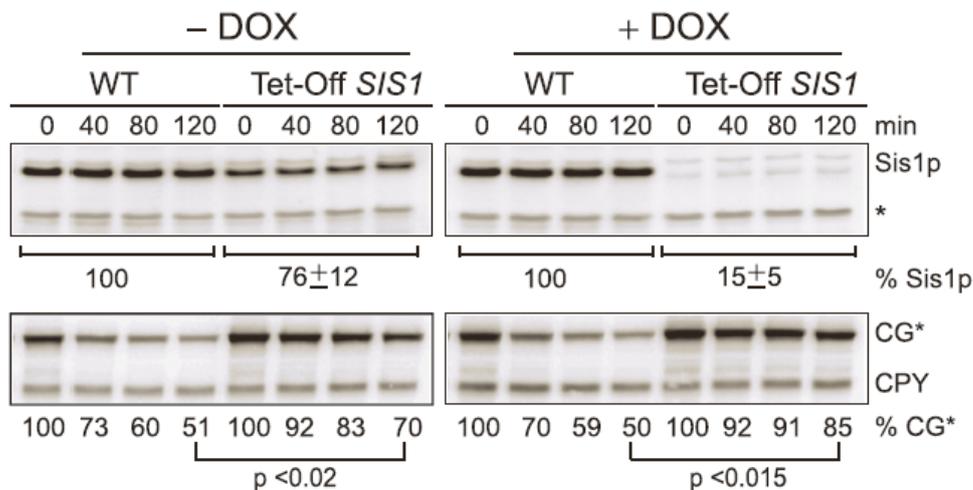
Figure 49. Moderate depletion of Sis1 results in CG* stabilization.

CG* was expressed in wild-type cells (R1158) and in Tet-Off SIS1 cells. Cells were grown for 20 hours without doxycycline (-DOX) or with 10 mg/ml doxycycline (+DOX). CG* degradation kinetics were analyzed. SDS-PAGE and immunoblotting were performed using anti-Sis1 and anti-CPY antibodies. Averages of at least three independent experiments and p-values for differences in the fractional CG* degradation after 120 min are indicated. A band cross-reacting with the anti-Sis1 antibody is indicated by the symbol *.Endogenous CPY was used as a loading control.

4.9.2 Sis1 cooperates with Hsp70 in the degradation of CG*

Sis1, as well as many other chaperones, requires other interacting partners to properly function. As the Sis1 protein belongs to the Hsp40 family type II protein, its interaction with the Hsp70

family depends on the HPD loop (Kampinga and Craig, 2010). This loop is situated in the J domain and consists of the amino acids His-Pro-Asp. We substituted the HPD-loop with an alanine amino acid sequence (Sis1AAA). Alternatively, we deleted the entire J domain corresponding to amino acids 1-76 (Sis1ΔJ).

Sis1AAA overexpression (in a wild-type Sis1-depleted background) did not increase the degradation kinetics of CG* as observed with wild-type Sis1 overexpression. In strains expressing Sis1AAA and CG*, CG* was stabilized, whereas the CG*degradation rate was increased in the presence of wild-type Sis1 (Figure 50).
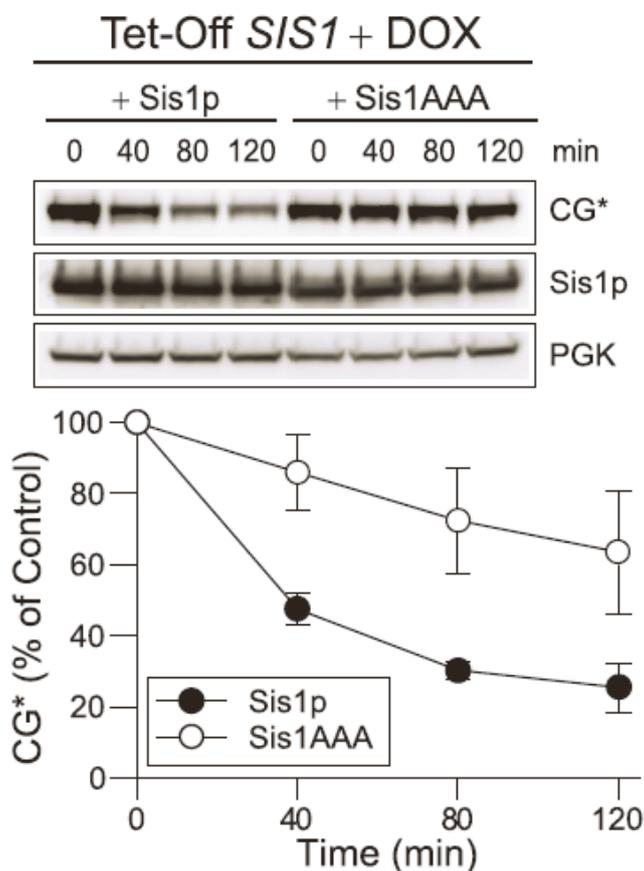
Figure 50. Sis1AAA cannot replace wild-type Sis1 for CG* degradation.

CG* was co-expressed with HA-tagged Sis1 or Sis1AAAin Tet-Off SIS1 cells. These cells were cultivated for 20 hours in the presence of DOX to deplete endogenous Sis1. CG* degradation was analyzed by CHX chase, SDS-PAGE and immunoblotting with anti-GFP, Sis1 and PGK antibodies.

Sis1, Sis1ΔJ, Sis1AAA and CG* were co-expressed in Tet-Off Sis1 cells. Sis1, Sis1ΔJ and Sis1AAA were immunoprecipitated with antibodies against their N-terminal HA-tag. These samples were subjected to SDS-PAGE and immunoblotting analysis. Sis1 and its mutants formed ternary

complexes with Ssa1 and CG*. Sis1ΔJ and Sis1AAA strongly interacted with CG*. Sis1ΔJ had weaker interactions with Ssa1 relative to the other Sis1 versions tested. We suspect that the Sis1 chaperone interacts with CG* and helps to recruit Ssa1 using its J domain (Figure 51).
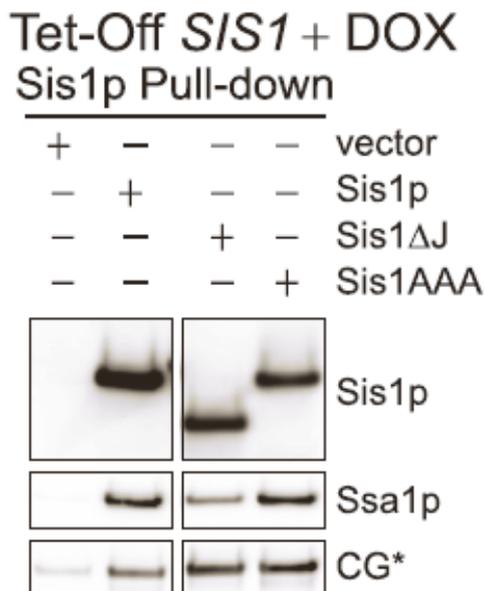
Figure 51. Sis1 interacts with Ssa1 and CG*.

CG* was co-expressed withSis1p, Sis1ΔJ or Sis1AAA in Tet-Off SIS1 cells. Strains were incubated in DOX-containing medium. Immunoprecipitation with anti-HA antibodies was performed followed by immunoblotting with anti-HA, anti-Ssa1 and anti-GFP antibodies.

4.9.3 Sis1 is not required for the degradation of short-lived regulatory proteins

Sis1 accelerated the degradation of CG* and NLS-CG* in cells expressing 96QmCh. The degradation of CG* was accelerated even in the presence of 20QmCh, under which conditions the UPS remained unimpaired. Therefore, Sis1 could be required for the degradation of misfolded cytosolic proteins. Fructose-1,6-bisphosphatase (FBPase) was chosen to represent normal cytosolic proteins. FBPase converts fructose-1,6-bisphosphate to fructose 6-phosphate during gluconeogenesis. FBPase is expressed when yeast cells are grown in media without a fermentable carbon source, such as in ethanol or acetate. However, FBPase is rapidly degraded via the UPS if glucose is the main carbon source (Juretschke et al., 2010).

FBPase expression was induced in Tet-Off SIS1 yeast cells and in wild-type cells by growing them on 2% ethanol medium. An abrupt shift to glucose-containing medium initiated the

degradation of FBPase, after which we performed a CHX chase assay. Sis1 depletion did not affect FBPase degradation kinetics (Figure 52).
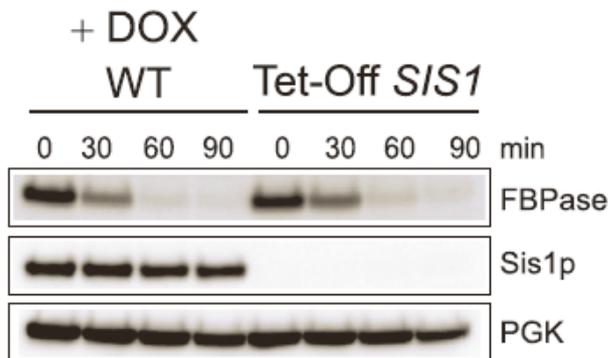
Figure 52. The catabolite-induced degradation of fructose-1,6-bisphosphatase (FBPase) is Sis1-independent.

Wild-type and Tet-Off SIS1 cells were grown for 20 hours in medium containing 2% ethanol and DOX. The degradation of FBPase was initiated by transferring the cells to medium containing 2% glucose and DOX. CHX chase and SDS-PAGE were performed. FBPase, Sis1 and PGK were analyzed by immunoblotting with the appropriate antibodies.

4.10 Sis1 is required for the delivery of CG* into the nucleus for degradation

4.10.1 Depletion of Sis1 results in the formation of cytoplasmic CG* inclusions

The majority of the proteasome complexes in yeast are localized in the nucleus. Consequently, some cytosolic misfolded proteins are degraded in the nucleus (Russell et al., 1999). Moreover, recent studies have shown that CG* is degraded in the nucleus (Heck et al., 2010;Prasad et al., 2010). However, the mechanism underlying this process remains unknown. In our work, we evaluated the potential involvement of Sis1 in this mechanism. We depleted 85% of Sis1 in cells expressing CG* (Figure 53), which caused the formation of large cytosolic CG*inclusions. These results suggest that CG* is degraded in the nucleus, and that Sis1 delivers CG* to the nucleus for degradation.
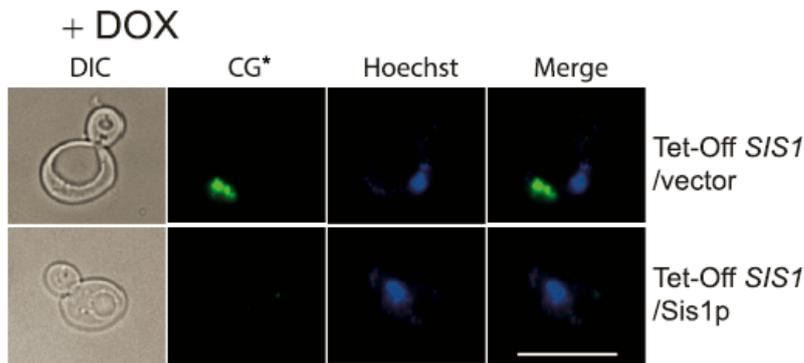
Figure 53. Sis1 depletion results in the formation of CG* inclusions.

CG* was expressed in Tet-Off *SIS1* cells and grown in the presence of DOX for 20 hours to deplete endogenous Sis1. Live cells were analyzed by DIC and fluorescence microscopy. Nuclei were counterstained with DAPI. Scale bar: 10 mm.

4.10.2 Targeting of CG* to the nucleus or to the cytoplasm significantly influences CG* degradation kinetics

Next, we modified CG* by fusing NLS and NES sequences to its N-terminus, which should result in the sequestration of NLS-CG* protein in nucleus and NES-CG* in the cytoplasm. Surprisingly, the NLS tag either increased or did not change the degradation kinetics of CG*assuming the delivery to the nucleus was efficient. In contrast, NES fusion led to the cytosolic localization of the NES-CG* protein.

We expressed NLS-CG*, CG* and NES-CG* in wild-type cells, after which CHX chase, SDS-PAGE and immunoblotting were performed (Figure 54). NLS-CG* degradation occurred more rapidly than CG* degradation. In contrast, NES-CG* was stabilized relative to CG*. These results strongly suggest that the CG* protein is degraded in the nucleus.
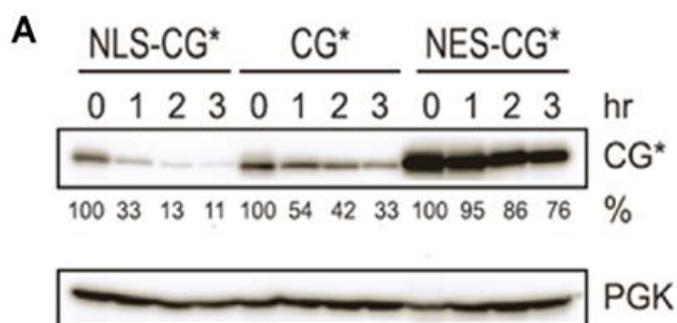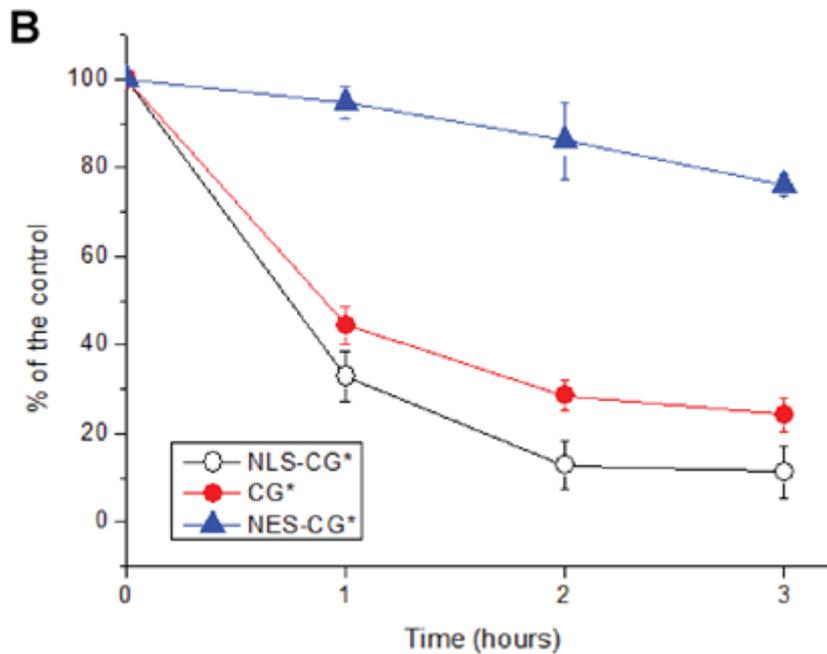
Figure 54. Nuclear degradation of CG*.

(A) NLS-CG*, NES-CG* and CG* degradation were analyzed in wild-type YPH499 cells. CHX chase was performed followed by SDS-PAGE and immunoblotting with anti-GFP and PGK antibodies. PGK levels were used as a loading control. (B) Densitometry analysis of NLS-CG*, CG* and NES-CG* in wild-type cells. Averages and the SD from three independent experiments are shown.

4.10.3 NES-CG* is exported from the nucleus via Crm1

We showed that the addition of a nuclear export signal to CG* leads to the stabilization of CG*. However, the addition of the NES tag could change the degradation kinetics based on the protein structure and not because of the localization properties of the NES sequence. Crm1 (Xpo1) is the nuclear export receptor for proteins containing NES sequences (Johnson et al., 2002;Maurer et al., 2001). To determine whether NES-CG* is specifically exported, we used temperature-sensitive *crm1-1ts* cells. In these cells, when the temperature is shifted to 37°C, the protein becomes unable to function properly. Therefore, this strain could be used to study the behavior of a given substrate in the presence and absence of the nuclear exporter Crm1. We expressed NES-CG* in wild-type and *crm1-1ts* cells. The results of the CHX chase experiments performed at 37°C are presented in Figure 55.

A

B
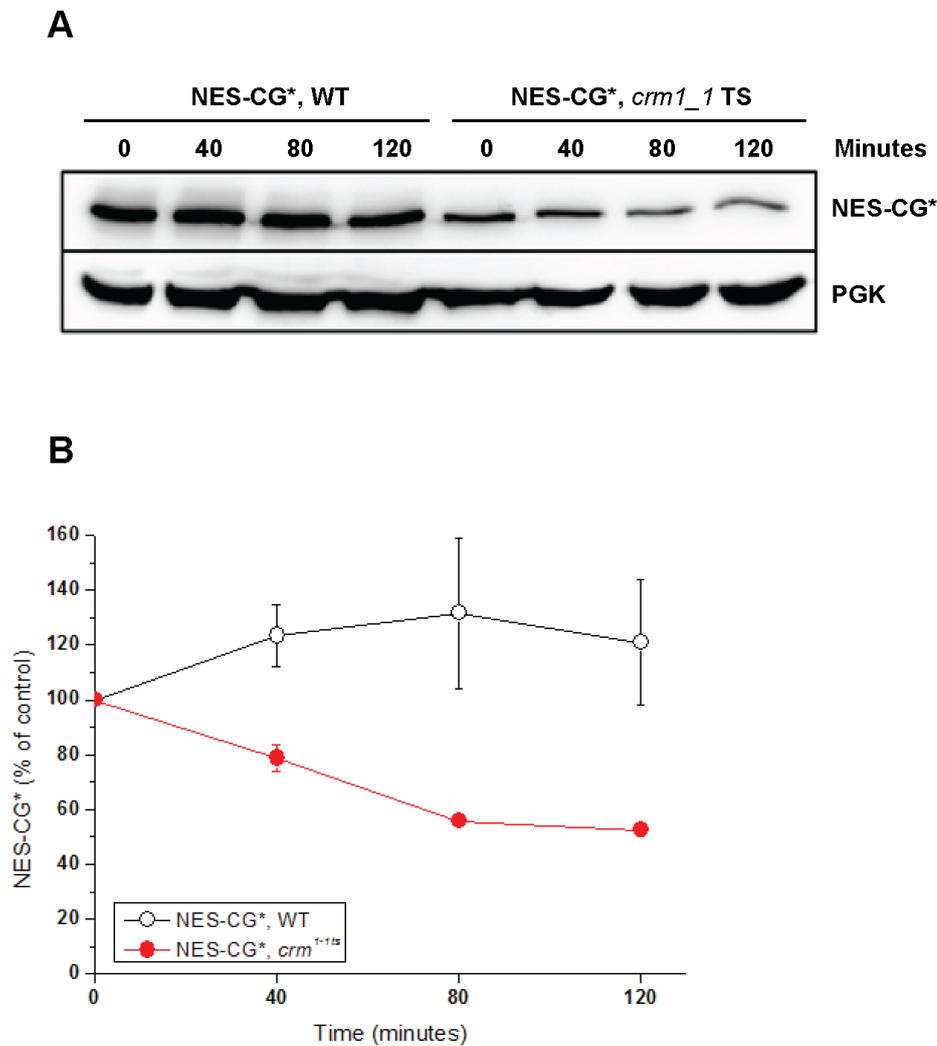
Figure 55. NES-CG* degradation is increased in *crm¹⁻¹ᵗˢ* cells at 37°C.

(A) NES-CG*degradation was analyzed in *crm¹⁻¹ᵗˢ* and in wild-type cells. A CHX chase was performed followed by SDS-PAGE and immunoblotting using anti-GFP and PGK antibodies. PGK levels were included as the loading control. (B) Densitometry analysis of NES-CG* in *crm¹⁻¹ᵗˢ* cells and wild-type cells. Averages and the SD from two independent experiments are shown.

We expressed CG* in *crm¹⁻¹ᵗˢ* and in wild-type cells and performed a CHX chase at 37°C. CG* was degraded more rapidly in the temperature-sensitive mutant relative to the wild-type strain. These results are presented in Figure 56.

A

B
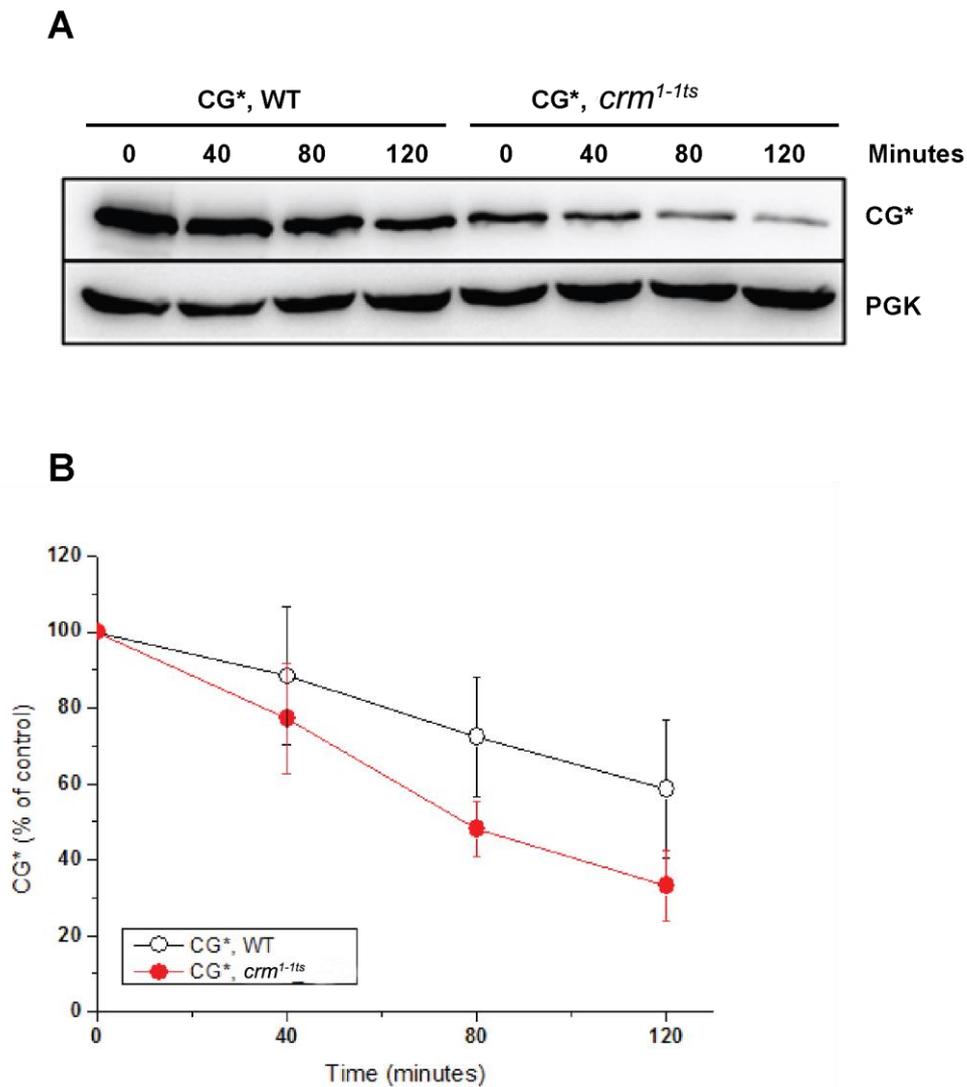
Figure 56. CG* degradation is increased in a *crm^{1-1ts}* mutant at 37°C.

CG* degradation was analyzed in *crm^{1-1ts}* and in wild-type cells. A CHX chase was performed followed by SDS-PAGE and immunoblotting using anti-GFP and PGK antibodies. PGK levels were included as the loading control. (B) Densitometry analysis of CG* in *crm^{1-1ts}* and wild-type cells. Averages and the SD from two independent experiments are shown.

4.10.4. CG* and Sis1 accumulation in the nucleus upon proteasome inhibition

CG* degradation can be inhibited by MG132. MG132 is a specific, reversible proteasome inhibitor. In yeast cells, MG132 functions most effectively in strains that lack the Pdr5 protein, a specific multi-drug transporter that is involved in the pleiotropic drug response (Ernst et al., 2005). To achieve MG132 accumulation, we used cells lacking the Pdr5 transporter, which tend to accumulate MG132. Fluorescence imaging was performed in cells expressing CG* in the *Δpdr5* strain (Figure 57). In these cells, MG132 caused the accumulation of CG* in a juxtanuclear manner. CG* was observed primarily as an aggregate, although the CG* signal was also

partially present in the nucleus in a diffuse manner suggesting solubility. Sis1 also accumulated

in the nucleus in MG132-treated cells.
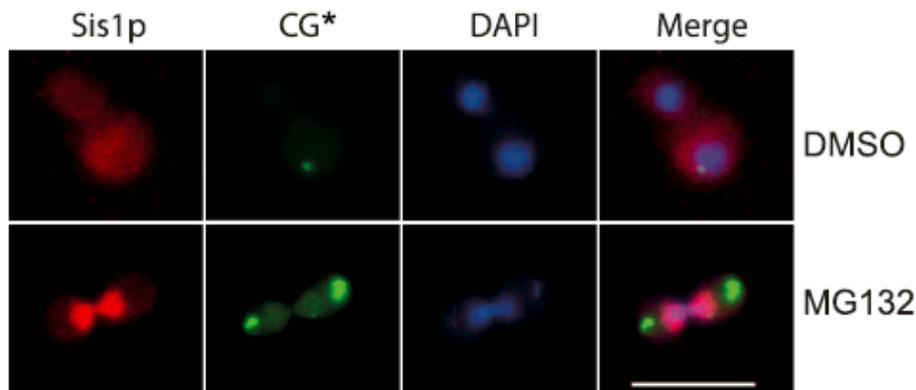
Figure 57. CG* and Sis1 accumulate in the nucleus upon proteasome inhibition.

CG* was expressed in Δ*pdr5* cells for 18 hours followed by the addition of 1% DMSO or 100 mMMG132 in DMSO for 2 hr. Sis1p was immunolabeled using rabbit anti-Sis1 antibody coupled to Cy3-conjugated goat anti-rabbit antibody, and CG* was labeled by GFP fluorescence. Nuclei were counterstained with DAPI. Scale bar: 10 mm.

4.10.5 CG* and Sis1 accumulate in the nucleus in Δ*san1 cells*

Another method to demonstrate that the nucleus is the primary degradation site for CG* is to

delete proteins that are essential for protein degradation via UPS in the nucleus. San1 is a

ubiquitin ligase involved in the degradation of aberrant nuclear proteins through the UPS

(Rosenbaum et al., 2011). CG* was expressed in Δ*san1* cells. Sis1 accumulated in the nucleus

(Figure 58), whereas CG* accumulated in a juxtanuclear manner and in the nucleus.
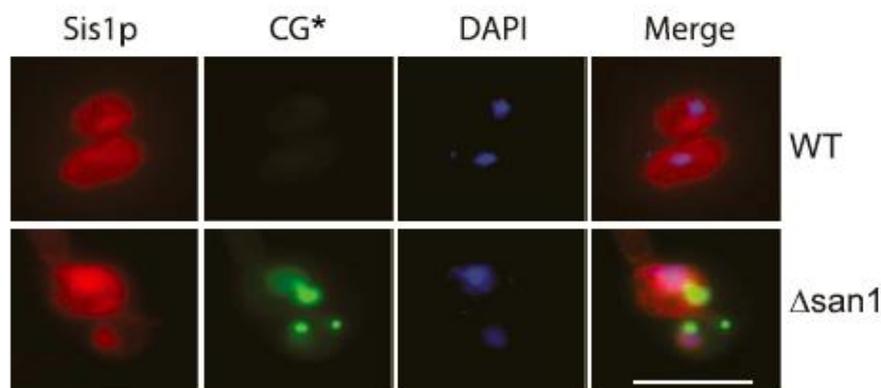
Figure 58. San1 deletion leads to CG* and Sis1 accumulation in the nucleus.

CG* was expressed in wild-type (WT) and in Δ*san1*cells for 18 hours, after which the cells were analyzed by immunofluorescence. Sis1 was immunolabeled with a rabbit anti-Sis1 antibody coupled to a Cy3-conjugated goat anti-rabbit antibody. CG* was observed by GFP fluorescence. Nuclei were stained with DAPI. Scale bar: 10 mm.

4.10.6 Sis1 shuttling is required for the degradation of misfolded proteins

Sis1 plays an important role in the delivery of CG* into the nucleus. When 96Q interacts with the Sis1 protein, it likely hinders Sis1 shuttling between the cytosol and the nucleus. To address this question, NES-Sis1 and NLS-Sis1 proteins were constructed. The Tet-Off SIS1 strain was used for the expression of NES-Sis1 or NLS-Sis1. When this strain was incubated in medium containing DOX, endogenous Sis1 was depleted. The results of this experiment and the intracellular distribution of these proteins are shown in Figure 59. In both cases, CG* was not properly degraded and showed the formation of inclusions in the cytosol.
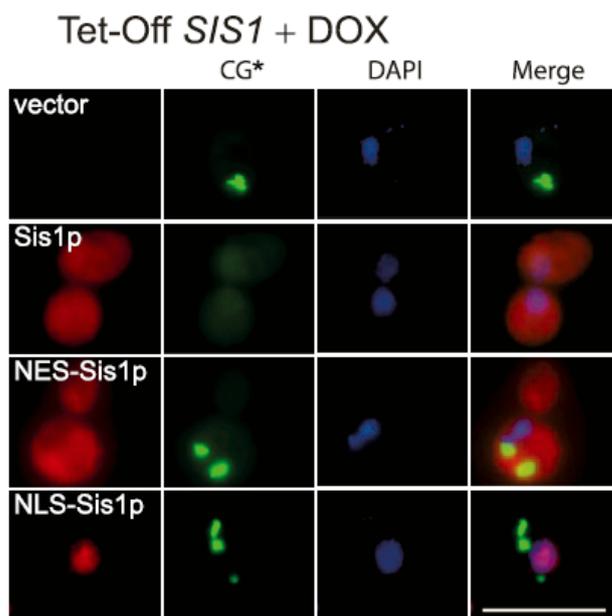
Figure 59. Sis1 shuttling between the cytoplasm and the nucleus is required for CG* degradation.

CG* co-expressed with Sis1, NLS-Sis1, or NES-Sis1 in Tet-Off SIS1 cells. Cells were incubated in medium containing DOX and GAL. Immunolabeling was performed using an anti-HA antibody modified by a Cy3-conjugated goat anti-mouse antibody, and CG* was monitored by GFP florescence. Nuclei were stained with DAPI stain. Scale bar: 10mm.

5   Discussion

According to the United Nations, the overall median age in developed countries rose from 28.0 years in 1950 to 40 in 2010 and is expected to increase to 44 years by 2050. The same trend applies to the global population: the median age was 24 years in 1950, which increased to 29 years by 2010 and is expected to increase to 36 years in 2050 (United Nations, Department of Economic and Social Affairs, Population Division, 2013). These data suggest that the population in developed countries and worldwide is quickly aging.

Age is the largest risk factor for the development of many neurodegenerative diseases. Therefore, one can expect a rise in the number of patients with neurodegenerative disorders. The worldwide prevalence of Alzheimer's disease was 26.6 million in 2006. By 2050, the number of people with this disease is expected to be approximately 80 million. In other words, one in 85 people in the world will be living with Alzheimer's disease(Brookmeyer et al., 2007). Finding a way to cure or at least effectively manage patients with neurodegenerative diseases is one of the biggest challenges for society and for the life sciences.

Neurodegenerative disorders are irreversible and incurable. There are no effective treatments available. Therefore, understanding the mechanisms of neurodegeneration as well as the links and similarities between different neurodegenerative disorders is crucial for the development of potential treatments. Among the most common neurodegenerative diseases, the following disorders are particularly important to investigate: Alzheimer's, Parkinson's and Huntington's. Little is known regarding the mechanisms underlying toxicity in these disorders and how potential therapies could be developed to counter these diseases. As of the writing of this work, six drugs are currently in phase III clinical trials, 39 are in phase II trials, and 38 are in phase I trials for the treatment of Alzheimer's disease. Yet, despite these attempts, hope for the development of an efficient treatment remains bleak, as only a few drugs, largely intended for symptomatic treatment, have been approved to date. New clinical trial designs using biomarkers based on the latest advances in neurodegenerative disease studies could help in the informed development of efficient drugs (Becker and Greig, 2008).

Patients with the abovementioned diseases display amyloidogenic aggregates in their brain tissues. There are intracellular inclusions in Parkinson's disease containing aggregated α-synuclein, aggregates in HD containing huntingtin and extracellular β-

amyloid plaques that are characteristic of Alzheimer's disease (Chiti and Dobson, 2006). Therefore, these aggregates are thought to be the major cause of toxicity in the cell (Pike et al., 1993;Shearman et al., 1994;Li et al., 2000). Some inconsistencies related to this theory have been noted such as poor correlation between neuron death and the number of visible aggregates (Yoo et al., 2003). Some studies have shown that the SDS-insoluble aggregates observed in these diseases are relatively harmless and that the toxic species are actually the soluble oligomeric intermediates(Hartley et al., 1999;Kuemmerle et al., 1999). A study by Kuemmerle et al. even suggested that SDS-insoluble aggregates of polyQs might play a cytoprotective role. Increasing evidence from different neurodegenerative disease studies has suggested that soluble oligomeric proteins formed before the development of SDS-insoluble inclusions may be responsible for the disease-related cytotoxicity (Haass and Selkoe, 2007;Sánchez et al., 2003). Oligomeric forms may increase the chance for interactions on susceptible hydrophobic surfaces, which primarily drive the aberrant interactions of these aggregate-prone proteins. In the insoluble fibrils, hydrophobic surfaces are buried in a compact β-structured core (Bolognesi et al., 2010). Another hypothesis with abundant supporting data postulates that the main species causing the toxicity are these soluble oligomeric species, while the role of SDS-insoluble aggregates remains controversial (Leitman et al., 2013;Behrends et al., 2006).

Huntington's disease is a good model for the analysis of neurodegenerative disorders and the identification of toxicity mechanisms. With age, the burden on the proteostasis network increases, and proteostasis collapse can occur (Morimoto, 2008). Moreover, studies have shown that longevity and proteotoxicity from misfolded proteins due to neurodegenerative disorders have a negative relationship (Cohen et al., 2006). In this study, we created a model to analyze the interplay between different misfolded proteins (polyQ- and CPY*-derived proteins). This model allowed us to simulate the fate of cells carrying an increased amount of misfolded proteins.

5.1 *Saccharomyces cerevisiae* as a model for studying UPS interference by polyQ proteins

We chose *S. cerevisiae*, a eukaryotic model with well-established molecular biology, easy genetic manipulations and a fully sequenced and well-annotated genome (Botstein et al., 1997; Engel et al., 2013). Gene disruptions via the introduction of mutations into existing

genes are relatively easy and straightforward to perform in this model. Furthermore, the *S. cerevisiae* yeast has been widely used to study neurodegenerative diseases (Behrends et al., 2006;Konopka et al., 2011;Duennwald, 2012).

In our model, we studied polyQ interference with the cellular protein quality control system. The polyQ-expanded protein 96Q inhibits the degradation of several misfolded proteins. We studied reporters in different cellular compartments and with different topologies: cytosolic (CG*), nuclear (NLS-CG*), ER lumenal (CPY*), and ER membrane proteins (CTG*) (Taxis et al., 2003). All of these proteins are based on CPY*, a terminally misfolded protein. We investigated the behavior of misfolded proteins in the different compartments of the cell in the presence of a polyQ-expanded protein. This model enabled us to obtain a systematic view of the chain of events caused by 96Q expression. Hopefully, this model will be used in future studies to analyze the fate of polyQ substrates in more detail, as these types of analyses were beyond the scope of the current study.

5.1.1 96Q interference with the degradation of misfolded proteins

Protein aggregates can strongly inhibit UPS function (Verhoef et al., 2002; Bence et al., 2001) prior to inclusion body formation (Bennett et al., 2005). The UPS may also be inhibited indirectly by pathogenic polyQ (Hipp et al., 2012). However, UPS impairment by pathogenically expanded polyQ proteins remains a controversial topic (Valera et al., 2007). Our model allowed us to systematically analyze polyQ interference with the UPS in the cell.

As shown in the Results section, 96Q stabilized several misfolded proteins: CG*, NLS-CG*, CPY* and CTG*. We observed that proteins containing a pathogenically expanded glutamine tract interfered with the degradation of proteins in the cytosol, nucleus and ER. Previous studies have shown that 47% of yeast proteins are cytoplasmic, 27% are nuclear/nucleolar and 13% are exocytic (including proteins of the ER and secretory vesicles) (Kumar et al., 2002). Taking into account published data from yeast proteome analyses, we speculate that our misfolded proteins represent more than 70% of the proteome. Therefore, CG*, NLS-CG*, CPY* and CTG* represented misfolded proteins in different compartments that could emerge at anytime.

Based on our results showing that 96Q stabilizes several misfolded proteins from different cellular compartments, we can assert that proteins containing a pathogenically expanded polyglutamine tract influenced misfolded proteins in the entire cell. Therefore, our results suggest that 96Q can influence the degradation of misfolded proteins to a greater extent than previously thought.

Misfolded proteins are often found in cells exposed to stress (such as heat shock or chemical stress) or with age (Cohen et al., 2006). If proteostasis capacity is overloaded by misfolded proteins, then cytotoxicity arises (Powers et al., 2009;Hartl et al., 2011). In our model, we simulated a natural situation: the capacity of the cell to counter misfolded protein stress was overloaded when 96Q was co-expressed with CG*, NLS-CG* or CTG*,whereas the cell capacity to handle misfolded protein stress was not overwhelmed in the case of 20Q co-expression with CG*, NLS-CG* or CTG*. Based on the results of our experiments, the expression of 96Q alone does not result in growth inhibition. Furthermore, co-expression of 96Q with either CG*, NLS-CG* or CTG* dramatically increases growth inhibition in our experiments. We hypothesize that the protein quality control system in these cases are not capable of handling all of the misfolded specimens. Proteostasis capacity of the cells and the ability to control misfolded species is reduced with age. In diseases caused by protein aggregation, misfolded proteins exert additional pressure on the proteostasis system in the cell (Taylor and Dillin, 2011;Cuanalo-Contreras et al., 2013). Our data are consistent with the idea that many neurodegenerative diseases (including Huntington's disease) have a certain age of onset. With age, proteostasis capacity diminishes and reaches the point where the protein quality control system is no longer able to handle the misfolded proteins; pathogenic polyQ-expanded proteins aggravate this problem.

Co-expression of 96Q and CG* not only led to cytotoxicity but also influenced the ability of the cells to respond to stress. According to our data, cells expressing 96Q and CG* were the least capable strains in inducing a stress response. In our experiments, the combination of these misfolded proteins impaired the heat shock response (Figure 20C). These data are supported by another observation made by our group: amyloid-like β-structured proteins deregulate the stress response in mammalian cells (Olzscha et al., 2011). In another study, the authors showed that full-length, non-aggregated polyQ-expanded Htt protein could block effective induction of the heat shock response (Chafekar and Duennwald, 2012). Thus, not only did 96Q and CG* expression overload

the proteostasis network, but the co-expression of these proteins also impaired the heat shock response. The diminished ability of the cell to withstand stress resulted in cytotoxic effects. Reduced ability of the cell to respond to stress will be further discussed in section 5.2.

The degradation of CG* and CTG* requires assistance from the Hsp70 chaperone Ssa1 and the Hsp40 co-chaperone Ydj1 (Park et al., 2007). According to the data from our SILAC proteomic analysis, 96Q was strongly associated with Sis1, Ssa1, Ssa2, Ssa4 and Ydj1. The association of these proteins with 96Q resulted in a reduced total chaperone capacity in the cell. Given that CG* and CTG* both require chaperone assistance, their degradation should be affected by the depletion of chaperone pool via 96Q expression. In the case of CG*,the Sis1 chaperone appears to be the limiting factor for CG* degradation. However, the chaperone or other protein that serves as the limiting factor for CTG* degradation remains unknown. Our results also showed that Dsk2 was strongly associated with 96Q in our SILAC experiments. Because a previous study has shown that CTG* depends on Dsk2 for its degradation (Medicherla et al., 2004), we hypothesize that Dsk2 depletion could explain the CTG* stabilization observed in our study.

As discussed above, the [PIN+] phenotype is important for the *de novo* formation of the [PSI+] phenotype but not for [PSI+] phenotype propagation (Derkatch et al., 1997; Derkatch et al., 2000). The [PIN+] phenotype is critical for the aggregation and cytotoxicity of pathogenic polyQ proteins in the cell (Meriin et al., 2002). Our data show that 96Q interference with misfolded proteins depends on the [PIN+] status of the cell. One possible explanation for this is that the [PIN+] prion is important for initial "seeding" of the amyloidal conformation in *S. cerevisiae*(Derkatch et al., 2004;Vitrenko et al., 2007). 96Q did not stabilize CG*, NLS-CG* and CTG* in the [pin-] background. Moreover, we demonstrated through immunoprecipitation experiments that 96Q bound significantly less of the chaperones and co-chaperonesSsa1, Sis1 and Ydj1 (Figure 34). Thus, we suspect that in [pin-] cells, 96Q existed in a different conformation that did not efficiently bind chaperones and other components of the proteostasis network. Based on several studies that have shown that polyQ aggregation and toxicity depend on the [PIN+] phenotype, we speculate that soluble oligomers and SDS-insoluble aggregates are not present in [pin-] cells(Meriin et al., 2002;Kurahashi et al., 2008). Therefore, the soluble oligomers and SDS-insoluble aggregates may be responsible for chaperone depletion and stabilization of

misfolded proteins in wild-type [PIN+] cells. However, further studies are required to identify which fraction (SDS-soluble or SDS-insoluble) causes CG* stabilization.

As shown in our results, the co-expression of 96Q and CG*, CTG* or NLS-CG* was not toxic in the [pin-] strain (Figure 30, 31 and 32). Under normal conditions, Sis1 interacts with prion fibrils of Rnq1 proteins in [PIN+] cells and with aggregated polyQ (Sondheimer et al., 2001). In [pin-] cells, Sis1 and other co-chaperones and chaperones interacted less with 96Q fibrils when compared with [PIN+] cells, which suggests that in [pin-] cells, various chaperones were not depleted from the available chaperone pool. This results in a greater chaperone capacity to handle misfolded proteins in the [pin-] strain. We hypothesize that increased chaperone availability in [pin-] cells overcomes the toxicity caused by 96Q and CG* co-expression.

In addition, our results showed that 96Q did not inhibit CG* degradation if these proteins were expressed for only 6 hours (Figure 11). The 96Q SDS-soluble fraction was abundantly present after 6 hours of incubation, which raises the question of which fraction of polyQ proteins is associated with chaperones. Monomeric or low molecular weight fractions found in the cell after 6 hours of incubation did not block CG* degradation. Moreover, the formation of the polymeric species of polyQ is not an instantaneous process (Krobitsch and Lindquist, 2000), and the period of 6 hours was likely not long enough for the formation of SDS-insoluble polymeric 96Q structures (not observed in filter retardation assay). SDS-insoluble polymeric 96Q structures were observed after 15 hours of expression (the presence of the SDS-insoluble fraction was detected by filter retardation assay); however, technical constraints prevented us from determining whether the SDS-soluble fraction or the SDS-insoluble polymer fraction was responsible for chaperone activity sequestration. More experiments are required to answer this question, but it seems likely that the conformation of the pathogenic polyQ protein plays a pivotal role in processes that are harmful to the cell.

In future studies, the construction of an unfolded reporter protein that could be targeted to the mitochondria could be useful. Indeed, a mitochondrial dysfunction has been observed in Huntington's disease (Oliveira, 2010). There are several theories explaining this phenomenon, but many of them do not consider protein quality control interference by polyQ in the cell. We have shown interaction between polyQ-expanded protein and many chaperones and co-chaperones (Ssa, Sis1 and Ydj1) and many other components of the proteostasis network (Table 2). In addition to these observations, Hsp70 and other

chaperones have been shown to be involved in the import of proteins into the mitochondria. Therefore, protein transport to the mitochondria could also be affected by polyQ. Sequestration of proteins that are important for mitochondrial transport could lead to mitochondrial dysfunction, which is characteristic of some neurodegenerative diseases.

5.1.2 PolyQ proteins do not directly inhibit the proteasome

Previous studies have suggested that the proteasome is inhibited in polyQ diseases due to the co-aggregation of pathogenically expanded polyQ proteins with ubiquitin and with proteasome subunits in patients with spinocerebellar ataxia type 1 and Huntington's disease (DiFiglia et al., 1997;Cummings et al., 1999). Thus, pathogenic polyQ proteins are thought to sequester proteasome subunits into the inclusions, which can lead to an imbalance in the UPS component stoichiometry and can result in the decrease of proteasomal function. Another model claims that UPS impairment is related to the fact that polyQ cannot be digested *in vitro* (Venkatraman et al., 2004).These findings were further supported by another study that revealed that proteins containing expanded polyQ tracts blocked the proteasome and prevented protein degradation(Raspe et al., 2009).

Our study provides evidence that conflict with both of these models. Cells expressing pathogenic polyQ retain the ability to degrade Ub^{G76V}-GFP, suggesting that the proteasome remains active (Figure 22). Moreover, GFPcODC can be degraded in cells co-expressing 96Q and CG*. Importantly, CG* was stabilized in this experiment due to the presence of 96Q. Therefore, these data suggest that the proteasome block was located upstream of the proteasome.

In addition, our data show that the proteasome is capable of degrading polyQ proteins if they are efficiently delivered to the proteasome upon the addition of cODC tags. These results suggest that long polyQ tracts do not physically encumber or sequester the proteasome. The data that we obtained from yeast are in accordance with studies performed in mammals. A previous study found that polyQ-expressing mice do not exhibit reduced proteasomal activity (Bett et al., 2006).

To summarize our results, the proteasome remains functional upon 96Q expression. Moreover, pathogenically expanded polyQ interferes with protein quality control upstream of the proteasome in yeast.

In addition, we found that CG* was fully ubiquitinated in the presence of 96Q. Pathogenic polyQ did not interfere with CG* ubiquitination, and therefore, CG* stabilization was due to a different cause. Previous studies support our finding that pathogenic polyQ protein interference with the proteasome is not linked to Ub-conjugation (Hipp et al., 2012). Moreover, overexpression of Ubr1 (an E3 ubiquitin ligase with a major role in targeting misfolded cytosolic proteins and CG* ubiquitination) did not improve CG* degradation (Eisele and Wolf, 2008; Heck et al., 2010; Park et al., 2013). However, disruption of Ubr1 in cells co-expressing 96Q and CG* resulted in increased cytotoxicity (Figure 27). This implies that Ubr1 plays an important role in CG* degradation, although it is not a limiting factor for degradation.

5.2   Expression of misfolded proteins reduces the ability of cells to respond to stress

The heat shock response is highly conserved in all organisms and is activated in response to different conditions such as exposure to high temperatures and the presence of misfolded proteins (Lindquist, 1986). The ability to respond to stress is very important for cell survival (Verghese et al., 2012). Cells expressing pathogenically expanded toxic polyQ proteins are not able to produce a strong stress response (Duennwald and Lindquist, 2008). Our results confirm this result based on our non-toxic 96Q protein. Neither 96Q alone nor in combination with CG* was able to induce a strong stress response (Figure 20A).

Moreover, the ability of the cells to produce a heat shock response was significantly impaired if both 96Q and CG* were co-expressed. CG* overexpression had a negative influence on stress induction in our experiments (Figure 20B). Summarizing the data from our experiments, we propose the following model: accumulation of misfolded proteins overwhelms the proteostasis network; however, cells cannot upregulate important proteostasis components because of the reduced ability to induce the appropriate stress

response in these cells. This results in the cytotoxicity we observed in cells co-expressing 96Q and CG*.

Interestingly, Sis1 overexpression (we will discuss this protein in more detail later) in 96Q-expressing cells led to a strong stress response induction even in the absence of heat shock (Figure 48). The intensity of the response in Sis1-overexpressing cells was similar to the response to heat shock. We speculate that Sis1 plays a role as a stress sensor and senses 96Q as a potentially dangerous misfolded protein, thereby triggering the upregulation of the stress response in the presence of 96Q. Sis1 is involved in the degradation of misfolded proteins and can also help upregulate other components of the proteostasis network to endure stress. Sis1 could act as a sensor for misfolded proteins in the cytosol and nucleus, which would represent a novel function of Sis1; however, more data are required to support this idea. Data from our stress assay with Sis1 overexpression should be further investigated on the mRNA level. Data from our laboratory suggest that high levels of Sis1 in the presence of 96Q increased the mRNA levels of several important players in the proteostasis network (personal communication with Dr. Julien Micoud).

5.3 Key 96Q interactors

Our data show that the proteasome remains active in the presence of 96Q. Stabilization of CG* and other proteins occurs upstream of the proteasome. We suspect that 96Q interacts with factor X, which is required for misfolded protein degradation. To identify factor X, we conducted a quantitative interactome analysis using SILAC (Ong and Mann, 2006). We identified proteins that showed enriched interaction with 96Q relative to 20Q. Approximately 100 proteins were enriched over 2-fold by co-immunoprecipitation in at least two of three independent experiments. These proteins were classified into 6 groups: chaperones, glutamine-rich proteins, yeast prion proteins, UPS components, nuclear pore complex proteins and vesicle transport proteins.

First, the association of prion proteins with 96Q reflects the requirement of prion status for the seeding of polyQ protein aggregation in yeast (Meriin et al., 2002). Moreover, many polyQ-rich proteins tend to co-aggregate with each other (Kazantsev et al., 1999; Schaffar et al., 2004). These studies suggest that polyQ-rich proteins exchange structural information with each other. 96Q expression might affect other polyQ-rich proteins by

encouraging the adoption of a misfolded configuration in a manner similar to prions. This would increase the likelihood that other proteins could have aberrant protein interactions. Two groups of 96Q-interacting proteins were notable: molecular chaperones (and co-chaperones) and proteins associated with the UPS. Molecular chaperones constitute the first line of defense against misfolded proteins; therefore, their increased interaction with 96Q was anticipated. In our study, we found that some very highly abundant chaperones, such as Ssa1, associated with 96Q. However, we also identified strong interacting proteins, such as the Sis1 protein, which is an Hsp40 chaperone with low abundance. We found that the overexpression of Sis1 restores CG* degradation, whereas overexpression of Ssa1 or Ydj1 fails to restore CG* clearance in 96Q-expressing cells. Our data also showed that as little as a 25% decrease in Sis1 expression led to the stabilization of CG* (Figure 49). Therefore, we concluded that Sis1 is a limiting factor for CG* degradation in the presence of 96Q.

UPS components also associated with 96Q. Our results showed that Dsk2 was highly enriched, and several subunits of the 19S proteasome complex were moderately enriched. We found that, despite the fact that Dsk2 is dispensable for CG* degradation, Dsk2 deletion accelerated CG* turnover (Medicherla et al., 2004; Park et al., 2013). Previous studies have shown that CTG* requires Dsk2 for its degradation (Medicherla et al., 2004). Therefore, the functional depletion of Dsk2 by 96Q could have caused the stabilization of CTG* observed in our study. However, additional experiments to investigate the mechanism of CTG* stabilization are required.

In summary, we found that 96Q interacts with several different types of proteins. 96Q interacts extensively with components of the proteostasis network particularly with chaperones. These results suggest that 96Q drastically affect the ability of the cell to maintain protein homeostasis by interacting with the proteostasis machinery.

5.4   Ssa1, Ydj1 and Sis1 interact with 96Q and are depleted from the pool of available proteins

First, we tried to overexpress Ssa1 and Ydj1, as these proteins were strongly associated with 96Q in our SILAC experiments, and they are required for CG* degradation (Park et al., 2007). Ssa1 and Ydj1 overexpression did not restore CG* degradation in 96Q-expressing cells. Moreover, Ssa1 and Ydj1 stabilized CG* levels (Figure 35 and Figure 36). Because chaperones act in a cooperative manner, one might expect that the upregulation of a single chaperone may lead to an imbalance between the components of the chaperone cycle (Hartl and Hayer-Hartl, 2002). Nonetheless, our results show that Ssa1 and Ydj1 are not limiting factors for CG* degradation in our model.

Chaperones are known modulators of polyQ aggregation and toxicity (Sakahira et al., 2002). Overexpression of Ssa1 and Ydj1 decreased the SDS-insoluble fraction of 96Q present in the cell but failed to restore the degradation of misfolded proteins. One possible explanation for this phenomenon is that the chaperones were trying to refold the terminally misfolded CPY*, which skewed the balance between refolding and degradation towards the refolding pathway. However, chaperone functions are beneficial to the cell. For example, Ydj1 overexpression resulted in reduced toxicity in cells co-expressing 96Q and CG* (Figure 38). We suspect that Ydj1 interacted with 96Q and thus was able to shield 96Q protein from potentially harmful interactions effectively substituting for some of the functions of the cognate Sis1 protein.

Second, we overexpressed the protein Sis1 based on the fact that Sis1was very strongly associated with 96Q in our SILAC experiments. CG* degradation in the presence of 96Q was greatly accelerated when Sis1 was overexpressed (Figure 40). Moreover, NLS-CG* degradation was accelerated by Sis1 overexpression (Figure 42). The effects of Sis1 on CG* and NLS-CG* degradation were quite specific, as all other reporters (CTG* and CPY*-HA) tested did not degrade faster in the presence of Sis1 (Figure 44 and Figure 46). This observation can be explained by the fact that Sis1 is localized in the cytosol and the nucleus and assists with the degradation of misfolded substrates in these compartments (Huh et al., 2003).

Ssa1 and Ydj1 sequestration by 96Q did not lead to stabilization of CG* protein because these two proteins are present in the cell in high quantities (269,000 and 119,000 molecules per cell, respectively), which makes their depletion by 96Q difficult (Ghaemmaghami et al., 2003). However, Sis1 protein exists in relatively low abundance, with only 20,300

molecules per cell, which suggests that 96Q could significantly deplete Sis1 protein. Altogether, 96Q depleted the chaperone pool by sequestering chaperones and co-chaperones. Depletion of the chaperone pool plays an important role in unbalancing the protein quality control system in the cell. Partial restoration of this balance due to Sis1 overexpression or due to [pin-] status of the cell leads to the alleviation of toxicity and significant improvements in CG* degradation (Figure 30 and Figure 40).

We showed that even a small reduction in Sis1 levels in the Sis1-Tet-Off strain resulted in the stabilization of CG*. As Sis1 is a protein of low abundance, we propose that pathogenic polyQ expression significantly depletes the pool of this chaperone.

We conclude that Sis1 sequestration by pathogenic polyQ protein explains the observed inhibition of CG* degradation. However, other proteins might contribute to CG* stabilization. 96Q associates with proteins from the nuclear pore or ubiquitin receptors (such as Dsk2). This might increase the observed defect in the degradation of misfolded proteins.

Our results suggest that Sis1 is a limiting factor in the degradation of CG* and NLS-CG*. However, the limiting factors for CPY* and CTG* remain unknown. We suspect that the limiting factor for CTG* degradation could be Dsk2, which should be confirmed with direct evidence. 96Q interaction with the proteostasis network is complex and should be further investigated.

5.5   Sis1 plays an important role in the degradation of misfolded proteins in the nucleus

Proteasomes are present in the cytoplasm and in the nucleus in significant quantities (Wójcik and DeMartino, 2003). Studies have shown that misfolded proteins are degraded not only in the cytoplasm but also in the nucleus (Heck et al., 2010;Prasad et al., 2010). However, the mechanism underlying such degradation remains poorly understood. In our study, we established that CG* is degraded in the nucleus. The nuclear substrate NLS-CG* was very quickly degraded, whereas the cytoplasmic substrate NES-CG* was stabilized (Figure 54). These data are in accordance with other studies (Heck et al., 2010). We also established the role of the Sis1 co-chaperone in CG* degradation. This chaperone is actively involved in the delivery of misfolded proteins to the nucleus (Figure 57, Figure 58 and Figure 59). Moreover, Sis1 tagged with NLS and NES failed to increase CG*

degradation (Figure 54). Therefore, shuttling of the Sis1 protein between the cytosol and the nucleus is important for its activity.

In support of our data showing that Sis1 is involved in the degradation of misfolded proteins, another terminally misfolded protein was reported to degrade with the assistance of Sis1: the short-lived version of GFP, slGFP. We hypothesize that if previous studies had inhibited the proteasome, slGFP would have localized to the nucleus (Summers et al., 2013). We also speculate that Sis1 is an essential protein given its involvement in the degradation of misfolded proteins in the nucleus. When Sis1 is depleted due to interactions with 96Q, misfolded proteins are no longer delivered to the nucleus. The accumulation of misfolded proteins results in cytotoxicity.

The idea that misfolded cytosolic proteins are generally degraded in the nucleus should be verified by future experiments.

As mutant studies have shown, a fully functional J domain is essential for Sis1 function. Sis1AAA or Sis1ΔJ mutants were unable to replace wild-type Sis1 for CG* degradation. Therefore, interaction with Hsp70 plays a pivotal role for Sis1. Sis1 interacts with Ssa1, presumably by binding to Ssa1/Ydj1 and substrate complexes or by replacing Ydj1 in those complexes. Despite the fact that Sis1 is a much less abundant protein relative to Ydj1 (20,300 to 119,000 per cell, respectively), Sis1 likely has a stronger affinity for misfolded proteins relative to Ydj1. Based on our data, we propose the following model: misfolded proteins are attempted to be refolded several times by Ssa1/Ydj1; then, Sis1 interacts with these complexes, substitutes for Ydj1 and targets the misfolded proteins for degradation. This model would explain why the overexpression of Ydj1 had some effect on CG* degradation but also stabilized CG*. Based on the fact that the proper ratio between the chaperones was perturbed by 96Q, Sis1 was not able to target proteins for degradation.

Whether Sis1 directly interacts with importin proteins and nuclear pore complexes remains unclear. The specific role of Sis1 in nuclear transport is supported by the following facts: CG* and Sis1 accumulated in the nucleus upon proteasome inhibition, and NLS-Sis1 or NES-Sis1 were unable to functionally replace normal Sis1. Re-export of Sis1 to the cytosol in our model is interconnected with the transfer of misfolded proteins to the nuclear proteasome machinery. A model for Sis1 degradation in the nucleus is shown in Figure 60.

Additionally, CG*, NLS-CG*, CTG* and CPY*-HA were stabilized in the presence of 96Q. Pathogenic polyQ protein sequestered many different proteins, particularly the molecular chaperones Ssa1, Ydj1 and Sis1. Moreover, CPY*-derived misfolded proteins require

chaperone assistance for degradation, and therefore contribute to the depletion of chaperone capacity. CG* and NLS-CG* were stabilized because the Sis1 co-chaperone was sequestered. CTG* and CPY*-HA were stabilized via different mechanisms, which we speculate occurred because chaperone capacity was depleted by 96Q or because Dsk2 was sequestered by 96Q. However, the exact mechanism of CTG* stabilization should be confirmed with direct evidence.

In addition, the [PIN+] prion affects the chaperone capacity of the cell. We suspect that [PIN+] fibrils cause many other aggregation-prone proteins to aggregate (Patel and Liebman, 2007). We hypothesize that polyQ aggregates in [PIN+] cells sequester chaperone capacity (Figure 60).
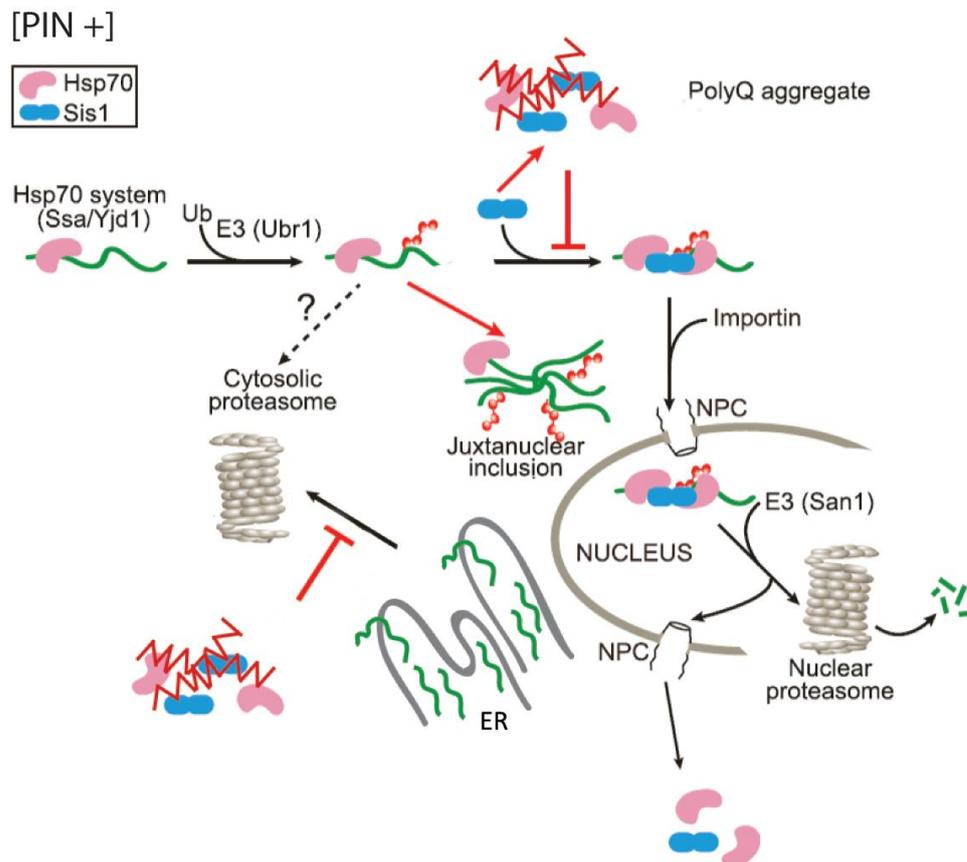
Figure 60. Model of the role of Sis1 in the degradation of misfolded cytosolic proteins.

CG*, CTG* and CPY*-HA are shown in the cytosol or ER. Misfolded proteins in the cytosol, such as CG* (green), are initially stabilized in their soluble form by Ssa1 in cooperation with Ydj1. CG* is a terminally misfolded protein; therefore, after several cycles of attempted refolding through protein binding and release, CG* remains unfolded and is ubiquitinated (most likely via Ubr1). Sis1 recognizes misfolded proteins and remodels the chaperone complex, shifting it from refolding to degradation mode. Sis1 stabilizes the association with Hsp70 and mediates protein import into the

nucleus for degradation by the proteasome. Red arrows indicate reactions where 96Q depletes Sis1. In addition, 96Q interferes with the degradation of CG*, CPY*-HA and CTG*. 96Q interacts with Sis1 and Hsp70 and sequesters them to the aggregates. Sis1 is required for CG* degradation. Chaperones are sequestered to aggregates and cannot assist in the degradation of misfolded proteins resulting in the accumulation of misfolded proteins. NLS-CG* is not shown in the figure but exhibits a similar mechanism of degradation to CG*.

Strikingly, 96Q does not inhibit the degradation of CG*, CTG* and NLS-CG* in [pin-] cells. Through immunoprecipitation and immunoblotting, our results show that 96Q does not interact with Ssa1, Ydj1 and Sis1 as strongly in [pin-] cells when compared with [PIN+] cells (Figure 34). Therefore, chaperone capacity was alleviated in [pin-] cells. This observation could help explain why different types of misfolded proteins were degraded normally in [pin-] cells. These results are summarized in Figure 61.
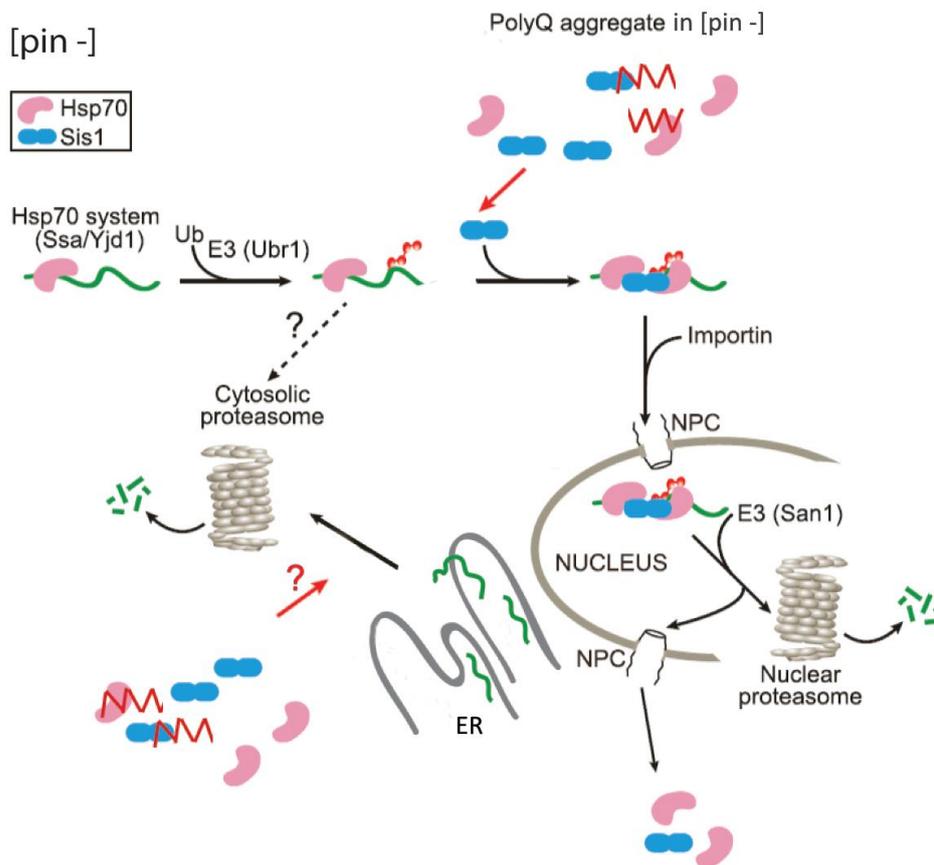
Figure 61. 96Q does not interfere with the degradation of CG*, CTG* and NLS-CG* in [pin-] cells.

In [pin-] cells, chaperone capacity is partially alleviated. CG*, NLS-CG* and CTG* are degraded normally even in the presence of 96Q. No significant accumulation of the studied misfolded proteins was observed in [pin-] cells.

# 6   References

Aebi, M., Bernasconi, R., Clerc, S., and Molinari, M. (2010). N-glycan structures: recognition and processing in the ER. Trends Biochem. Sci. *35*, 74–82.

Allen, K.D., Wegrzyn, R.D., Chernova, T.A., Müller, S., Newnam, G.P., Winslett, P.A., Wittich, K.B., Wilkinson, K.D., and Chernoff, Y.O. (2005). Hsp70 chaperones as modulators of prion life cycle: novel effects of Ssa and Ssb on the Saccharomyces cerevisiae prion [PSI+]. Genetics *169*, 1227–1242.

Anfinsen, C.B. (1973). Principles that govern the folding of protein chains. Science *181*, 223–230.

Arrasate, M., Mitra, S., Schweitzer, E.S., Segal, M.R., and Finkbeiner, S. (2004). Inclusion body formation reduces levels of mutant huntingtin and the risk of neuronal death. Nature *431*, 805–810.

Ballar, P., Pabuccuoglu, A., and Kose, F.A. (2011). Different p97/VCP complexes function in retrotranslocation step of mammalian ER-associated degradation (ERAD). Int. J. Biochem. Cell Biol. *43*, 613–621.

Barral, J.M., Broadley, S.A., Schaffar, G., and Hartl, F.U. (2004). Roles of molecular chaperones in protein misfolding diseases. Semin. Cell Dev. Biol. *15*, 17–29.

Bays, N.W., Gardner, R.G., Seelig, L.P., Joazeiro, C.A., and Hampton, R.Y. (2001a). Hrd1p/Der3p is a membrane-anchored ubiquitin ligase required for ER-associated degradation. Nat. Cell Biol. *3*, 24–29.

Bays, N.W., Wilhovsky, S.K., Goradia, A., Hodgkiss-Harlow, K., and Hampton, R.Y. (2001b). HRD4/NPL4 is required for the proteasomal processing of ubiquitinated ER proteins. Mol. Biol. Cell *12*, 4114–4128.

Becker, R.E., and Greig, N.H. (2008). Alzheimer's disease drug development: old problems require new priorities. CNS Neurol. Disord. Drug Targets *7*, 499–511.

Behrends, C., Langer, C.A., Boteva, R., Böttcher, U.M., Stemp, M.J., Schaffar, G., Rao, B.V., Giese, A., Kretzschmar, H., Siegers, K., et al. (2006). Chaperonin TRiC promotes the assembly of polyQ expansion proteins into nontoxic oligomers. Mol. Cell *23*, 887–897.

Bence, N.F., Sampat, R.M., and Kopito, R.R. (2001). Impairment of the ubiquitin-proteasome system by protein aggregation. Science *292*, 1552–1555.

Bennett, E.J., Bence, N.F., Jayakumar, R., and Kopito, R.R. (2005). Global impairment of the ubiquitin-proteasome system by nuclear or cytoplasmic protein aggregates precedes inclusion body formation. Mol. Cell *17*, 351–365.

Bennett, E.J., Shaler, T.A., Woodman, B., Ryu, K.-Y., Zaitseva, T.S., Becker, C.H., Bates, G.P., Schulman, H., and Kopito, R.R. (2007). Global changes to the ubiquitin system in Huntington's disease. Nature *448*, 704–708.

Bernasconi, R., Galli, C., Calanca, V., Nakajima, T., and Molinari, M. (2010). Stringent requirement for HRD1, SEL1L, and OS-9/XTP3-B for disposal of ERAD-LS substrates. J. Cell Biol. *188*, 223–235.

Bett, J.S., Goellner, G.M., Woodman, B., Pratt, G., Rechsteiner, M., and Bates, G.P. (2006). Proteasome impairment does not contribute to pathogenesis in R6/2 Huntington's disease mice: exclusion of proteasome activator REGgamma as a therapeutic target. Hum. Mol. Genet. *15*, 33–44.

Biggins, S., Ivanovska, I., and Rose, M.D. (1996). Yeast ubiquitin-like genes are involved in duplication of the microtubule organizing center. J. Cell Biol. *133*, 1331–1346.

Blond-Elguindi, S., Cwirla, S.E., Dower, W.J., Lipshutz, R.J., Sprang, S.R., Sambrook, J.F., and Gething, M.J. (1993). Affinity panning of a library of peptides displayed on bacteriophages reveals the binding specificity of BiP. Cell *75*, 717–728.

Bolognesi, B., Kumita, J.R., Barros, T.P., Esbjorner, E.K., Luheshi, L.M., Crowther, D.C., Wilson, M.R., Dobson, C.M., Favrin, G., and Yerbury, J.J. (2010). ANS binding reveals common features of cytotoxic amyloid species. ACS Chem. Biol. *5*, 735–740.

Boorstein, W.R., and Craig, E.A. (1990a). Transcriptional regulation of SSA3, an HSP70 gene from Saccharomyces cerevisiae. Mol. Cell. Biol. *10*, 3262–3267.

Boorstein, W.R., and Craig, E.A. (1990b). Regulation of a yeast HSP70 gene by a cAMP responsive transcriptional control element. EMBO J. *9*, 2543–2553.

Boorstein, W.R., Ziegelhoffer, T., and Craig, E.A. (1994). Molecular evolution of the HSP70 multigene family. J. Mol. Evol. *38*, 1–17.

Bordallo, J., Plemper, R.K., Finger, A., and Wolf, D.H. (1998). Der3p/Hrd1p is required for endoplasmic reticulum-associated degradation of misfolded lumenal and integral membrane proteins. Mol. Biol. Cell *9*, 209–222.

Botstein, D., Chervitz, S.A., and Cherry, J.M. (1997). Yeast as a model organism. Science *277*, 1259–1260.

Braakman, I., and Hebert, D.N. (2013). Protein folding in the endoplasmic reticulum. Cold Spring Harb. Perspect. Biol. *5*, a013201.

Brookmeyer, R., Johnson, E., Ziegler-Graham, K., and Arrighi, H.M. (2007). Forecasting the global burden of Alzheimer's disease. Alzheimers Dement. J. Alzheimers Assoc. *3*, 186–191.

Bukau, B., and Horwich, A.L. (1998). The Hsp70 and Hsp60 chaperone machines. Cell *92*, 351–366.

Burr, M.L., van den Boomen, D.J.H., Bye, H., Antrobus, R., Wiertz, E.J., and Lehner, P.J. (2013). MHC class I molecules are preferentially ubiquitinated on endoplasmic reticulum luminal residues during HRD1 ubiquitin E3 ligase-mediated dislocation. Proc. Natl. Acad. Sci. U. S. A. *110*, 14290–14295.

Carvalho, P., Goder, V., and Rapoport, T.A. (2006). Distinct ubiquitin-ligase complexes define convergent pathways for the degradation of ER proteins. Cell *126*, 361–373.

Carvalho, P., Stanley, A.M., and Rapoport, T.A. (2010). Retrotranslocation of a misfolded luminal ER protein by the ubiquitin-ligase Hrd1p. Cell *143*, 579–591.

Chafekar, S.M., and Duennwald, M.L. (2012). Impaired heat shock response in cells expressing full-length polyglutamine-expanded huntingtin. PloS One *7*, e37929.

Chang, Y.-W., Chuang, Y.-C., Ho, Y.-C., Cheng, M.-Y., Sun, Y.-J., Hsiao, C.-D., and Wang, C. (2010). Crystal structure of Get4-Get5 complex and its interactions with Sgt2, Get3, and Ydj1. J. Biol. Chem. *285*, 9962–9970.

Cheetham, M.E., and Caplan, A.J. (1998). Structure, function and evolution of DnaJ: conservation and adaptation of chaperone function. Cell Stress Chaperones *3*, 28–36.

Chiti, F., and Dobson, C.M. (2006). Protein misfolding, functional amyloid, and human disease. Annu. Rev. Biochem. *75*, 333–366.

Christianson, J.C., Olzmann, J.A., Shaler, T.A., Sowa, M.E., Bennett, E.J., Richter, C.M., Tyler, R.E., Greenblatt, E.J., Harper, J.W., and Kopito, R.R. (2012). Defining human ERAD networks through an integrative mapping strategy. Nat. Cell Biol. *14*, 93–105.

Ciechanover, A., and Brundin, P. (2003). The ubiquitin proteasome system in neurodegenerative diseases: sometimes the chicken, sometimes the egg. Neuron *40*, 427–446.

Claessen, J.H.L., and Ploegh, H.L. (2011). BAT3 guides misfolded glycoproteins out of the endoplasmic reticulum. PloS One *6*, e28542.

Clerc, S., Hirsch, C., Oggier, D.M., Deprez, P., Jakob, C., Sommer, T., and Aebi, M. (2009). Htm1 protein generates the N-glycan signal for glycoprotein degradation in the endoplasmic reticulum. J. Cell Biol. *184*, 159–172.

Cohen, A., Ross, L., Nachman, I., and Bar-Nun, S. (2012). Aggregation of polyQ proteins is increased upon yeast aging and affected by Sir2 and Hsf1: novel quantitative biochemical and microscopic assays. PloS One *7*, e44785.

Cohen, E., Bieschke, J., Perciavalle, R.M., Kelly, J.W., and Dillin, A. (2006). Opposing activities protect against age-onset proteotoxicity. Science *313*, 1604–1610.

Cox, J., and Mann, M. (2008). MaxQuant enables high peptide identification rates, individualized p.p.b.-range mass accuracies and proteome-wide protein quantification. Nat. Biotechnol. *26*, 1367–1372.

Cross, F.R. (1997). "Marker swap" plasmids: convenient tools for budding yeast molecular genetics. Yeast Chichester Engl. *13*, 647–653.

Cuanalo-Contreras, K., Mukherjee, A., and Soto, C. (2013). Role of protein misfolding and proteostasis deficiency in protein misfolding diseases and aging. Int. J. Cell Biol. *2013*, 638083.

Cummings, C.J., Orr, H.T., and Zoghbi, H.Y. (1999). Progress in pathogenesis studies of spinocerebellar ataxia type 1. Philos. Trans. R. Soc. Lond. B. Biol. Sci. *354*, 1079–1081.

Dantuma, N.P., Lindsten, K., Glas, R., Jellne, M., and Masucci, M.G. (2000). Short-lived green fluorescent proteins for quantifying ubiquitin/proteasome-dependent proteolysis in living cells. Nat. Biotechnol. *18*, 538–543.

Dehay, B., and Bertolotti, A. (2006). Critical role of the proline-rich region in Huntingtin for aggregation and cytotoxicity in yeast. J. Biol. Chem. *281*, 35608–35615.

Denic, V., Quan, E.M., and Weissman, J.S. (2006). A luminal surveillance complex that selects misfolded glycoproteins for ER-associated degradation. Cell *126*, 349–359.

Derkatch, I.L., Bradley, M.E., Zhou, P., Chernoff, Y.O., and Liebman, S.W. (1997). Genetic and environmental factors affecting the de novo appearance of the [PSI+] prion in Saccharomyces cerevisiae. Genetics *147*, 507–519.

Derkatch, I.L., Bradley, M.E., Masse, S.V., Zadorsky, S.P., Polozkov, G.V., Inge-Vechtomov, S.G., and Liebman, S.W. (2000). Dependence and independence of [PSI(+)] and [PIN(+)]: a two-prion system in yeast? EMBO J. *19*, 1942–1952.

Derkatch, I.L., Bradley, M.E., Hong, J.Y., and Liebman, S.W. (2001). Prions affect the appearance of other prions: the story of [PIN(+)]. Cell *106*, 171–182.

Derkatch, I.L., Uptain, S.M., Outeiro, T.F., Krishnan, R., Lindquist, S.L., and Liebman, S.W. (2004). Effects of Q/N-rich, polyQ, and non-polyQ amyloids on the de novo formation of the [PSI+] prion in yeast and aggregation of Sup35 in vitro. Proc. Natl. Acad. Sci. U. S. A. *101*, 12934–12939.

Deshaies, R.J., Koch, B.D., Werner-Washburne, M., Craig, E.A., and Schekman, R. (1988). A subfamily of stress proteins facilitates translocation of secretory and mitochondrial precursor polypeptides. Nature *332*, 800–805.

Díaz-Hernández, M., Valera, A.G., Morán, M.A., Gómez-Ramos, P., Alvarez-Castelao, B., Castaño, J.G., Hernández, F., and Lucas, J.J. (2006). Inhibition of 26S proteasome activity by huntingtin filaments but not inclusion bodies isolated from mouse and human brain. J. Neurochem. *98*, 1585–1596.

DiFiglia, M., Sapp, E., Chase, K., Schwarz, C., Meloni, A., Young, C., Martin, E., Vonsattel, J.P., Carraway, R., and Reeves, S.A. (1995). Huntingtin is a cytoplasmic protein associated with vesicles in human and rat brain neurons. Neuron *14*, 1075–1081.

DiFiglia, M., Sapp, E., Chase, K.O., Davies, S.W., Bates, G.P., Vonsattel, J.P., and Aronin, N. (1997). Aggregation of huntingtin in neuronal intranuclear inclusions and dystrophic neurites in brain. Science *277*, 1990–1993.

Dobson, C.M. (2004). Principles of protein folding, misfolding and aggregation. Semin. Cell Dev. Biol. *15*, 3–16.

Douglas, P.M., and Dillin, A. (2010). Protein homeostasis and aging in neurodegeneration. J. Cell Biol. *190*, 719–729.

Duennwald, M.L. (2012). Growth assays to assess polyglutamine toxicity in yeast. J. Vis. Exp. JoVE e3461.

Duennwald, M.L., and Lindquist, S. (2008). Impaired ERAD and ER stress are early and specific events in polyglutamine toxicity. Genes Dev. *22*, 3308–3319.

Duennwald, M.L., Jagadish, S., Muchowski, P.J., and Lindquist, S. (2006). Flanking sequences profoundly alter polyglutamine toxicity in yeast. Proc. Natl. Acad. Sci. U. S. A. *103*, 11045–11050.

Duyao, M., Ambrose, C., Myers, R., Novelletto, A., Persichetti, F., Frontali, M., Folstein, S., Ross, C., Franz, M., and Abbott, M. (1993). Trinucleotide repeat length instability and age of onset in Huntington's disease. Nat. Genet. *4*, 387–392.

Eichner, T., and Radford, S.E. (2011). A diversity of assembly mechanisms of a generic amyloid fold. Mol. Cell *43*, 8–18.

Eisele, F., and Wolf, D.H. (2008). Degradation of misfolded protein in the cytoplasm is mediated by the ubiquitin ligase Ubr1. FEBS Lett. *582*, 4143–4146.

Engel, S.R., Dietrich, F.S., Fisk, D.G., Binkley, G., Balakrishnan, R., Costanzo, M.C., Dwight, S.S., Hitz, B.C., Karra, K., Nash, R.S., et al. (2013). The Reference Genome Sequence of Saccharomyces cerevisiae: Then and Now. G3 Bethesda Md.

Ernst, R., Klemm, R., Schmitt, L., and Kuchler, K. (2005). Yeast ATP-binding cassette transporters: cellular cleaning pumps. Methods Enzymol. *400*, 460–484.

Fan, C.-Y., Lee, S., Ren, H.-Y., and Cyr, D.M. (2004). Exchangeable chaperone modules contribute to specification of type I and type II Hsp40 cellular function. Mol. Biol. Cell *15*, 761–773.

Faux, N.G., Bottomley, S.P., Lesk, A.M., Irving, J.A., Morrison, J.R., de la Banda, M.G., and Whisstock, J.C. (2005). Functional insights from the distribution and role of homopeptide repeat-containing proteins. Genome Res. *15*, 537–551.

Finkbeiner, S. (2011). Huntington's Disease. Cold Spring Harb. Perspect. Biol. *3*, a007476–a007476.

Fischer-Fantuzzi, L., and Vesco, C. (1988). Cell-dependent efficiency of reiterated nuclear signals in a mutant simian virus 40 oncoprotein targeted to the nucleus. Mol. Cell. Biol. *8*, 5495–5503.

Flaherty, K.M., DeLuca-Flaherty, C., and McKay, D.B. (1990). Three-dimensional structure of the ATPase fragment of a 70K heat-shock cognate protein. Nature *346*, 623–628.

Flynn, G.C., Pohl, J., Flocco, M.T., and Rothman, J.E. (1991). Peptide-binding specificity of the molecular chaperone BiP. Nature *353*, 726–730.

Folgueira, C., Carrión, J., Moreno, J., Saugar, J.M., Cañavate, C., and Requena, J.M. (2008). Effects of the disruption of the HSP70-II gene on the growth, morphology, and virulence of Leishmania infantum promastigotes. Int. Microbiol. Off. J. Span. Soc. Microbiol. *11*, 81–89.

Frydman, J. (2001). Folding of newly translated proteins in vivo: the role of molecular chaperones. Annu. Rev. Biochem. *70*, 603–647.

Gardner, R.G., Swarbrick, G.M., Bays, N.W., Cronin, S.R., Wilhovsky, S., Seelig, L., Kim, C., and Hampton, R.Y. (2000). Endoplasmic reticulum degradation requires lumen to cytosol signaling. Transmembrane control of Hrd1p by Hrd3p. J. Cell Biol. *151*, 69–82.

Gauss, R., Sommer, T., and Jarosch, E. (2006). The Hrd1p ligase complex forms a linchpin between ER-lumenal substrate selection and Cdc48p recruitment. EMBO J. *25*, 1827–1835.

Gerber, H.P., Seipel, K., Georgiev, O., Höfferer, M., Hug, M., Rusconi, S., and Schaffner, W. (1994). Transcriptional activation modulated by homopolymeric glutamine and proline stretches. Science *263*, 808–811.

Ghaemmaghami, S., Huh, W.-K., Bower, K., Howson, R.W., Belle, A., Dephoure, N., O'Shea, E.K., and Weissman, J.S. (2003). Global analysis of protein expression in yeast. Nature *425*, 737–741.

Gil, G., Faust, J.R., Chin, D.J., Goldstein, J.L., and Brown, M.S. (1985). Membrane-bound domain of HMG CoA reductase is required for sterol-enhanced degradation of the enzyme. Cell *41*, 249–258.

Glover, J.R., and Lindquist, S. (1998). Hsp104, Hsp70, and Hsp40: a novel chaperone system that rescues previously aggregated proteins. Cell *94*, 73–82.

Goldstein, G., Scheid, M., Hammerling, U., Schlesinger, D.H., Niall, H.D., and Boyse, E.A. (1975). Isolation of a polypeptide that has lymphocyte-differentiating properties and is probably represented universally in living cells. Proc. Natl. Acad. Sci. U. S. A. *72*, 11–15.

Gong, Y., Kakihara, Y., Krogan, N., Greenblatt, J., Emili, A., Zhang, Z., and Houry, W.A. (2009). An atlas of chaperone-protein interactions in Saccharomyces cerevisiae: implications to protein folding pathways in the cell. Mol. Syst. Biol. *5*, 275.

Greene, M.K., Maskos, K., and Landry, S.J. (1998). Role of the J-domain in the cooperation of Hsp40 with Hsp70. Proc. Natl. Acad. Sci. U. S. A. *95*, 6108–6113.

Guarente, L. (1983). Yeast promoters and lacZ fusions designed to study expression of cloned genes in yeast. Methods Enzymol. *101*, 181–191.

Gutekunst, C.A., Levey, A.I., Heilman, C.J., Whaley, W.L., Yi, H., Nash, N.R., Rees, H.D., Madden, J.J., and Hersch, S.M. (1995). Identification and localization of huntingtin in brain and human lymphoblastoid cell lines with anti-fusion protein antibodies. Proc. Natl. Acad. Sci. U. S. A. *92*, 8710–8714.

Haass, C., and Selkoe, D.J. (2007). Soluble protein oligomers in neurodegeneration: lessons from the Alzheimer's amyloid beta-peptide. Nat. Rev. Mol. Cell Biol. *8*, 101–112.

Hardy, J., and Orr, H. (2006). The genetics of neurodegenerative diseases. J. Neurochem. *97*, 1690–1699.

Harjes, P., and Wanker, E.E. (2003). The hunt for huntingtin function: interaction partners tell many different stories. Trends Biochem. Sci. *28*, 425–433.

Harrison, C.J., Hayer-Hartl, M., Di Liberto, M., Hartl, F., and Kuriyan, J. (1997). Crystal structure of the nucleotide exchange factor GrpE bound to the ATPase domain of the molecular chaperone DnaK. Science *276*, 431–435.

Hartl, F.U. (1996). Molecular chaperones in cellular protein folding. Nature *381*, 571–579.

Hartl, F.U., and Hayer-Hartl, M. (2002). Molecular chaperones in the cytosol: from nascent chain to folded protein. Science *295*, 1852–1858.

Hartl, F.U., and Hayer-Hartl, M. (2009). Converging concepts of protein folding in vitro and in vivo. Nat. Struct. Mol. Biol. *16*, 574–581.

Hartl, F.U., Bracher, A., and Hayer-Hartl, M. (2011). Molecular chaperones in protein folding and proteostasis. Nature *475*, 324–332.

Hartley, D.M., Walsh, D.M., Ye, C.P., Diehl, T., Vasquez, S., Vassilev, P.M., Teplow, D.B., and Selkoe, D.J. (1999). Protofibrillar intermediates of amyloid beta-protein induce acute electrophysiological changes and progressive neurotoxicity in cortical neurons. J. Neurosci. Off. J. Soc. Neurosci. *19*, 8876–8884.

Havel, L.S., Li, S., and Li, X.-J. (2009). Nuclear accumulation of polyglutamine disease proteins and neuropathology. Mol. Brain 2, 21.

Heck, J.W., Cheung, S.K., and Hampton, R.Y. (2010). Cytoplasmic protein quality control degradation mediated by parallel actions of the E3 ubiquitin ligases Ubr1 and San1. Proc. Natl. Acad. Sci. U. S. A. *107*, 1106–1111.

Heiser, V., Scherzinger, E., Boeddrich, A., Nordhoff, E., Lurz, R., Schugardt, N., Lehrach, H., and Wanker, E.E. (2000). Inhibition of huntingtin fibrillogenesis by specific antibodies and small molecules: implications for Huntington's disease therapy. Proc. Natl. Acad. Sci. U. S. A. *97*, 6739–6744.

Hershko, A., and Ciechanover, A. (1998). The ubiquitin system. Annu. Rev. Biochem. *67*, 425–479.

Hipp, M.S., Patel, C.N., Bersuker, K., Riley, B.E., Kaiser, S.E., Shaler, T.A., Brandeis, M., and Kopito, R.R. (2012). Indirect inhibition of 26S proteasome activity in a cellular model of Huntington's disease. J. Cell Biol. *196*, 573–587.

Hipp, M.S., Park, S.-H., and Hartl, F.U. (2014). Proteostasis impairment in protein-misfolding and -aggregation diseases. Trends Cell Biol. *24*, 506–514.

Hirakura, Y., Azimov, R., Azimova, R., and Kagan, B.L. (2000). Polyglutamine-induced ion channels: a possible mechanism for the neurotoxicity of Huntington and other CAG repeat diseases. J. Neurosci. Res. *60*, 490–494.

Höhfeld, J., Minami, Y., and Hartl, F.U. (1995). Hip, a novel cochaperone involved in the eukaryotic Hsc70/Hsp40 reaction cycle. Cell *83*, 589–598.

Hoogeveen, A.T., Willemsen, R., Meyer, N., de Rooij, K.E., Roos, R.A., van Ommen, G.J., and Galjaard, H. (1993). Characterization and localization of the Huntington disease gene product. Hum. Mol. Genet. *2*, 2069–2073.

Horn, S.C., Hanna, J., Hirsch, C., Volkwein, C., Schütz, A., Heinemann, U., Sommer, T., and Jarosch, E. (2009). Usa1 functions as a scaffold of the HRD-ubiquitin ligase. Mol. Cell *36*, 782–793.

Horton, L.E., James, P., Craig, E.A., and Hensold, J.O. (2001). The yeast hsp70 homologue Ssa is required for translation and interacts with Sis1 and Pab1 on translating ribosomes. J. Biol. Chem. *276*, 14426–14433.

Huh, W.-K., Falvo, J.V., Gerke, L.C., Carroll, A.S., Howson, R.W., Weissman, J.S., and O'Shea, E.K. (2003). Global analysis of protein localization in budding yeast. Nature *425*, 686–691.

Huyer, G., Piluek, W.F., Fansler, Z., Kreft, S.G., Hochstrasser, M., Brodsky, J.L., and Michaelis, S. (2004). Distinct machinery is required in Saccharomyces cerevisiae for the endoplasmic reticulum-associated degradation of a multispanning membrane protein and a soluble luminal protein. J. Biol. Chem. *279*, 38369–38378.

Jahn, T.R., and Radford, S.E. (2008). Folding versus aggregation: polypeptide conformations on competing pathways. Arch. Biochem. Biophys. *469*, 100–117.

Jana, N.R., Zemskov, E.A., Wang Gh, null, and Nukina, N. (2001). Altered proteasomal function due to the expression of polyglutamine-expanded truncated N-terminal huntingtin

induces apoptosis by caspase activation through mitochondrial cytochrome c release. Hum. Mol. Genet. *10*, 1049–1059.

Jentsch, S., and Rumpf, S. (2007). Cdc48 (p97): a "molecular gearbox" in the ubiquitin pathway? Trends Biochem. Sci. *32*, 6–11.

Johnson, A.W., Lund, E., and Dahlberg, J. (2002). Nuclear export of ribosomal subunits. Trends Biochem. Sci. *27*, 580–585.

Johnson, E.S., Ma, P.C., Ota, I.M., and Varshavsky, A. (1995). A proteolytic pathway that recognizes ubiquitin as a degradation signal. J. Biol. Chem. *270*, 17442–17456.

Jonikas, M.C., Collins, S.R., Denic, V., Oh, E., Quan, E.M., Schmid, V., Weibezahn, J., Schwappach, B., Walter, P., Weissman, J.S., et al. (2009). Comprehensive characterization of genes required for protein folding in the endoplasmic reticulum. Science *323*, 1693–1697.

Juenemann, K., Schipper-Krom, S., Wiemhoefer, A., Kloss, A., Sanz Sanz, A., and Reits, E.A.J. (2013). Expanded polyglutamine-containing N-terminal huntingtin fragments are entirely degraded by mammalian proteasomes. J. Biol. Chem. *288*, 27068–27084.

Jung, G., and Masison, D.C. (2001). Guanidine hydrochloride inhibits Hsp104 activity in vivo: a possible explanation for its effect in curing yeast prions. Curr. Microbiol. *43*, 7–10.

Juretschke, J., Menssen, R., Sickmann, A., and Wolf, D.H. (2010). The Hsp70 chaperone Ssa1 is essential for catabolite induced degradation of the gluconeogenic enzyme fructose-1,6-bisphosphatase. Biochem. Biophys. Res. Commun. *397*, 447–452.

Kaganovich, D., Kopito, R., and Frydman, J. (2008). Misfolded proteins partition between two distinct quality control compartments. Nature *454*, 1088–1095.

Kampinga, H.H., and Craig, E.A. (2010). The HSP70 chaperone machinery: J proteins as drivers of functional specificity. Nat. Rev. Mol. Cell Biol. *11*, 579–592.

Kanazawa, I. (1999). Molecular pathology of dentatorubral-pallidoluysian atrophy. Philos. Trans. R. Soc. Lond. B. Biol. Sci. *354*, 1069–1074.

Kazantsev, A., Preisinger, E., Dranovsky, A., Goldgaber, D., and Housman, D. (1999). Insoluble detergent-resistant aggregates form between pathological and nonpathological lengths of polyglutamine in mammalian cells. Proc. Natl. Acad. Sci. U. S. A. *96*, 11404–11409.

Kelley, W.L. (1998). The J-domain family and the recruitment of chaperone power. Trends Biochem. Sci. *23*, 222–227.

Kennedy, W.R., Alter, M., and Sung, J.H. (1968). Progressive proximal spinal and bulbar muscular atrophy of late onset. A sex-linked recessive trait. Neurology *18*, 671–680.

Kim, Y.E., Hipp, M.S., Bracher, A., Hayer-Hartl, M., and Hartl, F.U. (2013). Molecular chaperone functions in protein folding and proteostasis. Annu. Rev. Biochem. *82*, 323–355.

Kisselev, A.F., Kaganovich, D., and Goldberg, A.L. (2002). Binding of hydrophobic peptides to several non-catalytic sites promotes peptide hydrolysis by all active sites of 20 S proteasomes. Evidence for peptide-induced channel opening in the alpha-rings. J. Biol. Chem. *277*, 22260–22270.

Komander, D., and Rape, M. (2012). The ubiquitin code. Annu. Rev. Biochem. *81*, 203–229.

Konopka, C.A., Locke, M.N., Gallagher, P.S., Pham, N., Hart, M.P., Walker, C.J., Gitler, A.D., and Gardner, R.G. (2011). A yeast model for polyalanine-expansion aggregation and toxicity. Mol. Biol. Cell 22, 1971–1984.

Krobitsch, S., and Lindquist, S. (2000). Aggregation of huntingtin in yeast varies with the length of the polyglutamine expansion and the expression of chaperone proteins. Proc. Natl. Acad. Sci. U. S. A. 97, 1589–1594.

Kuemmerle, S., Gutekunst, C.A., Klein, A.M., Li, X.J., Li, S.H., Beal, M.F., Hersch, S.M., and Ferrante, R.J. (1999). Huntington aggregates may not predict neuronal death in Huntington's disease. Ann. Neurol. 46, 842–849.

Kumar, A., Agarwal, S., Heyman, J.A., Matson, S., Heidtman, M., Piccirillo, S., Umansky, L., Drawid, A., Jansen, R., Liu, Y., et al. (2002). Subcellular localization of the yeast proteome. Genes Dev. 16, 707–719.

Kurahashi, H., Ishiwata, M., Shibata, S., and Nakamura, Y. (2008). A regulatory role of the Rnq1 nonprion domain for prion propagation and polyglutamine aggregates. Mol. Cell. Biol. 28, 3313–3323.

Kushnirov, V.V., Kryndushkin, D.S., Boguta, M., Smirnov, V.N., and Ter-Avanesyan, M.D. (2000). Chaperones that cure yeast artificial [PSI+] and their prion-specific effects. Curr. Biol. CB 10, 1443–1446.

Laemmli, U.K. (1970). Cleavage of structural proteins during the assembly of the head of bacteriophage T4. Nature 227, 680–685.

Lange, O.F., Lakomek, N.-A., Farès, C., Schröder, G.F., Walter, K.F.A., Becker, S., Meiler, J., Grubmüller, H., Griesinger, C., and de Groot, B.L. (2008). Recognition dynamics up to microseconds revealed from an RDC-derived ubiquitin ensemble in solution. Science 320, 1471–1475.

Langer, T., Lu, C., Echols, H., Flanagan, J., Hayer, M.K., and Hartl, F.U. (1992). Successive action of DnaK, DnaJ and GroEL along the pathway of chaperone-mediated protein folding. Nature 356, 683–689.

Lebre, A.-S., and Brice, A. (2003). Spinocerebellar ataxia 7 (SCA7). Cytogenet. Genome Res. 100, 154–163.

Lee, S., Fan, C.Y., Younger, J.M., Ren, H., and Cyr, D.M. (2002). Identification of essential residues in the type II Hsp40 Sis1 that function in polypeptide binding. J. Biol. Chem. 277, 21675–21682.

Leitman, J., Ulrich Hartl, F., and Lederkremer, G.Z. (2013). Soluble forms of polyQ-expanded huntingtin rather than large aggregates cause endoplasmic reticulum stress. Nat. Commun. 4, 2753.

Li, S.-H., and Li, X.-J. (2004). Huntingtin and its role in neuronal degeneration. Neurosci. Rev. J. Bringing Neurobiol. Neurol. Psychiatry 10, 467–475.

Li, H., Li, S.H., Johnston, H., Shelbourne, P.F., and Li, X.J. (2000). Amino-terminal fragments of mutant huntingtin show selective accumulation in striatal neurons and synaptic toxicity. Nat. Genet. 25, 385–389.

Li, S.H., Cheng, A.L., Li, H., and Li, X.J. (1999). Cellular defects and altered gene expression in PC12 cells stably expressing mutant huntingtin. J. Neurosci. Off. J. Soc. Neurosci. *19*, 5159–5172.

Li, Z., Hartl, F.U., and Bracher, A. (2013). Structure and function of Hip, an attenuator of the Hsp70 chaperone cycle. Nat. Struct. Mol. Biol. *20*, 929–935.

Lindquist, S. (1986). The heat-shock response. Annu. Rev. Biochem. *55*, 1151–1191.

Lindquist, S., Krobitsch, S., Li, L., and Sondheimer, N. (2001). Investigating protein conformation-based inheritance and disease in yeast. Philos. Trans. R. Soc. Lond. B. Biol. Sci. *356*, 169–176.

Lippincott-Schwartz, J., Bonifacino, J.S., Yuan, L.C., and Klausner, R.D. (1988). Degradation from the endoplasmic reticulum: disposing of newly synthesized proteins. Cell *54*, 209–220.

Lopez, N., Aron, R., and Craig, E.A. (2003). Specificity of class II Hsp40 Sis1 in maintenance of yeast prion [RNQ+]. Mol. Biol. Cell *14*, 1172–1181.

Luke, M.M., Sutton, A., and Arndt, K.T. (1991). Characterization of SIS1, a Saccharomyces cerevisiae homologue of bacterial dnaJ proteins. J. Cell Biol. *114*, 623–638.

Mangiarini, L., Sathasivam, K., Seller, M., Cozens, B., Harper, A., Hetherington, C., Lawton, M., Trottier, Y., Lehrach, H., Davies, S.W., et al. (1996). Exon 1 of the HD gene with an expanded CAG repeat is sufficient to cause a progressive neurological phenotype in transgenic mice. Cell *87*, 493–506.

Manogaran, A.L., Fajardo, V.M., Reid, R.J.D., Rothstein, R., and Liebman, S.W. (2010). Most, but not all, yeast strains in the deletion library contain the [PIN(+)] prion. Yeast Chichester Engl. *27*, 159–166.

Martinez-Yamout, M., Legge, G.B., Zhang, O., Wright, P.E., and Dyson, H.J. (2000). Solution structure of the cysteine-rich domain of the Escherichia coli chaperone protein DnaJ. J. Mol. Biol. *300*, 805–818.

Mathur, V., Hong, J.Y., and Liebman, S.W. (2009). Ssa1 overexpression and [PIN(+)] variants cure [PSI(+)] by dilution of aggregates. J. Mol. Biol. *390*, 155–167.

Maurer, P., Redd, M., Solsbacher, J., Bischoff, F.R., Greiner, M., Podtelejnikov, A.V., Mann, M., Stade, K., Weis, K., and Schlenstedt, G. (2001). The nuclear export receptor Xpo1p forms distinct complexes with NES transport substrates and the yeast Ran binding protein 1 (Yrb1p). Mol. Biol. Cell *12*, 539–549.

Mayer, M.P. (2010). Gymnastics of molecular chaperones. Mol. Cell *39*, 321–331.

Maynard, C.J., Böttcher, C., Ortega, Z., Smith, R., Florea, B.I., Díaz-Hernández, M., Brundin, P., Overkleeft, H.S., Li, J.-Y., Lucas, J.J., et al. (2009). Accumulation of ubiquitin conjugates in a polyglutamine disease model occurs without global ubiquitin/proteasome system impairment. Proc. Natl. Acad. Sci. U. S. A. *106*, 13986–13991.

McGowan, D.P., van Roon-Mom, W., Holloway, H., Bates, G.P., Mangiarini, L., Cooper, G.J., Faull, R.L., and Snell, R.G. (2000). Amyloid-like inclusions in Huntington's disease. Neuroscience *100*, 677–680.

McKeehan, W., and Hardesty, B. (1969). The mechanism of cycloheximide inhibition of protein synthesis in rabbit reticulocytes. Biochem. Biophys. Res. Commun. *36*, 625–630.

Medicherla, B., Kostova, Z., Schaefer, A., and Wolf, D.H. (2004). A genomic screen identifies Dsk2p and Rad23p as essential components of ER-associated degradation. EMBO Rep. *5*, 692–697.

Mehnert, M., Sommer, T., and Jarosch, E. (2014). Der1 promotes movement of misfolded proteins through the endoplasmic reticulum membrane. Nat. Cell Biol. *16*, 77–86.

Meriin, A.B., Zhang, X., He, X., Newnam, G.P., Chernoff, Y.O., and Sherman, M.Y. (2002). Huntington toxicity in yeast model depends on polyglutamine aggregation mediated by a prion-like protein Rnq1. J. Cell Biol. *157*, 997–1004.

Michalik, A., and Van Broeckhoven, C. (2004). Proteasome degrades soluble expanded polyglutamine completely and efficiently. Neurobiol. Dis. *16*, 202–211.

Minton, A.P. (2000). Effects of excluded surface area and adsorbate clustering on surface adsorption of proteins I. Equilibrium models. Biophys. Chem. *86*, 239–247.

Miranda, M., and Sorkin, A. (2007). Regulation of receptors and transporters by ubiquitination: new insights into surprisingly similar mechanisms. Mol. Interv. *7*, 157–167.

Monoi, H., Futaki, S., Kugimiya, S., Minakata, H., and Yoshihara, K. (2000). Poly-L-glutamine forms cation channels: relevance to the pathogenesis of the polyglutamine diseases. Biophys. J. *78*, 2892–2899.

Morimoto, R.I. (2008). Proteotoxic stress and inducible chaperone networks in neurodegenerative disease and aging. Genes Dev. *22*, 1427–1438.

Mukai, H., Kuno, T., Tanaka, H., Hirata, D., Miyakawa, T., and Tanaka, C. (1993). Isolation and characterization of SSE1 and SSE2, new members of the yeast HSP70 multigene family. Gene *132*, 57–66.

Mutsuddi, M., and Rebay, I. (2005). Molecular genetics of spinocerebellar ataxia type 8 (SCA8). RNA Biol. *2*, 49–52.

Nakatsukasa, K., Huyer, G., Michaelis, S., and Brodsky, J.L. (2008). Dissecting the ER-associated degradation of a misfolded polytopic membrane protein. Cell *132*, 101–112.

Nance, M.A., Mathias-Hagen, V., Breningstall, G., Wick, M.J., and McGlennen, R.C. (1999). Analysis of a very large trinucleotide repeat in a patient with juvenile Huntington's disease. Neurology *52*, 392–394.

Nucifora, F.C., Jr, Sasaki, M., Peters, M.F., Huang, H., Cooper, J.K., Yamada, M., Takahashi, H., Tsuji, S., Troncoso, J., Dawson, V.L., et al. (2001). Interference by huntingtin and atrophin-1 with cbp-mediated transcription leading to cellular toxicity. Science *291*, 2423–2428.

Ohtsuka, K. (1993). Cloning of a cDNA for heat-shock protein hsp40, a human homologue of bacterial DnaJ. Biochem. Biophys. Res. Commun. *197*, 235–240.

Oliveira, J.M.A. (2010). Nature and cause of mitochondrial dysfunction in Huntington's disease: focusing on huntingtin and the striatum. J. Neurochem. *114*, 1–12.

Olzscha, H., Schermann, S.M., Woerner, A.C., Pinkert, S., Hecht, M.H., Tartaglia, G.G., Vendruscolo, M., Hayer-Hartl, M., Hartl, F.U., and Vabulas, R.M. (2011). Amyloid-like aggregates sequester numerous metastable proteins with essential cellular functions. Cell *144*, 67–78.

Ong, S.-E., and Mann, M. (2006). A practical recipe for stable isotope labeling by amino acids in cell culture (SILAC). Nat. Protoc. *1*, 2650–2660.

Ortega, Z., Díaz-Hernández, M., Maynard, C.J., Hernández, F., Dantuma, N.P., and Lucas, J.J. (2010). Acute polyglutamine expression in inducible mouse model unravels ubiquitin/proteasome system impairment and permanent recovery attributable to aggregate formation. J. Neurosci. Off. J. Soc. Neurosci. *30*, 3675–3688.

Pandey, U.B., Nie, Z., Batlevi, Y., McCray, B.A., Ritson, G.P., Nedelsky, N.B., Schwartz, S.L., DiProspero, N.A., Knight, M.A., Schuldiner, O., et al. (2007). HDAC6 rescues neurodegeneration and provides an essential link between autophagy and the UPS. Nature *447*, 859–863.

Park, S.-H., Bolender, N., Eisele, F., Kostova, Z., Takeuchi, J., Coffino, P., and Wolf, D.H. (2007a). The cytoplasmic Hsp70 chaperone machinery subjects misfolded and endoplasmic reticulum import-incompetent proteins to degradation via the ubiquitin-proteasome system. Mol. Biol. Cell *18*, 153–165.

Park, S.-H., Bolender, N., Eisele, F., Kostova, Z., Takeuchi, J., Coffino, P., and Wolf, D.H. (2007b). The cytoplasmic Hsp70 chaperone machinery subjects misfolded and endoplasmic reticulum import-incompetent proteins to degradation via the ubiquitin-proteasome system. Mol. Biol. Cell *18*, 153–165.

Park, S.-H., Kukushkin, Y., Gupta, R., Chen, T., Konagai, A., Hipp, M.S., Hayer-Hartl, M., and Hartl, F.U. (2013). PolyQ proteins interfere with nuclear degradation of cytosolic proteins by sequestering the Sis1p chaperone. Cell *154*, 134–145.

Patel, B.K., and Liebman, S.W. (2007). "Prion-proof" for [PIN+]: infection with in vitro-made amyloid aggregates of Rnq1p-(132-405) induces [PIN+]. J. Mol. Biol. *365*, 773–782.

Patino, M.M., Liu, J.J., Glover, J.R., and Lindquist, S. (1996). Support for the prion hypothesis for inheritance of a phenotypic trait in yeast. Science *273*, 622–626.

PAULING, L., and COREY, R.B. (1951). Atomic coordinates and structure factors for two helical configurations of polypeptide chains. Proc. Natl. Acad. Sci. U. S. A. *37*, 235–240.

PAULING, L., COREY, R.B., and BRANSON, H.R. (1951). The structure of proteins; two hydrogen-bonded helical configurations of the polypeptide chain. Proc. Natl. Acad. Sci. U. S. A. *37*, 205–211.

Paushkin, S.V., Kushnirov, V.V., Smirnov, V.N., and Ter-Avanesyan, M.D. (1996). Propagation of the yeast prion-like [psi+] determinant is mediated by oligomerization of the SUP35-encoded polypeptide chain release factor. EMBO J. *15*, 3127–3134.

Pellecchia, M., Szyperski, T., Wall, D., Georgopoulos, C., and Wüthrich, K. (1996). NMR structure of the J-domain and the Gly/Phe-rich region of the Escherichia coli DnaJ chaperone. J. Mol. Biol. *260*, 236–250.

Perutz, M.F., Johnson, T., Suzuki, M., and Finch, J.T. (1994). Glutamine repeats as polar zippers: their possible role in inherited neurodegenerative diseases. Proc. Natl. Acad. Sci. U. S. A. *91*, 5355–5358.

Peters, J.M., Franke, W.W., and Kleinschmidt, J.A. (1994). Distinct 19 S and 20 S subcomplexes of the 26 S proteasome and their distribution in the nucleus and the cytoplasm. J. Biol. Chem. *269*, 7709–7718.

Piccioni, F., Pinton, P., Simeoni, S., Pozzi, P., Fascio, U., Vismara, G., Martini, L., Rizzuto, R., and Poletti, A. (2002). Androgen receptor with elongated polyglutamine tract forms aggregates that alter axonal trafficking and mitochondrial distribution in motor neuronal processes. FASEB J. Off. Publ. Fed. Am. Soc. Exp. Biol. *16*, 1418–1420.

Pickart, C.M. (2001). Mechanisms underlying ubiquitination. Annu. Rev. Biochem. *70*, 503–533.

Pike, C.J., Burdick, D., Walencewicz, A.J., Glabe, C.G., and Cotman, C.W. (1993). Neurodegeneration induced by beta-amyloid peptides in vitro: the role of peptide assembly state. J. Neurosci. Off. J. Soc. Neurosci. *13*, 1676–1687.

Pilon, M., Schekman, R., and Römisch, K. (1997). Sec61p mediates export of a misfolded secretory protein from the endoplasmic reticulum to the cytosol for degradation. EMBO J. *16*, 4540–4548.

Plemper, R.K., Böhmler, S., Bordallo, J., Sommer, T., and Wolf, D.H. (1997). Mutant analysis links the translocon and BiP to retrograde protein transport for ER degradation. Nature *388*, 891–895.

Polier, S., Dragovic, Z., Hartl, F.U., and Bracher, A. (2008). Structural basis for the cooperation of Hsp70 and Hsp110 chaperones in protein folding. Cell *133*, 1068–1079.

Powers, E.T., Morimoto, R.I., Dillin, A., Kelly, J.W., and Balch, W.E. (2009). Biological and chemical approaches to diseases of proteostasis deficiency. Annu. Rev. Biochem. *78*, 959–991.

Prasad, R., Kawaguchi, S., and Ng, D.T.W. (2010). A nucleus-based quality control mechanism for cytosolic proteins. Mol. Biol. Cell *21*, 2117–2127.

Qian, Y.Q., Patel, D., Hartl, F.U., and McColl, D.J. (1996). Nuclear magnetic resonance solution structure of the human Hsp40 (HDJ-1) J-domain. J. Mol. Biol. *260*, 224–235.

Qiu, X.-B., Shao, Y.-M., Miao, S., and Wang, L. (2006). The diversity of the DnaJ/Hsp40 family, the crucial partners for Hsp70 chaperones. Cell. Mol. Life Sci. CMLS *63*, 2560–2570.

Quan, E.M., Kamiya, Y., Kamiya, D., Denic, V., Weibezahn, J., Kato, K., and Weissman, J.S. (2008). Defining the glycan destruction signal for endoplasmic reticulum-associated degradation. Mol. Cell *32*, 870–877.

Rabinovich, E., Kerem, A., Fröhlich, K.-U., Diamant, N., and Bar-Nun, S. (2002). AAA-ATPase p97/Cdc48p, a cytosolic chaperone required for endoplasmic reticulum-associated protein degradation. Mol. Cell. Biol. *22*, 626–634.

Rajan, V.B.V., and D'Silva, P. (2009). Arabidopsis thaliana J-class heat shock proteins: cellular stress sensors. Funct. Integr. Genomics *9*, 433–446.

Rajan, R.S., Illing, M.E., Bence, N.F., and Kopito, R.R. (2001). Specificity in intracellular protein aggregation and inclusion body formation. Proc. Natl. Acad. Sci. U. S. A. *98*, 13060–13065.

Rapoport, T.A. (2007). Protein translocation across the eukaryotic endoplasmic reticulum and bacterial plasma membranes. Nature *450*, 663–669.

Raspe, M., Gillis, J., Krol, H., Krom, S., Bosch, K., van Veen, H., and Reits, E. (2009). Mimicking proteasomal release of polyglutamine peptides initiates aggregation and toxicity. J. Cell Sci. *122*, 3262–3271.

Ravid, T., Kreft, S.G., and Hochstrasser, M. (2006). Membrane and soluble substrates of the Doa10 ubiquitin ligase are degraded by distinct pathways. EMBO J. *25*, 533–543.

Richly, H., Rape, M., Braun, S., Rumpf, S., Hoege, C., and Jentsch, S. (2005). A series of ubiquitin binding factors connects CDC48/p97 to substrate multiubiquitylation and proteasomal targeting. Cell *120*, 73–84.

Robertson, A.L., Bate, M.A., Androulakis, S.G., Bottomley, S.P., and Buckle, A.M. (2011). PolyQ: a database describing the sequence and domain context of polyglutamine repeats in proteins. Nucleic Acids Res. *39*, D272–D276.

Romanos, M.A., Scorer, C.A., and Clare, J.J. (1992). Foreign gene expression in yeast: a review. Yeast Chichester Engl. *8*, 423–488.

De Rooij, K.E., Dorsman, J.C., Smoor, M.A., Den Dunnen, J.T., and Van Ommen, G.J. (1996). Subcellular localization of the Huntington's disease gene product in cell lines by immunofluorescence and biochemical subcellular fractionation. Hum. Mol. Genet. *5*, 1093–1099.

Rosenbaum, J.C., Fredrickson, E.K., Oeser, M.L., Garrett-Engele, C.M., Locke, M.N., Richardson, L.A., Nelson, Z.W., Hetrick, E.D., Milac, T.I., Gottschling, D.E., et al. (2011). Disorder targets misorder in nuclear quality control degradation: a disordered ubiquitin ligase directly recognizes its misfolded substrates. Mol. Cell *41*, 93–106.

Rout, M.P., Aitchison, J.D., Suprapto, A., Hjertaas, K., Zhao, Y., and Chait, B.T. (2000). The yeast nuclear pore complex: composition, architecture, and transport mechanism. J. Cell Biol. *148*, 635–651.

Rubenstein, E.M., Kreft, S.G., Greenblatt, W., Swanson, R., and Hochstrasser, M. (2012). Aberrant substrate engagement of the ER translocon triggers degradation by the Hrd1 ubiquitin ligase. J. Cell Biol. *197*, 761–773.

Rüdiger, S., Germeroth, L., Schneider-Mergener, J., and Bukau, B. (1997). Substrate specificity of the DnaK chaperone determined by screening cellulose-bound peptide libraries. EMBO J. *16*, 1501–1507.

Rumpf, S., and Jentsch, S. (2006). Functional division of substrate processing cofactors of the ubiquitin-selective Cdc48 chaperone. Mol. Cell *21*, 261–269.

Russell, S.J., Steger, K.A., and Johnston, S.A. (1999). Subcellular localization, stoichiometry, and protein levels of 26 S proteasome subunits in yeast. J. Biol. Chem. *274*, 21943–21952.

Sakahira, H., Breuer, P., Hayer-Hartl, M.K., and Hartl, F.U. (2002). Molecular chaperones as modulators of polyglutamine protein aggregation and toxicity. Proc. Natl. Acad. Sci. U. S. A. *99 Suppl 4*, 16412–16418.

Sánchez, I., Mahlke, C., and Yuan, J. (2003). Pivotal role of oligomerization in expanded polyglutamine neurodegenerative disorders. Nature *421*, 373–379.

Sato, B.K., Schulz, D., Do, P.H., and Hampton, R.Y. (2009). Misfolded membrane proteins are specifically recognized by the transmembrane domain of the Hrd1p ubiquitin ligase. Mol. Cell *34*, 212–222.

Schaffar, G., Breuer, P., Boteva, R., Behrends, C., Tzvetkov, N., Strippel, N., Sakahira, H., Siegers, K., Hayer-Hartl, M., and Hartl, F.U. (2004). Cellular toxicity of polyglutamine expansion proteins: mechanism of transcription factor deactivation. Mol. Cell *15*, 95–105.

Scheufler, C., Brinker, A., Bourenkov, G., Pegoraro, S., Moroder, L., Bartunik, H., Hartl, F.U., and Moarefi, I. (2000). Structure of TPR domain-peptide complexes: critical elements in the assembly of the Hsp70-Hsp90 multichaperone machine. Cell *101*, 199–210.

Schmitz, A., Herrgen, H., Winkeler, A., and Herzog, V. (2000). Cholera toxin is exported from microsomes by the Sec61p complex. J. Cell Biol. *148*, 1203–1212.

Schulze, A., Standera, S., Buerger, E., Kikkert, M., van Voorden, S., Wiertz, E., Koning, F., Kloetzel, P.-M., and Seeger, M. (2005). The ubiquitin-domain protein HERP forms a complex with components of the endoplasmic reticulum associated degradation pathway. J. Mol. Biol. *354*, 1021–1027.

Seo, H., Sonntag, K.-C., and Isacson, O. (2004). Generalized brain and skin proteasome inhibition in Huntington's disease. Ann. Neurol. *56*, 319–328.

Seo, H., Sonntag, K.-C., Kim, W., Cattaneo, E., and Isacson, O. (2007). Proteasome activator enhances survival of Huntington's disease neuronal model cells. PloS One *2*, e238.

Sha, B., Lee, S., and Cyr, D.M. (2000). The crystal structure of the peptide-binding fragment from the yeast Hsp40 protein Sis1. Struct. Lond. Engl. 1993 *8*, 799–807.

Sharma, J., and Liebman, S.W. (2013). Exploring the basis of [PIN(+)] variant differences in [PSI(+)] induction. J. Mol. Biol. *425*, 3046–3059.

Sharp, A.H., Loev, S.J., Schilling, G., Li, S.H., Li, X.J., Bao, J., Wagster, M.V., Kotzuk, J.A., Steiner, J.P., and Lo, A. (1995). Widespread expression of Huntington's disease gene (IT15) protein product. Neuron *14*, 1065–1074.

Shearman, M.S., Ragan, C.I., and Iversen, L.L. (1994). Inhibition of PC12 cell redox activity is a specific, early indicator of the mechanism of beta-amyloid-mediated cell death. Proc. Natl. Acad. Sci. U. S. A. *91*, 1470–1474.

Shi, Y., Hong, X., and Wang, C. (2005). The C-terminal (331-376) sequence of Escherichia coli DnaJ is essential for dimerization and chaperone activity: a small angle X-ray scattering study in solution. J. Biol. Chem. *280*, 22761–22768.

Singer, D., Zauner, T., Genz, M., Hoffmann, R., and Zuchner, T. (2010). Synthesis of pathological and nonpathological human exon 1 huntingtin. J. Pept. Sci. Off. Publ. Eur. Pept. Soc. *16*, 358–363.

Sipe, J.D., and Cohen, A.S. (2000). Review: history of the amyloid fibril. J. Struct. Biol. *130*, 88–98.

Sondheimer, N., and Lindquist, S. (2000). Rnq1: an epigenetic modifier of protein function in yeast. Mol. Cell *5*, 163–172.

Sondheimer, N., Lopez, N., Craig, E.A., and Lindquist, S. (2001). The role of Sis1 in the maintenance of the [RNQ+] prion. EMBO J. *20*, 2435–2442.

Stanley, A.M., Carvalho, P., and Rapoport, T. (2011). Recognition of an ERAD-L substrate analyzed by site-specific in vivo photocrosslinking. FEBS Lett. *585*, 1281–1286.

Steffan, J.S., Kazantsev, A., Spasic-Boskovic, O., Greenwald, M., Zhu, Y.Z., Gohler, H., Wanker, E.E., Bates, G.P., Housman, D.E., and Thompson, L.M. (2000). The Huntington's disease protein interacts with p53 and CREB-binding protein and represses transcription. Proc. Natl. Acad. Sci. U. S. A. *97*, 6763–6768.

Stirling, P.C., Lundin, V.F., and Leroux, M.R. (2003). Getting a grip on non-native proteins. EMBO Rep. *4*, 565–570.

Summers, D.W., Douglas, P.M., and Cyr, D.M. (2009). Prion propagation by Hsp40 molecular chaperones. Prion *3*, 59–64.

Summers, D.W., Wolfe, K.J., Ren, H.Y., and Cyr, D.M. (2013). The Type II Hsp40 Sis1 cooperates with Hsp70 and the E3 ligase Ubr1 to promote degradation of terminally misfolded cytosolic protein. PloS One *8*, e52099.

Sun, T., Guo, J., Shallow, H., Yang, T., Xu, J., Li, W., Hanson, C., Wu, J.G., Li, X., Massaeli, H., et al. (2011). The role of monoubiquitination in endocytic degradation of human ether-a-go-go-related gene (hERG) channels under low K+ conditions. J. Biol. Chem. *286*, 6751–6759.

Sunde, M., and Blake, C. (1997). The structure of amyloid fibrils by electron microscopy and X-ray diffraction. Adv. Protein Chem. *50*, 123–159.

Swanson, R., Locher, M., and Hochstrasser, M. (2001). A conserved ubiquitin ligase of the nuclear envelope/endoplasmic reticulum that functions in both ER-associated and Matalpha2 repressor degradation. Genes Dev. *15*, 2660–2674.

Sweeny, E.A., and Shorter, J. (2008). Prion proteostasis: Hsp104 meets its supporting cast. Prion *2*, 135–140.

Szabo, A., Langer, T., Schröder, H., Flanagan, J., Bukau, B., and Hartl, F.U. (1994). The ATP hydrolysis-dependent reaction cycle of the Escherichia coli Hsp70 system DnaK, DnaJ, and GrpE. Proc. Natl. Acad. Sci. U. S. A. *91*, 10345–10349.

Szathmary, R., Bielmann, R., Nita-Lazar, M., Burda, P., and Jakob, C.A. (2005). Yos9 protein is essential for degradation of misfolded glycoproteins and may function as lectin in ERAD. Mol. Cell *19*, 765–775.

Takeuchi, J., Chen, H., and Coffino, P. (2007). Proteasome substrate degradation requires association plus extended peptide. EMBO J. *26*, 123–131.

Takeuchi, J., Chen, H., Hoyt, M.A., and Coffino, P. (2008). Structural elements of the ubiquitin-independent proteasome degron of ornithine decarboxylase. Biochem. J. *410*, 401–407.

Taxis, C., Hitt, R., Park, S.-H., Deak, P.M., Kostova, Z., and Wolf, D.H. (2003). Use of modular substrates demonstrates mechanistic diversity and reveals differences in chaperone requirement of ERAD. J. Biol. Chem. *278*, 35903–35913.

Taylor, R.C., and Dillin, A. (2011). Aging as an event of proteostasis collapse. Cold Spring Harb. Perspect. Biol. *3*.

Thrower, J.S., Hoffman, L., Rechsteiner, M., and Pickart, C.M. (2000). Recognition of the polyubiquitin proteolytic signal. EMBO J. *19*, 94–102.

Trottier, Y., Devys, D., Imbert, G., Saudou, F., An, I., Lutz, Y., Weber, C., Agid, Y., Hirsch, E.C., and Mandel, J.L. (1995). Cellular localization of the Huntington's disease protein and discrimination of the normal and mutated form. Nat. Genet. *10*, 104–110.

Trushina, E., and McMurray, C.T. (2007). Oxidative stress and mitochondrial dysfunction in neurodegenerative diseases. Neuroscience *145*, 1233–1248.

Tuite, M., Stojanovski, K., Ness, F., Merritt, G., and Koloteva-Levine, N. (2008). Cellular factors important for the de novo formation of yeast prions. Biochem. Soc. Trans. *36*, 1083–1087.

Tycko, R. (2004). Progress towards a molecular-level structural understanding of amyloid fibrils. Curr. Opin. Struct. Biol. *14*, 96–103.

Valera, A.G., Díaz-Hernández, M., Hernández, F., and Lucas, J.J. (2007). Testing the possible inhibition of proteasome by direct interaction with ubiquitylated and aggregated huntingtin. Brain Res. Bull. *72*, 121–123.

Varga, K., Jurkuvenaite, A., Wakefield, J., Hong, J.S., Guimbellot, J.S., Venglarik, C.J., Niraj, A., Mazur, M., Sorscher, E.J., Collawn, J.F., et al. (2004). Efficient intracellular processing of the endogenous cystic fibrosis transmembrane conductance regulator in epithelial cell lines. J. Biol. Chem. *279*, 22578–22584.

Varshavsky, A. (2012). The ubiquitin system, an immense realm. Annu. Rev. Biochem. *81*, 167–176.

Vashist, S., and Ng, D.T.W. (2004). Misfolded proteins are sorted by a sequential checkpoint mechanism of ER quality control. J. Cell Biol. *165*, 41–52.

Vattemi, G., Engel, W.K., McFerrin, J., and Askanas, V. (2004). Endoplasmic reticulum stress and unfolded protein response in inclusion body myositis muscle. Am. J. Pathol. *164*, 1–7.

Venkatraman, P., Wetzel, R., Tanaka, M., Nukina, N., and Goldberg, A.L. (2004). Eukaryotic proteasomes cannot digest polyglutamine sequences and release them during degradation of polyglutamine-containing proteins. Mol. Cell *14*, 95–104.

Verghese, J., Abrams, J., Wang, Y., and Morano, K.A. (2012). Biology of the heat shock response and protein chaperones: budding yeast (Saccharomyces cerevisiae) as a model system. Microbiol. Mol. Biol. Rev. MMBR *76*, 115–158.

Vijay-Kumar, S., Bugg, C.E., and Cook, W.J. (1987). Structure of ubiquitin refined at 1.8 A resolution. J. Mol. Biol. *194*, 531–544.

Vitrenko, Y.A., Gracheva, E.O., Richmond, J.E., and Liebman, S.W. (2007). Visualization of aggregation of the Rnq1 prion domain and cross-seeding interactions with Sup35NM. J. Biol. Chem. *282*, 1779–1787.

Voges, D., Zwickl, P., and Baumeister, W. (1999). The 26S proteasome: a molecular machine designed for controlled proteolysis. Annu. Rev. Biochem. *68*, 1015–1068.

Vonsattel, J.P., Myers, R.H., Stevens, T.J., Ferrante, R.J., Bird, E.D., and Richardson, E.P., Jr (1985). Neuropathological classification of Huntington's disease. J. Neuropathol. Exp. Neurol. *44*, 559–577.

Wahlman, J., DeMartino, G.N., Skach, W.R., Bulleid, N.J., Brodsky, J.L., and Johnson, A.E. (2007). Real-time fluorescence detection of ERAD substrate retrotranslocation in a mammalian in vitro system. Cell *129*, 943–955.

Walker, F.O. (2007). Huntington's disease. Lancet *369*, 218–228.

Walsh, P., Bursać, D., Law, Y.C., Cyr, D., and Lithgow, T. (2004). The J-protein family: modulating protein assembly, disassembly and translocation. EMBO Rep. *5*, 567–571.

Wang, J., Wang, C.-E., Orr, A., Tydlacka, S., Li, S.-H., and Li, X.-J. (2008). Impaired ubiquitin-proteasome system activity in the synapses of Huntington's disease mice. J. Cell Biol. *180*, 1177–1189.

Wang, Q., Liu, Y., Soetandyo, N., Baek, K., Hegde, R., and Ye, Y. (2011). A ubiquitin ligase-associated chaperone holdase maintains polypeptides in soluble states for proteasome degradation. Mol. Cell *42*, 758–770.

Wendland, B., McCaffery, J.M., Xiao, Q., and Emr, S.D. (1996). A novel fluorescence-activated cell sorter-based screen for yeast endocytosis mutants identifies a yeast homologue of mammalian eps15. J. Cell Biol. *135*, 1485–1500.

Werner-Washburne, M., Stone, D.E., and Craig, E.A. (1987). Complex interactions among members of an essential subfamily of hsp70 genes in Saccharomyces cerevisiae. Mol. Cell. Biol. *7*, 2568–2577.

Werner-Washburne, M., Becker, J., Kosic-Smithers, J., and Craig, E.A. (1989). Yeast Hsp70 RNA levels vary in response to the physiological status of the cell. J. Bacteriol. *171*, 2680–2688.

Westermark, P., Benson, M.D., Buxbaum, J.N., Cohen, A.S., Frangione, B., Ikeda, S.-I., Masters, C.L., Merlini, G., Saraiva, M.J., Sipe, J.D., et al. (2005). Amyloid: toward terminology clarification. Report from the Nomenclature Committee of the International Society of Amyloidosis. Amyloid Int. J. Exp. Clin. Investig. Off. J. Int. Soc. Amyloidosis *12*, 1–4.

Wickner, R.B. (1994). [URE3] as an altered URE2 protein: evidence for a prion analog in Saccharomyces cerevisiae. Science *264*, 566–569.

Wickner, R.B., Dyda, F., and Tycko, R. (2008). Amyloid of Rnq1p, the basis of the [PIN+] prion, has a parallel in-register beta-sheet structure. Proc. Natl. Acad. Sci. U. S. A. *105*, 2403–2408.

Wiertz, E.J., Jones, T.R., Sun, L., Bogyo, M., Geuze, H.J., and Ploegh, H.L. (1996). The human cytomegalovirus US11 gene product dislocates MHC class I heavy chains from the endoplasmic reticulum to the cytosol. Cell *84*, 769–779.

Wilkinson, K.D. (1999). Ubiquitin-dependent signaling: the role of ubiquitination in the response of cells to their environment. J. Nutr. *129*, 1933–1936.

Willmund, F., del Alamo, M., Pechmann, S., Chen, T., Albanèse, V., Dammer, E.B., Peng, J., and Frydman, J. (2013). The cotranslational function of ribosome-associated Hsp70 in eukaryotic protein homeostasis. Cell *152*, 196–209.

Wójcik, C., and DeMartino, G.N. (2003). Intracellular localization of proteasomes. Int. J. Biochem. Cell Biol. *35*, 579–589.

Wolf, D.H., and Hilt, W. (2004). The proteasome: a proteolytic nanomachine of cell regulation and waste disposal. Biochim. Biophys. Acta *1695*, 19–31.

Woudstra, E.C., Gilbert, C., Fellows, J., Jansen, L., Brouwer, J., Erdjument-Bromage, H., Tempst, P., and Svejstrup, J.Q. (2002). A Rad26-Def1 complex coordinates repair and RNA pol II proteolysis in response to DNA damage. Nature *415*, 929–933.

Xie, W., Kanehara, K., Sayeed, A., and Ng, D.T.W. (2009). Intrinsic conformational determinants signal protein misfolding to the Hrd1/Htm1 endoplasmic reticulum-associated degradation system. Mol. Biol. Cell *20*, 3317–3329.

Yan, W., and Craig, E.A. (1999). The glycine-phenylalanine-rich region determines the specificity of the yeast Hsp40 Sis1. Mol. Cell. Biol. *19*, 7751–7758.

Ye, Y., Meyer, H.H., and Rapoport, T.A. (2001). The AAA ATPase Cdc48/p97 and its partners transport proteins from the ER into the cytosol. Nature *414*, 652–656.

Yoo, S.Y., Pennesi, M.E., Weeber, E.J., Xu, B., Atkinson, R., Chen, S., Armstrong, D.L., Wu, S.M., Sweatt, J.D., and Zoghbi, H.Y. (2003). SCA7 knockin mice model human SCA7 and reveal gradual accumulation of mutant ataxin-7 in neurons and abnormalities in short-term plasticity. Neuron *37*, 383–401.

Young, M.R., and Craig, E.A. (1993). Saccharomyces cerevisiae HSP70 heat shock elements are functionally distinct. Mol. Cell. Biol. *13*, 5637–5646.

Zhong, T., and Arndt, K.T. (1993). The yeast SIS1 protein, a DnaJ homolog, is required for the initiation of translation. Cell *73*, 1175–1186.

Zhu, X., Zhao, X., Burkholder, W.F., Gragerov, A., Ogata, C.M., Gottesman, M.E., and Hendrickson, W.A. (1996). Structural analysis of substrate binding by the molecular chaperone DnaK. Science *272*, 1606–1614.

Zimmerman, S.B., and Minton, A.P. (1993). Macromolecular crowding: biochemical, biophysical, and physiological consequences. Annu. Rev. Biophys. Biomol. Struct. *22*, 27–65.

Zimmerman, S.B., and Trach, S.O. (1991). Estimation of macromolecule concentrations and excluded volume effects for the cytoplasm of Escherichia coli. J. Mol. Biol. *222*, 599–620.

Zuiderweg, E.R.P., Bertelsen, E.B., Rousaki, A., Mayer, M.P., Gestwicki, J.E., and Ahmad, A. (2013). Allostery in the Hsp70 chaperone proteins. Top. Curr. Chem. *328*, 99–153.

7   Appendix

7.1   Abbreviations

Units are expressed according to the international system of units (SI). Protein and gene names are abbreviated according to their SWISSPROT database entries.

ADP	adenosine 5'-diphosphate
Amp	ampicillin
APS	ammonium peroxydisulfate
ATP	adenosine 5'-triphosphate
bp	base pair
BSA	albumin bovine serum
Cen.	centromeric plasmid
cODC	c-terminal 37 amino acids of ornithine decarboxylase
CHX	cycloheximide
Da	dalton
DAPI	4,6-diamidin-2-phenylindol
DMSO	dimethylsulfoxid
DNA	deoxyribonucleic acid
dNTP	dideoxynucleoside triphosphate
Dox	doxycycline
DTT	dithiothreitol
E.coli	*Escherichia coli*
EDTA	ethylenediaminetetraacetic acid
ER	endoplasmic reticulum
ERAD	ER-associated degradation
FBPase	fructose 1,6-bisphosphatase
FITC	fluorescein-isothiocyanate
g	acceleration of gravity, 9.81 m/s2
Gal	galactose
GFP	green fluorescent protein
Glu	glucose

GuCL	guanidinium hydrochloride
HD	Huntington's disease
HRP	horseradish peroxidase
HS	heat shock
Hsp	heat shock protein
Hsp70	heat shock proteins with molecular *weight* 70 kilodaltons
Hsp40	heat shock proteins with molecular *weight* 40 kilodaltons
HSR	heat shock response
IB	inclusion body
IP	immunoprecipitation
LB	Luria-Bertani
mCherry	monomeric red fluorescent protein
mRNA	messenger RNA
myc	protein tag derived from the c-myc protein
NEF	nucleotide-exchange factor
NES	nuclear export signal
NLS	nuclear localization signal
OD	optical density
OD420	optical density at a wavelength of 420nm
OD600	optical density at a wavelength of 600nm
ONPG	ortho-Nitrophenyl-β-galactoside
PAGE	polyacrylamide Gel Electrophoresis
PBS	phosphate-buffered saline
PCR	Polymerase Chain Reaction
PEG	polyethylene glycol
PGK	phosphoglycerate kinase
Pi	inorganic Phosphate
PMSF	phenylmethylsulfonyl fluoride
RNA	ribonucleic acid
PolyQ	polyglutamine
Poly-Ub	polyubiquitin
S. cerevisiae	*Saccharomyces cerevisiae*
SD	standard deviation
SDS	sodium dodecylsulfate
SDS-PAGE	sodium dodecyl sulfate polyacrylamide gel electrophoresis

SILAC	stable isotope labeling by amino acids in cell culture
SBD	substrate binding domain
TCA	trichloroacetic acid
TEMED	N,N,N',N'-tetramethylethylendiamine
Tet	tetracycline
Tris	tris(hydroxymethyl)aminomethane
Triton X-100	octyl phenol ethoxylate
Tween 20	polyoxyethylen-sorbitan-monolaurate
Ub	ubiquitin
UPR	unfolded protein response
UPS	ubiquitin-proteasome system
WT	wild-type
2µ	multicopy plasmid

7.2 Publications and conference abstracts

7.2.1 Publications

Park SH, Kukushkin Y, Gupta R, Chen T, Konagai A, Hipp MS, Hayer-Hartl M, Hartl FU (2013) PolyQ proteins interfere with nuclear degradation of cytosolic proteins by sequestering the Sis1p chaperone. Cell 154:134–145

7.2.2 Conference abstracts

Yuri Kukushkin, Sae-Hun Park, Ulrich Hartl.
"PolyQ-expanded Huntingtin disturbs protein quality control in the cell." The 9th Eibsee meeting of Alzheimer's Disease November, 2009, Eibsee

7.3 Curriculum vitae

KukushkinYury S.
July 11, 1983
Russia/Russian

E-mail: **yury.kukushkin@gmail.com**

Career/Employment:

07/2007- 09/2012   PhD student in **Max Planck Institute of Biochemistry,**   Martinsried, Germany

Education:

09/2000 –07/ 2005 M. Sc. in Biochemistry, Biological department of Moscow State University (rank №1 in Russia). Graduated with honor.

09/1990 – 06/2000   Physics and mathematics school #1636, Moscow.

Co-Organizer:

Future Biotech - nonprofit organization stimulating research and commercialize scientific findings in life sciences in Russia and worldwide.

Future Biotech aims to bring together the most talented and ambitious master, PhD students and young postdocs to discuss applications of scientific knowledge and commercialization of scientific findings. Our aim is to strengthen the connection between fundamental science and entrepreneurship, promote networking, and discuss some of the most appealing areas in biology and possible career paths in fundamental science and entrepreneurship around the world.

Professional skills:

Languages:
Russian – native
English – fluent
German – low intermediate

Computer skills, advanced level: Microsoft Word, Microsoft Excel (including macro usage), Microsoft Power Point, Microsoft Access (+ basic understanding of SQL), Microsoft Visio.
Statistical programs: SPSS 11, Statistica 6.0, Sigma Plot